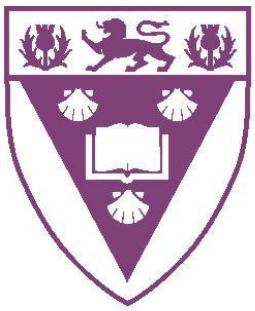

RHODES UNIVERSITY

Grahamstown • 6140 • South Africa

Gold mineralisation at Masumbi Au-Cu Prospect, West Kenya: Implication for gold exploration in the Archaean Ndori Greenstone Belt of Kenya

Luckmore Salimo

A thesis submitted in partial fulfilment of the requirements for the degree of

MASTER OF SCIENCE (Exploration Geology)

Rhodes University

Grahamstown 6140

South Africa

November 2013

DECLARATION

Name:	**Luckmore Salimo**
Student Number:	**G13S7334**
Programme:	**MSc. Exploration Geology**

1. I, Luckmore Salimo, do hereby solemnly declare that this thesis is the result of my own investigation and research, except to the extent indicated in the acknowledgements and references included in the body of the thesis.
2. I am fully aware that plagiarism is an academic offence. Plagiarism is to use another's work and pretend that it is one's own.
3. I have used the Economic Geology system of referencing where the author and date are used for citation and referencing.
4. I have not allowed, and will not allow, anyone to copy my work with the intention of passing it off as his or her own work.

Signature_____ Date: 29/11/2013

Supervisor's signature_____ Date: 29/11/2013

ABSTRACT

The Masumbi Au-Cu deposit in the Ndori Greenstone Belt of western Kenya is hosted in dacitic volcanics of the Nyanzian Group (2710 ± 340 Ma) and dioritic to granodioritic felsic intrusives (2504 ± 48 Ma). The deposit is characterised by gold and copper mineralisation that is associated with quartz-sulphide veins and veinlets. The copper mineralisation typically occurs as chalcopyrite. Gold is closely associated with pyrite in mineralogy and its pathfinder elements silver, bismuth, tellurium and selenium in geochemistry. The gold occurs in two forms that may indicate two generations of precipitation: the equant and the elongate forms. Based on Au/Ag ratios, the equant gold grains can be classified as native gold as their gold content is greater than 90 wt%. The elongate gold grains can be classified as electrums as their silver content is greater than 38 wt%.

While there is a strong Au-Ag association within individual gold grains supporting an orogenic model for the gold mineralisation, mineralisation at the Masumbi Prospect appears atypical of Archaean orogenic gold deposits because of the abundance of copper (up to 0.43%). The enrichment of silver, copper, bismuth and tellurium in ore assemblages is common in porphyry, VMS and epithermal systems, but their presence at Masumbi does not preclude the formation as an orogenic deposit.

Assay results from three Masumbi diamond drill-holes show an apparent correlation between gold and copper. However, petrography and electron probe microanalyses results from this study indicate that chalcopyrite is an earlier phase than pyrite as it occasionally occurs as inclusions in pyrite. This petrogenetic relationship between pyrite and chalcopyrite suggests that there is no temporal relationship between gold and copper mineralisation. Statistical analysis of the assays shows no linear correlation between gold and copper thereby supporting the above findings. The gold and copper mineralisation have been interpreted as forming as two separate events with copper forming first followed by gold. These events are both related to the intrusion of the felsic rocks that are associated with the Aruan metamorphic event that has been responsible for the bulk of the gold mineralisation on the Tanzanian Craton.

The common alteration assemblage in the Masumbi rocks comprises chlorite and epidote. This alteration assemblage is typical of regional greenschist metamorphic facies grading into amphibolite metamorphic facies in the Nyanzian Group of Kenya. However, these alteration

minerals could possibly be products of propylitic alteration in the rock groundmass. Other alteration mineral assemblages, possibly of hydrothermal origin, comprise muscovite, sericite, quartz, carbonate, associated with the sulphides pyrite and chalcopyrite. Although the occurrence of gold appears to be controlled by the presence of pyrite, it is also associated with silicification.

Exploration methods have been proposed to target undiscovered gold deposits in the Ndori Greenstone Belt that are similar to the Masumbi deposit. These methods could probably be applied to vein-type gold deposits in other granite-greenstone terranes in the Lake Victoria Goldfields.

DEDICATION

This thesis is dedicated to my beautiful wife Anna, who supported me in each step of the way, and to our amazing children, Panashe and Paidamoyo.

ACKNOWLEDGEMENTS

As a 2013 recipient of the Julian Baring Scholarship, I am hugely indebted to the trustees of the Fund for affording me a great opportunity to attend the world-renowned MSc. Exploration Geology programme at Rhodes University. Thank you so much for a full sponsorship.

I wish to thank the management of Rock and Stock Investments, Mr. Joshua Hattingh, Mrs. Cecelia Hattingh and Mr. Ernie Venter, for granting me a special year-long, uninterrupted and paid study leave. Your support and encouragement during the course of my study are greatly appreciated.

This thesis would not have been possible without project data and drill-core samples supplied by African Barrick Gold. Special thanks are extended to the Vice President for Exploration - Mr. Peter Spora, the Technical Director for Exploration - Mr. Glen Edwards and the Exploration Manager for Kenya - Dr. Timothy Sharp for your support. To Mr. Collins Aseto, thanks mate for coordinating sample collection and dispatch.

Many thanks are due to Professor Yong Yao of Rhodes University, my supervisor and director of the MSc. Exploration Geology programme, for the guidance and supervision rendered throughout the duration of my studies. Particular thanks are due to Dr. Marian Munteanu for guidance during Electron Probe Micro-Analyses and reviewing drafts of this thesis. Heartfelt thanks to Mrs. Ashley Goddard, the Administrator of the programme, for introducing me to the Julian Baring Scholarship and being a caring mother throughout the year. All members of the academic and technical staff of the Geology Department are acknowledged for their assistance throughout the duration of the programme.

I would like to thank my classmates, Demand Gwatinetsa, Thomas Branson, Tsholofelo Malatji, Godfrey Bitesigirwe and Ali Assane, for their stimulating discussions during the year.

The use of JEOL JXA 8230 Superprobe, instrument sponsored by NRF/NEP grant 40113 (UID 74464) is kindly acknowledged.

To my wife Anna, thank you sweetheart for being my pillar of strength during trying times and enduring loneliness when I was in Grahamstown. To my son Panashe and daughter Paidamoyo, thank you for understanding when dad missed your functions - concerts, award ceremonies, etc.

TABLE OF CONTENTS

LIST OF FIGURES

LIST OF TABLES

CHAPTER 1 INTRODUCTION

1.1 Background

Aviva Mining Kenya Limited (AMKL) is a wholly-owned subsidiary of African Barrick Gold (ABG) that is in the business of mineral exploration in Kenya. ABG acquired AMKL from ASX-listed Aviva Corporation Ltd (Aviva) in October 2012, thereby acquired AMKL's interests in the West Kenya Project. AMKL has now been incorporated into ABG Kenya Exploration Limited that is currently conducting gold and base metal exploration in five special prospecting licences in western Kenya of which SPL123 (Ndori) and SPL213 (Siaya) cover the largest proportion of the total area. Figure 1 shows the location of SPL123 (Ndori) and SPL213 (Siaya).

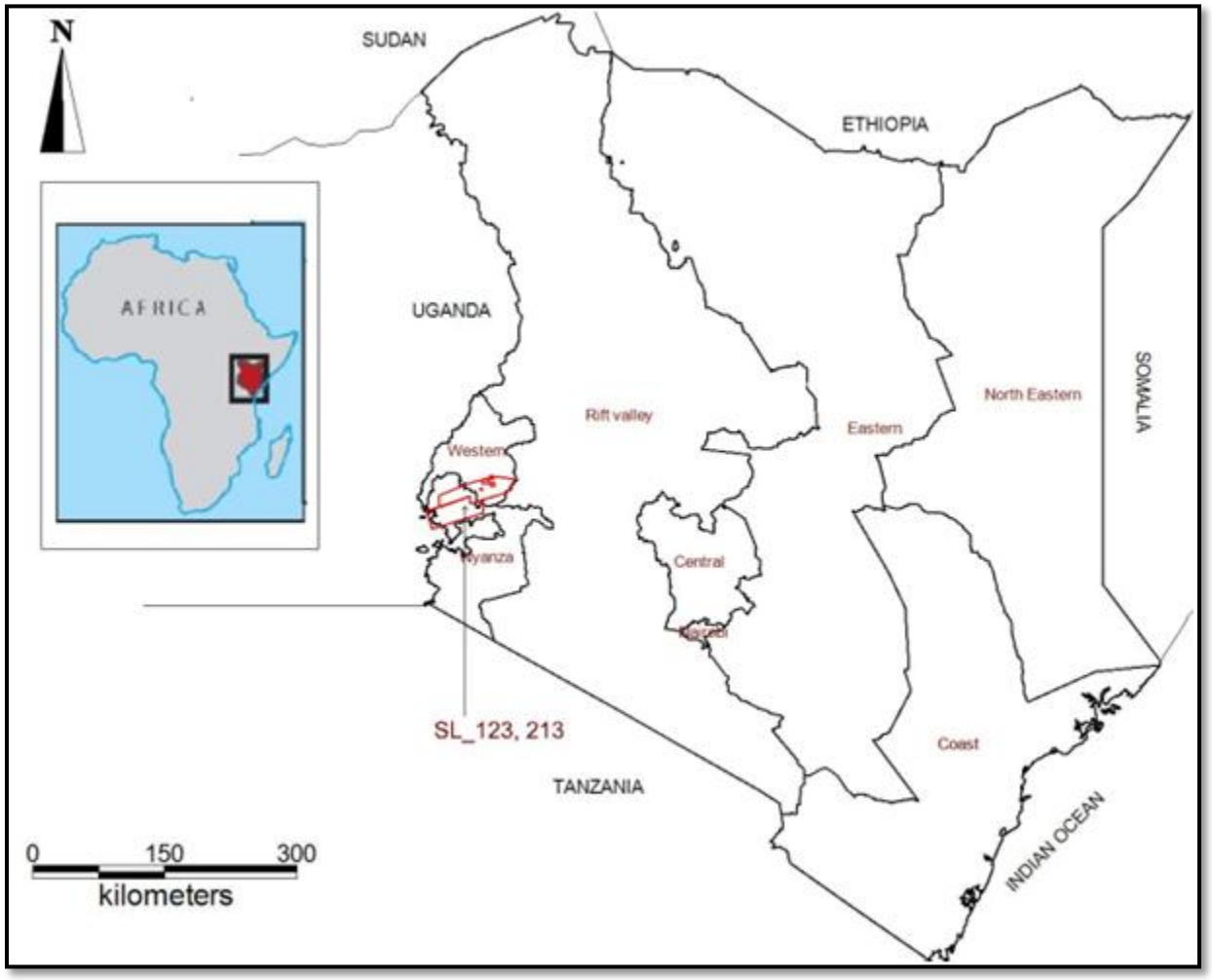

Figure 1. Location of AMKL's licence area in western Kenya.

SPL123 (Ndori) and SPL213 (Siaya) have a combined extent of 2,800km^2 and account for the bulk of the highly-prospective Ndori Greenstone Belt in Kenya, which forms part of the Archaean Tanzanian Craton. There are more than 200 recorded gold deposits and occurrences within the licence area that include historical mines Rosterman and Ramba-Lumba. In line with ABG's exploration strategy, AMKL has embarked on an extensive exploration programme with the aim of delivering significant economic gold resources. Several gold targets have been generated on the licences using a variety of exploration techniques. The Masumbi Au-Cu Prospect is one of the targets generated on SPL123 (Ndori) in the southwest portion of the Ndori Greenstone Belt.

1.2 Objectives of this study

The Masumbi deposit is unusual in some respects when compared with Archaean gold deposits. The majority of Archaean gold deposits are gold only, with only traces of base metals present in and around the mineralised zones (Colvine, 1988; Groves et al., 1990). In contrast, gold mineralisation at Masumbi is associated with significant quantities of copper (up to 0.43%). The Archaean gold deposits are commonly hosted by quartz lodes and show clear spatial and genetic associations with contemporaneous structures such as faults, shear zones and fold hinges (Allibone et al., 1998). Gold and copper mineralisation at Masumbi, however, is hosted in quartz-sulphide veinlets, some of which have epidote-rich selvages. Mineralisation at Masumbi is also associated with alteration that has been referred to as 'propylitic' (Grant, 2006). This alteration assemblage is not generally associated with Archaean lode-style gold deposits but with porphyry-related settings (Allibone et al., 1998).

In order to explore for similar deposits in the Ndori Greenstone Belt, it is imperative to better understand the association of gold mineralisation at Masumbi with copper mineralisation, alteration assemblages and pathfinder elements. Therefore, the objectives of this thesis include the following: to investigate if there is temporal relationship between gold and copper mineralisation at Masumbi; to determine if gold mineralisation at Masumbi is associated with particular alteration assemblages; to analyse pathfinder elements associated with gold mineralisation at Masumbi; and to integrate appropriate exploration methods for gold deposits with characteristics similar to the Masumbi Au-Cu deposit.

CHAPTER 2 PREVIOUS WORK

2.1 Introduction

This chapter chronicles exploration and mining history of Masumbi Au-Cu Prospect and discusses the recent exploration work conducted by AMKL. Prior to AMKL tenure, there is scanty published literature on the exploration and mining history. The information contained in this chapter largely comes from unpublished internal company reports and memorandums.

2.2 Exploration history

Exploration and mining at the Masumbi Au-Cu Prospect can be dated back to 1929 when colonials targeted small-scale workings on high grade veins, eluvial and alluvial deposits. This early work was terminated in 1945 due to the World War II. From 1997 to 1998, Pan African Resources Corporation (PARC) conducted grassroots exploration that included trenching and augering. Between 2003 and 2006, AfriOre conducted ground magnetic and induced polarisation (IP) surveys, drilled more than 2,000 m of percussion drilling and 845 m of diamond drilling, conducted soil geochemical sampling and trenching. AfriOre was taken over by Lonmin who conducted exploration from 2007 to 2008. As part of their regional soil sampling programme covering all prospective gold-bearing areas, Lonmin conducted soil geochemical sampling at Masumbi. No exploration work took place from 2009 to 2010 and then Aviva formed a joint venture with Lonmin. From 2010 to 2011, AMKL conducted a detailed surface mapping exercise, drilled 1,009.37 m of diamond drilling, 833 m of reverse circulation (RC) drilling and IP and resistivity surveys. Details of exploration work by AMKL are discussed in the next section. A summary of the exploration history for the Masumbi Au-Cu Prospect is outline in Table 1.

Although intermittent mineral exploration at the Masumbi Prospect spans over eight decades, a significant economic gold resource is yet to be delivered. However, the soil geochemical sampling programme conducted by AfriOre delineated a 5 km x 2 km gold-in-soil anomaly that prompted the RC and diamond drilling programmes. Results from the drilling programmes by AfriOre and later by AMKL culminated in potential mineralisation of 3.6 million tonnes of gold ore grading at 1.19 g/t and containing approximately 138,200 ounces of gold.

Table 1. Summary exploration history of the Masumbi Prospect

From	To	Company	Activities undertaken
1929	1945	Colonial workers	• Small-scale workings on high grade veins, eluvial and alluvial deposits.
1997	1998	PARC	• Semi-detailed work that included trenching and hand augering.
2003	2006	AfriOre	• Ground magnetic and IP surveys, • > 2000m of percussion drilling, • 845m of diamond drilling, • soil geochemical sampling, and • trenching
2007	2008	Lonmin	• Soil geochemical sampling
2010	2012	AMKL	• Detailed surface geological mapping, • 1009.37m of diamond drilling, • 833.00m of RC drilling and • Ground IP and resistivity surveys

2.3 Recent exploration work on Masumbi Au-Cu Prospect

Exploration work conducted by AMKL on the Masumbi Au-Cu Prospect includes detailed surface geological mapping, petrographic description characterising the rocks from drill core, a resistivity and IP survey, RC drilling, diamond drilling and a review of the gold grade and mineralisation potential.

2.3.1 Geological mapping

Field mapping of the AMKL's licence areas at a scale of 1:250,000 in western Kenya, incorporating the Masumbi Prospect, coincided with acquisition of new geophysical data and a combination of these new data enabled an interpretation of the geology and structure of the licence areas that would aid exploration efforts in the area. The geological interpretation details the stratigraphy of the area and includes a structural model whose framework is dominated by early-formed syn-sedimentary extensional fault structures that developed during deposition of

the Kavirondian sediments. A progressive, protracted contractional deformation event followed sedimentation and involved inversion of some syn-sedimentary structures. The contractional deformation is suggested to have overlapped with gold mineralisation with both events envisaged as punctuated multi-increment processes. Structural associations with known mineralisation support this suggestion with gold mineralisation occurring in structural settings that range from low-strain, high differential stress environments to higher strain complexly deformed areas that involve dilation with attendant faulting and veining (Mason, 2010).

2.3.2 Petrographic description of rocks drilled at Masumbi Prospect

Diamond drill logging at the Masumbi Prospect suggests that the rocks include a sequence of dacitic lavas which have been intruded by several varieties of felsic igneous rocks. However, there is some lack of consistency with the logging with regards to grain sizes and textures and deciding whether rock units are intrusive or extrusive in nature. In order to better characterise these rocks, twenty three samples from four diamond drill-holes were submitted for thin section preparation and petrographic description.

On the basis of petrographic observations on the twenty three samples submitted, Crawford (2011) argues that the rocks logged as dacites have been correctly logged. They were almost certainly glassy plagioclase-phyric and aphyric dacitic lavas in which the glass devitrified before the lava pile was intruded by at least one and probably more suites of dioritic to granodioritic intrusive rock. Heat and hydrothermal fluids from the intruding felsic magmas led to recrystallisation and coarsening of the devitrified glass in the dacitic host lavas, leading to textures very difficult to separate from true intrusive textures in the associated diorites and granodiorites (Crawford, 2011).

2.3.3 Resistivity and IP survey

Gradient array resistivity and IP surveys were undertaken at the Masumbi Prospect. The goal of resistivity mapping was to detect the contrasts in resistivity that would facilitate mapping of resistive units beyond the immediate known mineralised zone. The gradient array was chosen because it allows the provision of an effective surface map of the resistivity distribution which in turn aids in the interpretation of a geology map. The purpose of the survey was to explore the apparent resistivity and chargeability expression of the gold mineralised intrusive units at Masumbi; to investigate any possible strike extension or parallel repetition of the known

mineralisation system; and to better target drilling within the 5 km x 2 km gold-in-soil anomaly over Masumbi (Buckingham, 2012).

A single line of pole-dipole array resistivity and IP data were collected across the Masumbi mineralisation to investigate the geometry of the gradient array anomalies at depth. The resistivity data collected reveals that the Masumbi mineralisation sits within one of several mappable resistive units trending north to northwest, coincident with a wider chargeability zone. Gradient array resistivity data and gradient array chargeability data are illustrated in Figure 2 and Figure 3 respectively. The survey confirmed the potential for strike extension as well as parallel repetition of units exhibiting a similar electrical response to those hosting the known gold mineralisation (Buckingham, 2012).

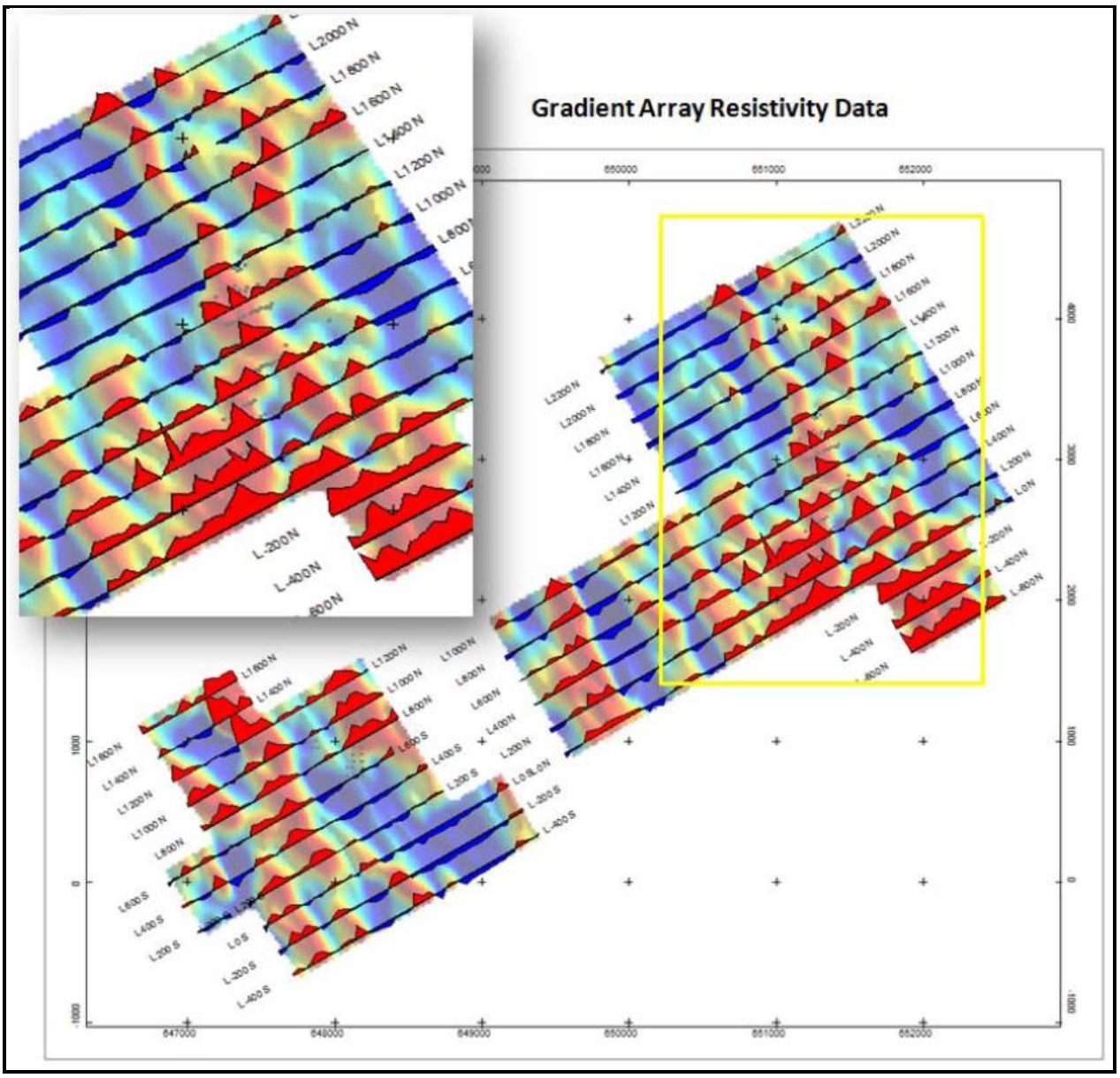

Figure 2. Gradient array resistivity data for the Masumbi Prospect (in yellow block). Adapted from Buckingham (2012).

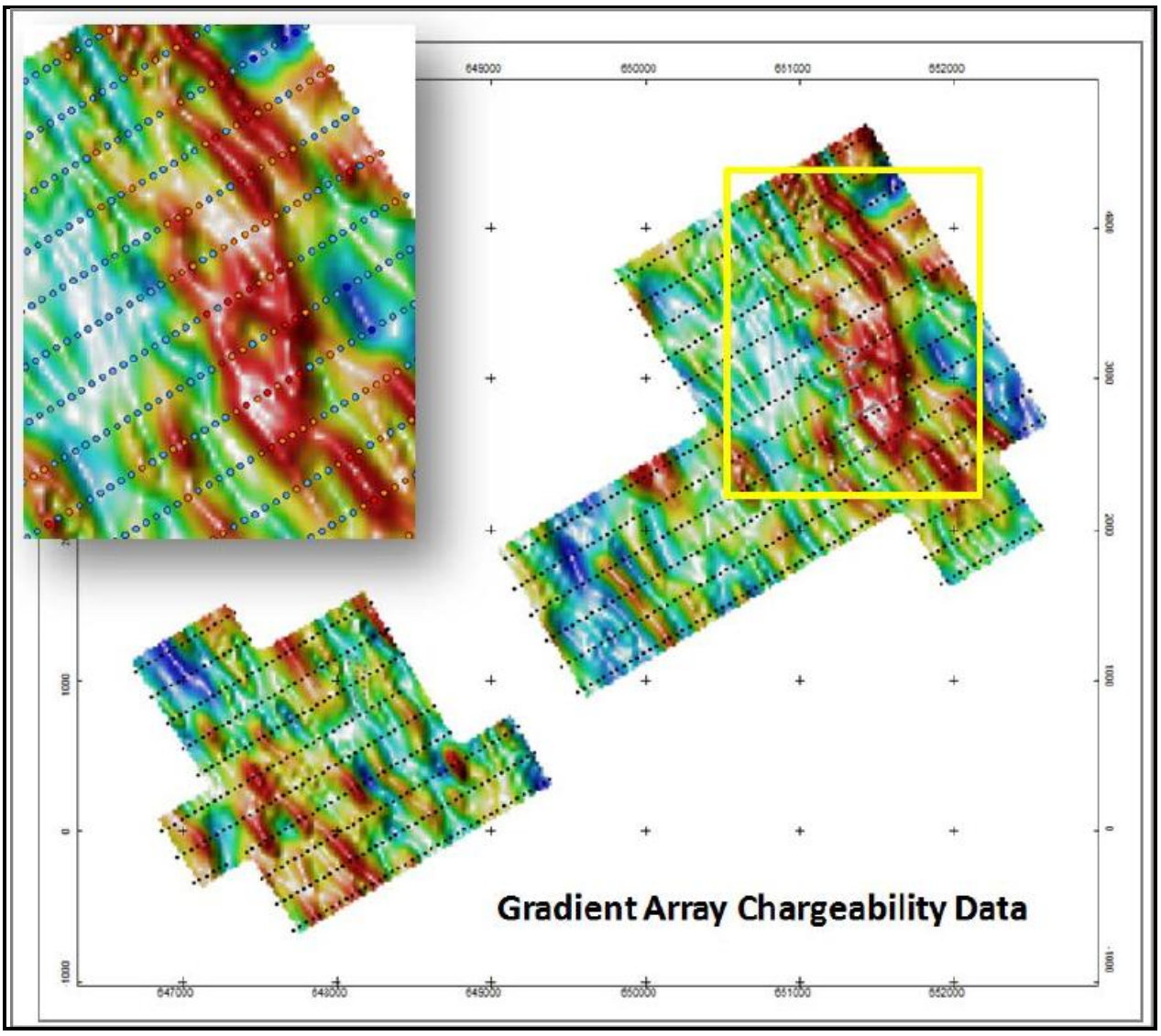

Figure 3. Gradient array chargeability data for the Masumbi Prospect (in yellow block). Adapted from Buckingham (2012).

An interpretation of the gradient array data was carried out in an attempt to better understand the possible geometry and extent of the intrusive units, and to assist in identifying areas of interest for drilling (Buckingham, 2012). The map in Figure 4 is primarily a geological interpretation of the gradient array and IP data over the Masumbi Prospect area.

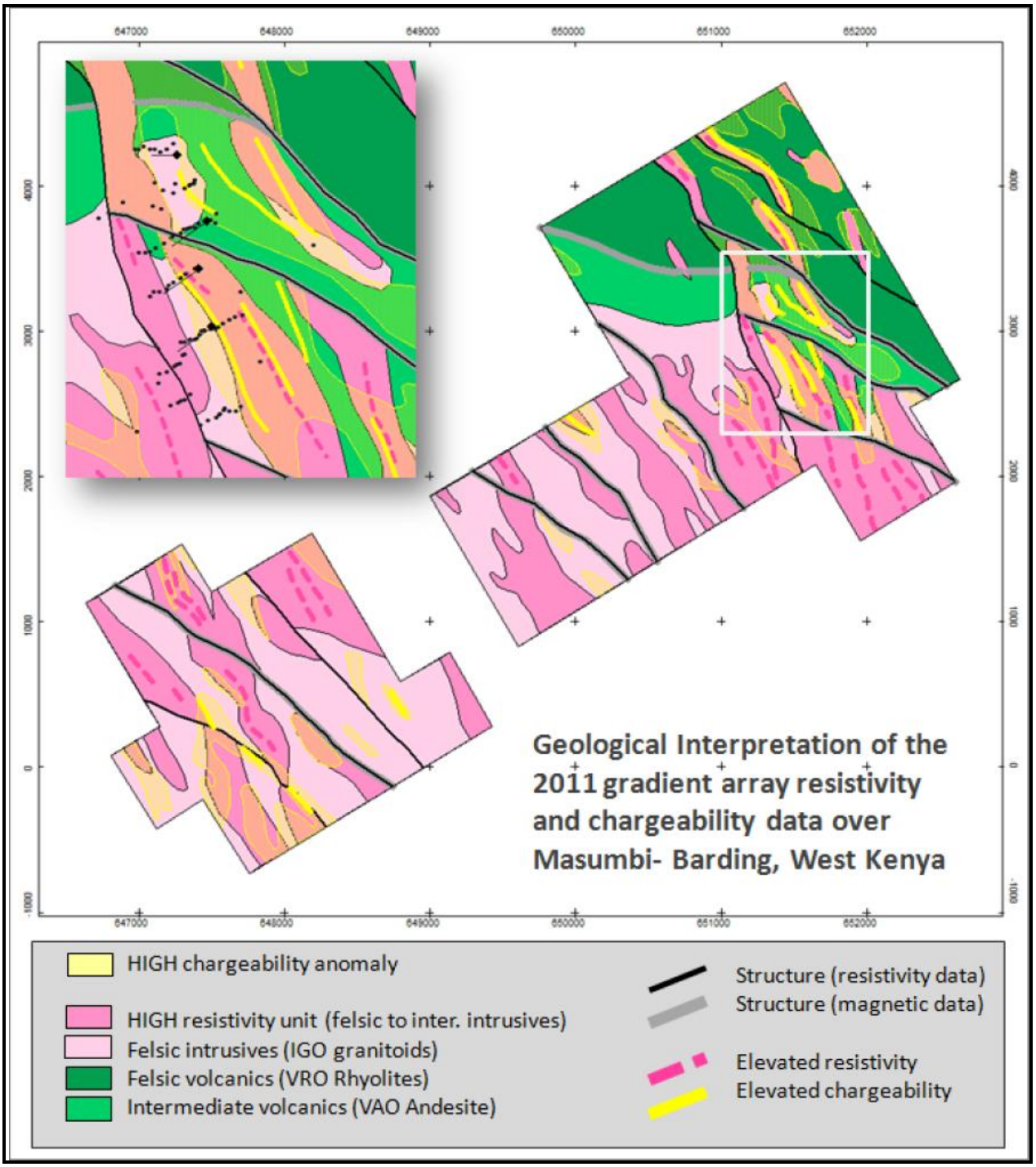

Figure 4. Geological interpretation of the gradient array resistivity and chargeability data over Masumbi Prospect (in white block). Adapted from Buckingham (2012).

2.3.4 RC and Diamond drilling

RC and diamond drilling programmes conducted at the Masumbi Prospect focused on an area measuring approximately 1 km x 0.3 km. The RC drilling programme achieved nine drill-holes totalling 833 m; seven of the nine drill-holes intersected zones of gold mineralisation. The diamond drilling programme achieved five drill-holes totalling 1,009.37 m; all the five diamond drill-holes intersected zones of gold mineralisation as well as zones of copper mineralisation. Table 2 and Table 3 summarise the RC and the diamond drilling programmes respectively.

Table 2. Summary of the Masumbi RC drilling programme

Drill-hole ID	Drilled metres	No. of samples	Gold mineralisation intersected
ASRC038	96	112	Yes
ASRC039	91	107	Yes
ASRC040	120	133	Yes
ASRC041	160	187	Yes
ASRC042	31	28	No
ASRC043	152	176	Yes
ASRC044	40	46	Yes
ASRC045	63	72	No
ASRC046	80	91	Yes
Total	**833**	**952**	

Table 3. Summary of the Masumbi Diamond drilling programme

Drill-hole ID	Drilled metres	No. of samples	Gold mineralisation intersected
ANMDD001	197.96	250	Yes
ANMDD002	200.82	214	Yes
ANMDD003	200.91	220	Yes
ANMDD004	158.64	164	Yes
ANMDD005	251.04	227	Yes
Total	**1,009.37**	**1,075**	

2.3.5 Gold mineralisation

In order to develop an understanding of the mineralisation extent and grade continuity at the Masumbi Prospect, all data available within the prospect were reviewed by Optiro Pty Ltd. These data include collar, survey, assay and geological logging data. The database contained 102 individual drill-holes for 2,634 gold assays. Drill-hole data were imported into Datamine software to allow 3D visualisation and statistical analysis to be performed (Gray and Jones, 2011).

According to Gray and Jones (2011), assessment and definition of potential mineralisation involved four processes: 3D visualisation of recorded geology and assay results, statistical analysis to identify mineralisation populations and directions of continuity of mineralisation (variography), the creation and interpretation of indicator models for high and low grade mineralisation populations to further assist in defining mineralised domains, and the wireframing of mineralisation domains to define potential ore material volumes and grade. Five individual wireframe volumes, referred to as domains, were generated; Domains 10, 20 and 30 define the main high grade mineralisation zone, Domain 40 defines a discrete shallow area of mineralisation to the west of the main zone and Domain 50 captures a poorly defined area of shallow (<30 m) low grade mineralisation to the east of the main zone. Gray and Jones (2011) argue that the main zone of mineralisation appears to be structurally controlled because it cross-cuts several different logged lithologies and is associated with the occurrence of pyrite and quartz veins (Gray and Jones, 2011). Figure 5 illustrates the wireframes generated for the Masumbi Prospect.

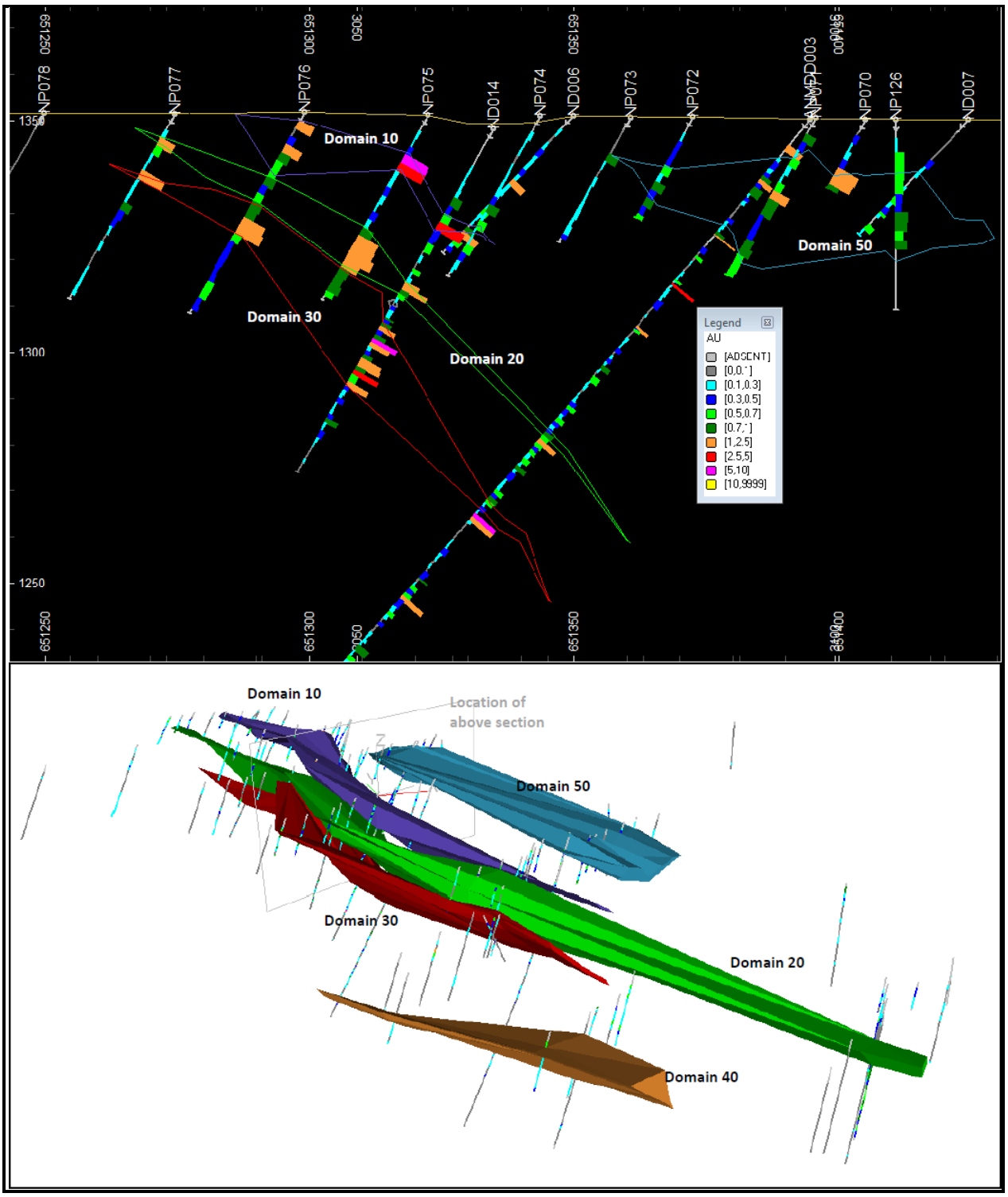

Figure 5. Wireframe domains generated for the Masumbi Prospect (Gray and Jones, 2011)**.**

CHAPTER 3 ARCHAEAN OROGENIC GOLD DEPOSITS

3.1 Introduction

Archaean orogenic gold deposits form a distinctive class of epigenetic precious-metal deposit that has been the source for much of world gold and are also a characteristic feature of granite-greenstone terrains (Gebre-Mariam et al., 1995; Groves et al., 1998; Kerrich et al., 2000). They are generated at mid-crustal (4 – 16 km) levels proximal to terrane boundaries (Kerrich et al., 2000) and are formed during compressional to transpressional deformation processes at convergent plate margins in accretionary and collisional orogens (Groves et al., 1998). These deposits, characterised by a high gold/silver ratio and great vertical extent, were deposited by low-salinity, near neutral, H_2O-CO_2±CH_4 fluids which transported gold as a reduced sulphur complex (Groves et al., 1998). This chapter discusses classification, tectonic setting, geological characteristics, structure, ore fluids, crustal environment and ore genesis of Archaean orogenic deposits.

3.2 Classification

There has been a proliferation of classification schemes and terms defining lode gold deposits. Based on wallrock-alteration mineral assemblages, Mueller and Groves (1991) classified epigenetic, greenstone-hosted gold deposits into two large groups; high-temperature deposits and medium-temperature (mesothermal) deposits. The high-temperature deposits are usually located in metamorphic terranes of medium grade (amphibolites facies), and are characterised by microcline-muscovite-andalusite, garnet-pyroxene-biotite or amphibole-biotite-calcite alteration in the ore zones. The medium-temperature deposits are usually located in metamorphic terranes of low grade (greenschist facies), and are characterised by biotite-ankerite-albite or sericite-ankerite-albite alteration in the ore zones (Mueller and Groves, 1991).

Another form of classification of gold deposits is based on crustal setting, from deep hypothermal to near-surface epithermal (Poulsen, 1996). The term mesothermal or mesozonal has been used in view of their predominance in mid-crustal, greenschist environments. However, according to Kerrich et al. (2000), the deposits are now known to have formed over a range of crustal depths from greater than 25 km to the near surface environment therefore those terms are

not appropriate. Groves et al (1998) proposed that mesothermal gold deposits should be termed orogenic, due to their unique temporal and spatial association with orogeny.

3.3 Tectonic setting

Orogenic gold shows a spatial association with collisional orogens irrespective of whether they are hosted in Archaean or Proterozoic greenstone belts or Proterozoic and Phanerozoic sedimentary rock sequences (Kerrich and Cassidy, 1994; Groves et al., 1998; Goldfarb et al., 2001). The concept of a general spatial association between the gold deposits and subduction-related thermal processes in accretionary orogens was popularised in the mid-1980s. Groves et al. (1998) argue that collisional (or internal) and accretionary (or peripheral) orogens may represent end-members of a continuous process. Any continent-continent collision will be preceded by closure of an ocean basin, and therefore is nothing more than a final stage of a peripheral orogen (Groves et al., 1998).

Groves et al. (2005) summarised the tectonic setting of various gold deposit types into a schematic diagram shown in Figure 6 (Groves et al., 2005). Orogenic gold deposits develop in the fore-arc region of a convergent continental margin over a wide range of crustal depths and may also develop in deformed back-arc sedimentary sequences of the craton margin (Goldfarb et al., 2005).

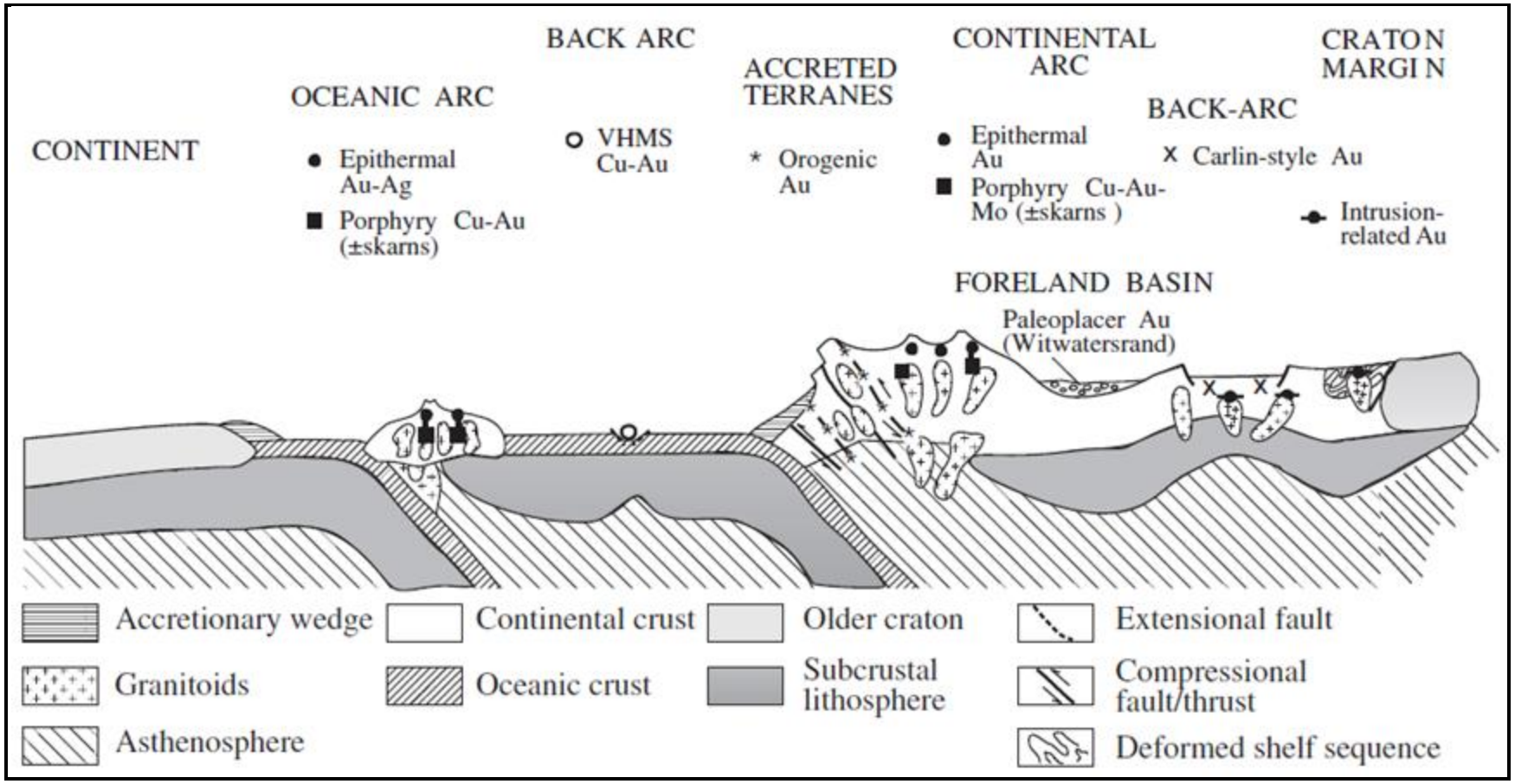

Figure 6. Schematic diagram showing the tectonic setting of various gold deposit types. Modified after Groves et al. (2005).

3.4 Geological characteristics

3.4.1 Geology of host terranes

The arguably single most common characteristic of orogenic gold deposits is their consistent association with deformed metamorphic terranes of all ages (Groves et al., 1998). Although some significant deposits occur in higher metamorphic grade Archaean terranes (McCuaig et al., 1993) or in lower metamorphic grade domains, there is a strong association of gold and greenschist facies rocks (Groves et al., 1998). Pre-metamorphic protoliths for the auriferous Archaean greenstone belts are essentially volcano-plutonic terranes of oceanic back-arc basalt and felsic to mafic arc rocks. Younger ores that are important in some Archaean terranes such as Slave Province in Canada are hosted by clastic marine sedimentary rock-dominant terranes that were metamorphosed to greywacke, argillite, schist and phyllite (Groves et al., 1998).

3.4.2 Structure

Groves et al. (1998) argue that there is a strong structural control of mineralisation at different scales. Most productive gold provinces in metamorphic belts are linked to first-order, ore-controlling regional faults that are typically several hundred kilometres long and a few hundred metres wide. However, although spatially and temporally associated with structures of regional extent, orogenic gold deposits are rarely located within these first-order structures (Kerrich et al., 2000); instead, gold deposits are normally sited in second- or higher-order splays of the regional structures (Groves et al., 1998; Goldfarb et al., 2005).

Colvine et al. (1984) and Weinberg et al. (2004) postulate that areas of jogs, changes in strike, or bifurcations of the first-order systems are favourable sites for fluid focusing into lower order faults (Colvine, 1984; Weinberg et al., 2004). Regional fault intersections, areas of regional uplift or anticlines, and zones of competency contrast such as along granitoid margins are also favourable areas with low or minimum stress (Goldfarb et al., 2005). Mineralised structures have small syn- and post-mineralisation displacements, but the gold deposits commonly have extensive down-plunge continuity ranging from hundreds of metres to kilometres (Groves et al., 1998). Similarly, another team of collaborators also noted that the structures have high-angle oblique displacement, usually with reverse slip, but with some examples in transcurrent fault regimes (Kerrich et al., 2000). Orogenic gold deposits are commonly restricted to the brittle-

ductile transition, with syn-kinematic gold precipitation (Groves et al., 1998; Kerrich et al., 2000; Goldfarb et al., 2005).

3.4.3 Deposit mineralogy

Orogenic gold deposits are characterised by abundant quartz ± carbonate veins and low sulphide volume (Goldfarb et al., 2001). Typically, the vein systems comprise ≤ 3-5% sulphide minerals (mostly Fe-sulphides) and ≤ 5-15% carbonate minerals (Groves et al., 1998). Common gangue phases in veins in greenschist-facies rocks are albite, white mica or fuchsite, chlorite, scheelite and tourmaline (Groves et al., 1998). Although zoning of metal content occurs at the scale of an entire mining district, vein systems within a given deposit can be continuous along a vertical extent of more than 2 km with little change in mineralogy or gold grade (Groves et al., 1998; Kerrich et al., 2000). Gold/silver ratios range from 5/1 to 10/1, with ore in places being in the veins and elsewhere in sulphidised wallrocks (Groves et al., 1998; Goldfarb et al., 2005).

Arsenopyrite is the most common sulphide mineral in deposits that are hosted by metasedimentary rocks, whereas pyrite or pyrrhotite is dominant in metamorphosed igneous rocks. Auriferous veins exhibit variable enrichments in As, B, Bi, Hg, Sb, Te and W; Cu, Pb and Zn concentrations are generally only slightly elevated above regional backgrounds (Groves et al., 1998; Kerrich et al., 2000).

3.4.4 Hydrothermal alteration

Hydrothermal alteration assemblages in wallrocks that host orogenic gold deposits reflect the interaction of an H_2O-CO_2-H_2S (±CH_4 and N_2) fluid with different rock types at various temperatures (Ridley and Diamond, 2000). Strong lateral zonation of alteration phases from proximal to distal assemblages on scales of metres characterise the orogenic gold deposits. Within the alteration zones, mineralogical assemblages generally vary with wallrock type and crustal level (Groves et al., 1998). Wallrock alteration in greenschist facies involves the addition of significant amounts of CO_2, S, K, H_2O, SiO_2 ± Na and large-ion lithophile elements (Groves et al., 1998). According to Kerrich et al. (2000), the alteration mineral paragenesis in greenschist facies domains is dominated by quartz, carbonate, mica, (± albite), chlorite, and pyrite (± scheelite and tourmaline).

Alteration is a highly visible and important characteristic of orogenic gold deposits. Carbonatisation is the most prominent and most common alteration assemblage. Sulphidisation, silicification, oxidation and alkali-metasomatism are other important alteration types. Groves et al (1998) argue that in most instances, carbonates include ankerite, dolomite or calcite; sulphides include pyrite, pyrrhotite or arsenopyrite; alkali metasomatism involves sericitisation or, less commonly, formation of fuchsite, biotite or K-feldspar and albitisation and mafic minerals are highly chloritised.

3.4.5 Ore genesis

Orogenic gold ores were deposited from dilute aqueous carbonic fluids, with uniformly low-salinity (typically <6wt% NaCl equivalent), near-neutral pH, and composed of H_2O-CO_2±CH_4 (Groves et al., 1998; Kerrich et al., 2000; Goldfarb et al., 2005). These fluids transported gold as a reduced sulphur complex and are notable by their consistently elevated CO_2 concentrations of ≤ 5 mol %. Typical $\delta^{18}O$ values for hydrothermal fluids are approximately 5-8 per ml in the Archaean greenstone belts and approximately 2 per ml higher in the Phanerozoic gold lodes (Groves et al., 1998). Numerous models have been proposed for the generation of the gold-transporting hydrothermal fluid of orogenic gold deposits. The main models include the following:

i. *Devolatilisation of felsic magmas*. According to Burrows et al. (1986), this model is based on field relations, stable isotope compositions of carbon, and the similarity of the element suite of the orogenic gold deposits to some granite-related ore deposit types. With gold having been concentrated in the magmatic fluid as a consequence of being an incompatible element during crystallisation, the fluid is considered to be exsolved from crystallising granitic magmas (second boiling) (Ridley and Diamond, 2000).
ii. *Fluid release during crystallisation of gold-rich shoshonitic lamprophyre magmas or their interaction with crustal rocks*. The spatial and temporal association of calc-alkalic lamprophyres with gold deposits has been interpreted in terms of intrinsically gold-rich alkaline magmas derived from the core-mantle boundary (Rock et al., 1989). Contrary to this proposition by Rock et al. (1989), Kerrich and Wyman (1994) demonstrated that fresh shoshonitic dykes are characterised by normal background gold contents. Therefore, these later collaborators concluded that lamprophyres are not intrinsically enriched either in gold or

elements affiliated with orogenic gold deposits, and accordingly do not constitute a special source rock (Kerrich and Wyman, 1994).

iii. *A mantle fluid that is initially CO_2 rich but is modified as it induces granulite facies metamorphism in the lower crust.* This model is based on the synchronicity of mineralisation and lower crustal granulite facies metamorphism and of complementary geochemical depletions in granulites and enrichments in the ore deposits (Krogh, 1993).

iv. *Meteoric waters that have circulated to depths in the crust*. This model, based on hydrogen isotope analyses of fluid inclusions, was criticised after it was demonstrated that the data used do not reflect the ore fluid but instead reflects later fluids that infiltrated the deposits (Ridley and Diamond, 2000).

v. *Devolatilisation during prograde metamorphism*. The metamorphogenic model of ore genesis was first proposed by Boyle (1961) and developed by Kerrich and Fyfe (1981). This model considered fluids to have been released from hydrous and carbonate minerals on their breakdown in prograde metamorphic reactions (Boyle, 1960; Kerrich and Fyfe, 1981). They argue that since shear zones and other structures consist of too small a volume of altered rock to supply the amount of gold in the deposits, then the gold must have been leached either from the dehydrating rocks or from nearby rocks along the flow path, before the fluid was channelized (Kerrich and Fyfe, 1981; Ridley and Diamond, 2000).

According to Ridley and Diamond (2000), the models that have stood up to scrutiny and testing are those models invoking metamorphic devolatilisation and devolatilisation of felsic magmas. In both these models, the ore fluid is assumed to have stayed intact from its source to the deposit, without being diluted or significantly modified by mixing with fluids from other sources (Ridley and Diamond, 2000).

The scale and form of orogenic hydrothermal systems involving a single fluid are illustrated in Figure 7. Single-pass flow is focused from a large volume of source rock from which gold is leached and may travel over several kilometres along channelways to the deposit. At the deposit, the fluid is constrained to relatively narrow channelways,with formation of alteration halos as a result of fluid dispersion and diffusion into adject wall rock (Ridley and Diamond, 2000).

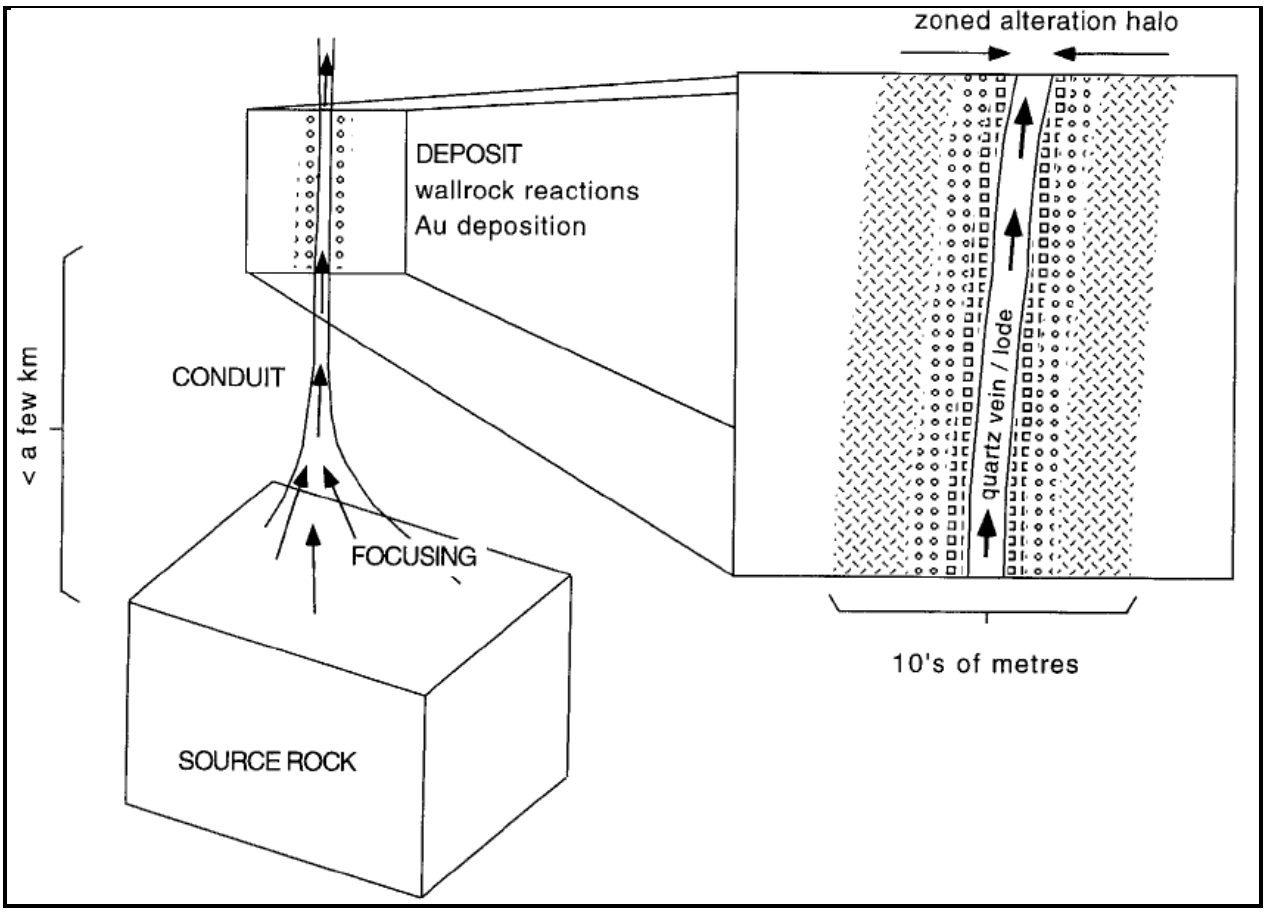

Figure 7. Schematic architecture of orogenic hydrothermal systems (Ridley and Diamond, 2000)**.**

3.5 Crustal environment

Most orogenic gold deposits are located in ductile to brittle structures. They have proximal alteration assemblages of Fe-sulphide –carbonate – sericite ± albite and were deposited at 300 ± 50°C and 1 – 3 kbar. These deposits are consistently syn- to post-peak-metamorphic and were emplaced at temperatures commonly within 100°C of peak metamorphic temperatures experienced by the surrounding host rocks (Groves et al., 1998). However, geobarometry studies by Hagemann and Brown (1996) in mainly Archaean greenstone belts have extended the temperature and pressure ranges, and therefore extended the inferred crustal range of formation of the deposits into higher- and lower-grade metamorphic rocks. The evidence for formation of these gold deposits over temperature and pressure ranges of about 180 - 700°C and < 1 -5 kbar implies vertically extensive hydrothermal systems that contrast sharply with other continental-

margin gold systems that are apparently restricted to the upper 5 km or so of crust. Figure 8 is a schematic representation of crustal environments of orogenic gold deposits in terms of depth of formation.

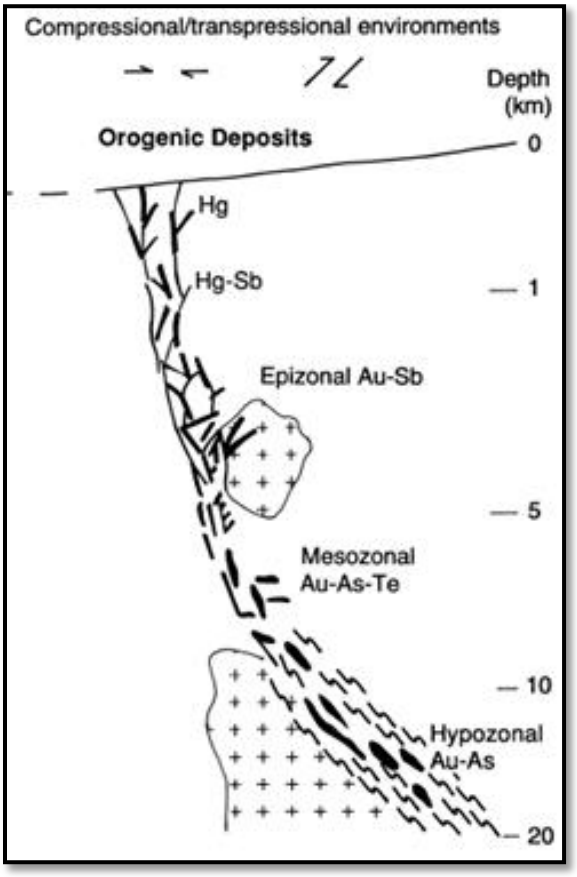

Figure 8. Schematic representation of crustal environments of orogenic gold deposits in terms of depth of formation. Modified after Groves et al. (1998).

CHAPTER 4 TANZANIA CRATON

4.1 Introduction

The basic fabric of Africa consists of several major Archaean cratons and smaller cratonic fragments, stitched together and flanked by younger fold belts (Begg et al., 2009). Tanzania Craton is one of the important tectonic and physiographic terranes in which Archaean rocks in Africa are preserved. The other important tectonic and physiographic terranes are: the Zimbabwe Craton; the Kaapvaal Craton of South Africa; the North Zaire (now Democratic Republic of Congo) Massif which extends into the Central African Republic; the Kasai-Angola Massif of southern Democratic Republic of Congo (formerly Zaire); the Atlantic Rise of Cameroun, Gabon, and Congo extending southwards to the Malanje 'Strip' of northern Angola; the Guinea Rise of Guinea, Sierra Leone, and Liberia; and the Reguibat Rise of Mauritania, Morocco, and northwest Algeria (Foster and Piper, 1993).

This section discusses the tectonic setting and stratigraphic framework of the Tanzania Craton as well as geological characteristics and geochronology of the granite-greenstone terranes within the craton.

4.2 Tectonic setting

Two Archaean cratons cover a significant portion of the Central and East African massif: the Tanzania Craton and the NE-Zaire Craton of the Democratic Republic of Congo (Chamberlain, 2003). These cratons were earlier considered to be two separate shield areas (Clifford, 1970) but later studies recorded similarities between them. According to Kröner (1977) and Cahen et al. (1984), there are similarities between lithostratigraphy and ages of greenstone belts within them. These cratons were regarded to be linked by the Uganda Basement Gneisses before the onset of Proterozoic cratonisation (Kröner, 1977; Cahen et al., 1984). A geological map illustrating the location and geometry of the Tanzania and NE-Zaire Cratons is shown in Figure 9.

The Tanzania Craton occupies the Central Plateau of Tanzania and extends northward into western Kenya and south-eastern Uganda (Ichang'i and MacLean, 1991; Chamberlain, 2003). During the Proterozoic, the margins of the Tanzania Craton were caught up in successive orogenic belts that now form the structural framework of East Africa (Cahen et al., 1984; Chamberlain, 2003).

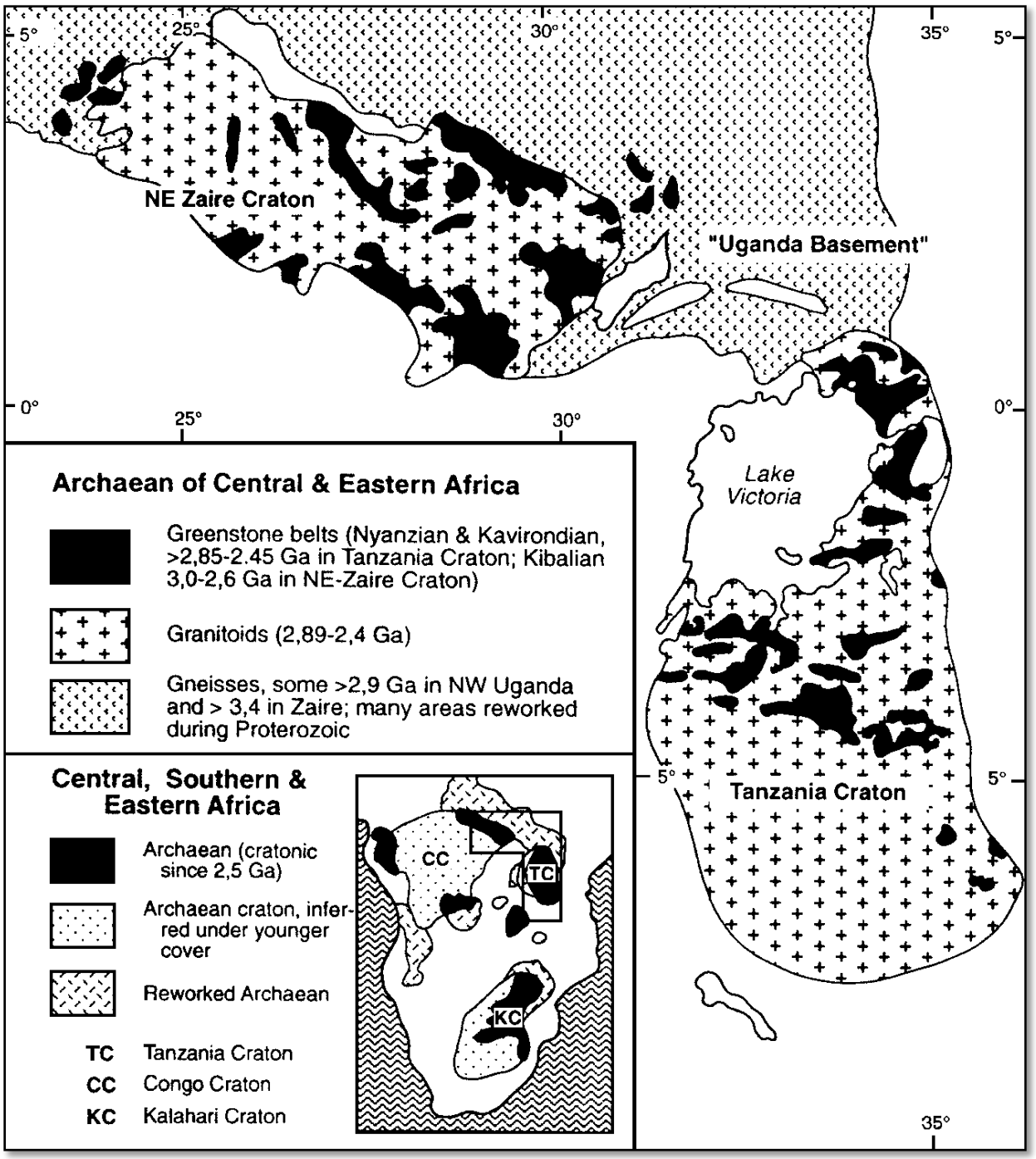

Figure 9. Geological map showing the Tanzania and NE-Zaire Cratons. The insert map illustrates the regional setting of these cratons within the Archaean framework of central and southern Africa. (Borg and Shackleton, 1997)**.**

The craton is bounded to the east by the Late Proterozoic (900-500 Ma) collisional Mozambique Mobile Belt and to the southeast by the Lower to Middle Proterozoic Usagaran Belt (2.0-1.8 Ga). To the southwest, it is bounded by the Early to Middle Proterozoic Ubendian Belt (2.0 Ga) and to the northwest by the Kibaran Mobile Belt (Late Proterozoic Karagwe-Ankolean Belt in Uganda; 1310 Ma). The contact with the Ruwenzorian Mobile Belt of Uganda (2.0 Ga) defines the northern margin of the Tanzania Craton (Ichang'i and MacLean, 1991; Ngecu and Gaciri, 1995; Borg and Shackleton, 1997; Chamberlain, 2003). As a consequence of these Proterozoic orogenies, the Archaean sequences are presumed to exist as reactivated basement slices in some of these belts and are only preserved in relatively pristine form within the Tanzania Craton itself (Chamberlain, 2003). Figure 10 illustrates the Tanzanian Craton and the surrounding mobile belts.

Figure 10. The Tanzanian Craton and the surrounding mobile belts. T - Tanzanian, Z = Zimbabwe, K = Kaapvaal Cratons (Ichang'i and MacLean, 1991)**.**

In western Kenya, the craton is divided by the Winam (Kavirondo) Rift valley into a northern and a southern terrane (Shackleton, 1950; Ichang'i and MacLean, 1991; Ngecu and Gaciri, 1995) as shown in Figure 11. The Winam Rift is an arm of the East African Rift System (Ichang'i and MacLean, 1991). Continuity of the craton across the rift is demonstrated by greenstones and granites that are exposed in the southwestern end of the rift in the vicinity of the Rangwa carbonatite complex (MacCall, 1958), and also in the northeast (Saggerson, 1952).

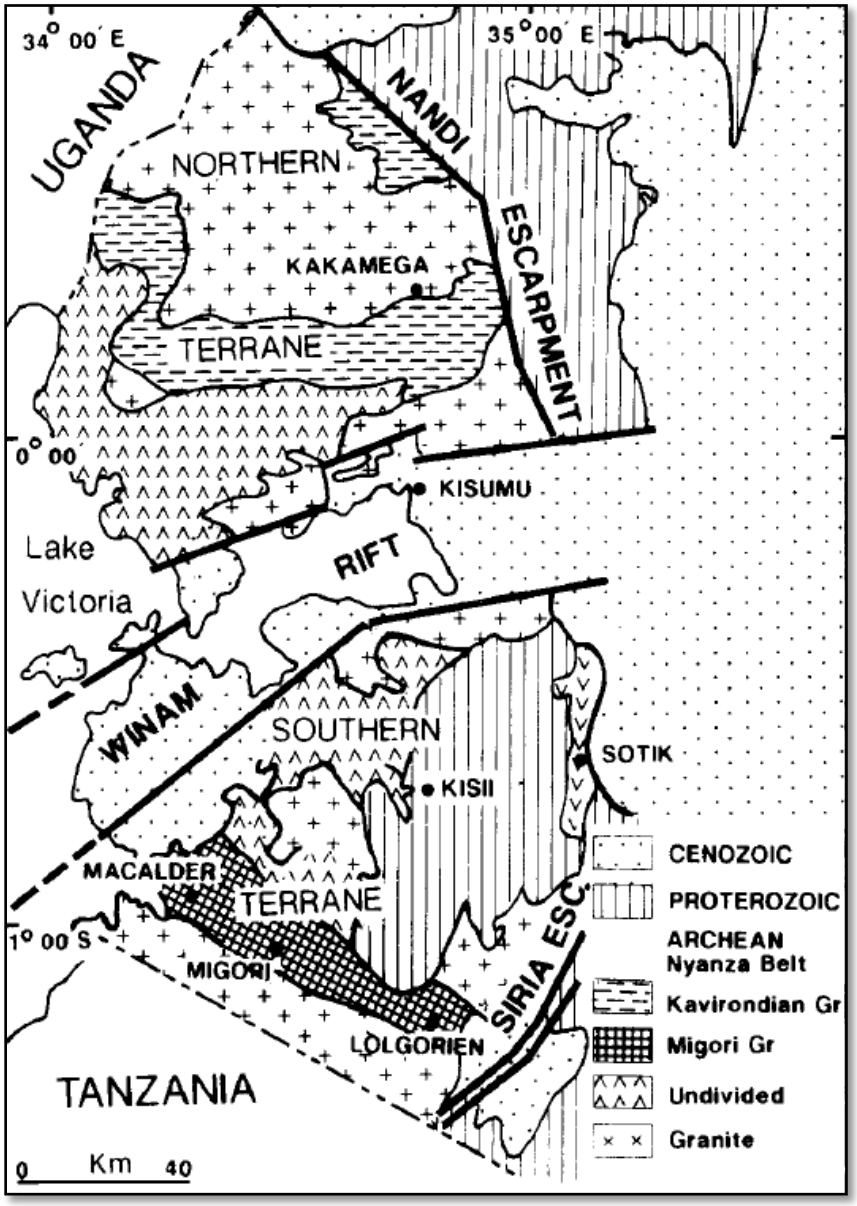

Figure 11. The Tanzanian Craton in western Kenya, divided into a northern and southern terrane by the Winam (Kavirondo) Rift (Ichang'i and MacLean, 1991)**.**

4.3 Lithostratigraphy

The Tanzania Craton, underlying an area of *ca*. 500,000 km^2, consists of a series volcano-sedimentary greenstone sequences deposited from *ca*. 2.8 Ga to at least 2.66 Ga that were affected by successive phases of deformation and pulses of granitoid emplacement dated from 2.73 to 2.58 Ga (Pinna et al., 2000). The granite-greenstone sequences exhibit many features that are characteristic of Archaean cratons. The features include the existence of numerous gold deposits, granitoids within and surrounding the greenstones, a predominance of greenschist facies regional metamorphism, and regional deformation (Chamberlain, 2003).

Quennel *et al*. (1956) classified the basement rocks of the Tanzania Craton *sensu stricto* as the 'Dodoman System' and placed all the Archaean supracrustal rocks within the 'Nyanzian Supergroup' (Quennel et al., 1956; Chamberlain, 2003). However, Clifford (1970) subdivided the craton into three systems: the 'Dodoman System', comprising granitoid and migmatitic rocks (the Tanzanian Craton *sensu stricto*) and high-grade metamorphic supracrustal rocks of the 'Dodoman Series'; the 'Nyanzian System' (dominantly greenstone belt assemblage), composed of mafic, intermediate and felsic volcanic, metamorphosed greywackes, pelites and banded ironstones; and the unconformably overlying 'Kavirondian System' (dominantly greenstone belt molasse), consisting of conglomerates, arenaceous and argillaceous sediments and volcanic rocks (Clifford, 1970; Gabert, 1990). Consequently, Clifford (1970) subdivided the 'Nyanzian Supergroup' of Quennel et al. (1956) into the 'Nyanzian System' and the 'Kavirondian System'.

Ichang'i and MacLean (1991) together with Ngecu and Gaciri (1995) argue that the chronostratigraphic terms 'System' and 'Series' as used by Stockley (1943) and later researchers to categorise various greenstone volcano-sedimentary sequences imply wide ranging time stratigraphic correlations which may not be valid. Instead, they prefer the term 'Group' because the former terms were not applied in accordance with the conventional lithostratigraphical classification of the International Subcommission on Stratigraphic Classification (ISSC) (Hedberg, 1976), the North American Commission on Stratigraphic Nomenclature (1983) and Whittaker et al. (1991) (Stockley, 1943; Ichang'i and MacLean, 1991; Whittaker et al., 1991; Ngecu and Gaciri, 1995). Similarly, in this thesis the term 'Group' has been adopted over 'System'.

4.3.1 The Dodoman Group

The southern half of the craton, in the central region of Tanzania, is composed of granitic rocks, felsic gneisses and migmatites with narrow enclaves of amphibolite facies greenstones of the Dodoman Group (Quennel et al., 1956; Ichang'i and MacLean, 1991). Equivalents of the rocks of the Dodoman Group have been identified in the Kenya-Tanzania border region (Cahen and Snelling, 1966; Chamberlain, 2003).

Typical rocks of the Dodoman Group occur near Dodoma where there is a series of elongate east-southeast trending outcrops of a variety of high-grade metamorphic rocks that include banded and ferruginous quartzites, biotite-hornblende gneisses, and ironstones (Chamberlain, 2003). Also identified in the area are granulite-facies assemblages and pyroxene gneisses together with lower grade talc-chlorite, sericite, and corundum-bearing schists. These rocks are intruded by post-migmatitic aplites, pegmatites, olivine-monzonites and monzodiorites (Quennel et al., 1956).

The tectono-stratigraphic relationship between the Dodoman and the Nyanzian Groups, as well as the temporal relations between the different lithostratigraphic units within each domain, is not clear (Manya and Maboko, 2003). According to Harpum (1970), the Dodoman Group represents highly metamorphosed equivalents of the Nyanzian, and that the metamorphism of the Dodoman took place before deposition of the Nyanzian (Harpum, 1970; Chamberlain, 2003; Manya and Maboko, 2003). Therefore, the Dodoman is considered by more traditional views as constituting the basement to the Nyanzian.

However, later authors (Kröner, 1977, Bell & Dodson, 1981 and Cahen *et al*., 1984) interpreted the Dodoman gneisses and the Uganda Basement Gneisses to be a lower crustal equivalent of the Nyanzian (Kröner, 1977; Bell and Dodson, 1981; Cahen et al., 1984). More recently, Borg and Krogh (1999) demonstrated using U-Pb geochronology that the high-grade metamorphic rocks do not constitute the basement to the Nyanzian (Borg and Krogh, 1999; Manya and Maboko, 2003).

4.3.2 The Nyanzian Group

Borg and Shackleton (1997) recognised eight distinct belts of Nyanzian stratigraphy; they extend through southeast Uganda, southwest Kenya and northwest Tanzania as illustrated in

Figure 12. These belts are collectively termed the ‘Lake Victoria Goldfields’ (Chamberlain, 2003), of which the Busia-Kakamega Greenstone Belt is one of them. The Ndori Greenstone Belt forms part of the larger Busia-Kakamega Greenstone Belt.

Typical greenstone belt assemblages of mafic and felsic volcanics, banded iron formation (BIF) and associated low-grade metasediments characterise these belts of Nyanzian stratigraphy. These greenstone belts occur as irregularly shaped lenses that are surrounded by granitoids and characterised by intense folding representing steeply dipping synclinal remnants within the Tanzania Craton (Gabert, 1990; Chamberlain, 2003). According to Ichang’i and MacLean (1991), abundant high-K dacites and rhyolites in the northerly greenstone belts such as the Migori Greenstone Belt in Kenya indicate the presence of underlying continental crust. In contrast, tholeiitic basalts dominate in the southerly greenstone belts and granite-derived sediments are absent (Ichang'i and MacLean, 1991; Chamberlain, 2003).

Based on their work on the Migori Greenstone Belt of southwest Kenya, Ichang’i & MacLean (1991) established that the volcanics are bimodal mafic tholeiitic basalt and dolerite, and felsic calc-alkaline dacite-rhyolite and high-K dacite. Felsic units comprise three quarters of the volcanic stratigraphy. Basalts, calc-alkaline dacites and rhyolites were deposited in a submarine environment while the voluminous high-K dacites were erupted subaerially. Greenstone belts in the Lake Victoria Goldfields are dominated by calc-alkaline felsic volcanics in contrast to the komatiites-tholeiitic basalt volcanism in the Kaapvaal Craton of South Africa, and a mixture of the two types in the Zimbabwe Craton (Ichang'i and MacLean, 1991).

4.3.3 The Kavirondian Group

The Kavirondian Group represents the molasse facies of the greenstone belt (Harpum, 1970; Gabert, 1990). It unconformably overlies the Nyanzian Group (Gabert, 1990; Kuehn et al., 1990) and is folded on E-W trending axes (Gabert, 1990). The Kavirondian Group comprises conglomerates, quartzites, arkosic and feldspathic grits, sandstones and siltstones, shales and phyllites, and tuffs (Gabert, 1990). In western Kenya, Ngecu and Gaciri (1995) classified the Kavirondian Group into three formations: Shivakala Formation, Igukhu Formation and Mudaa Formation.

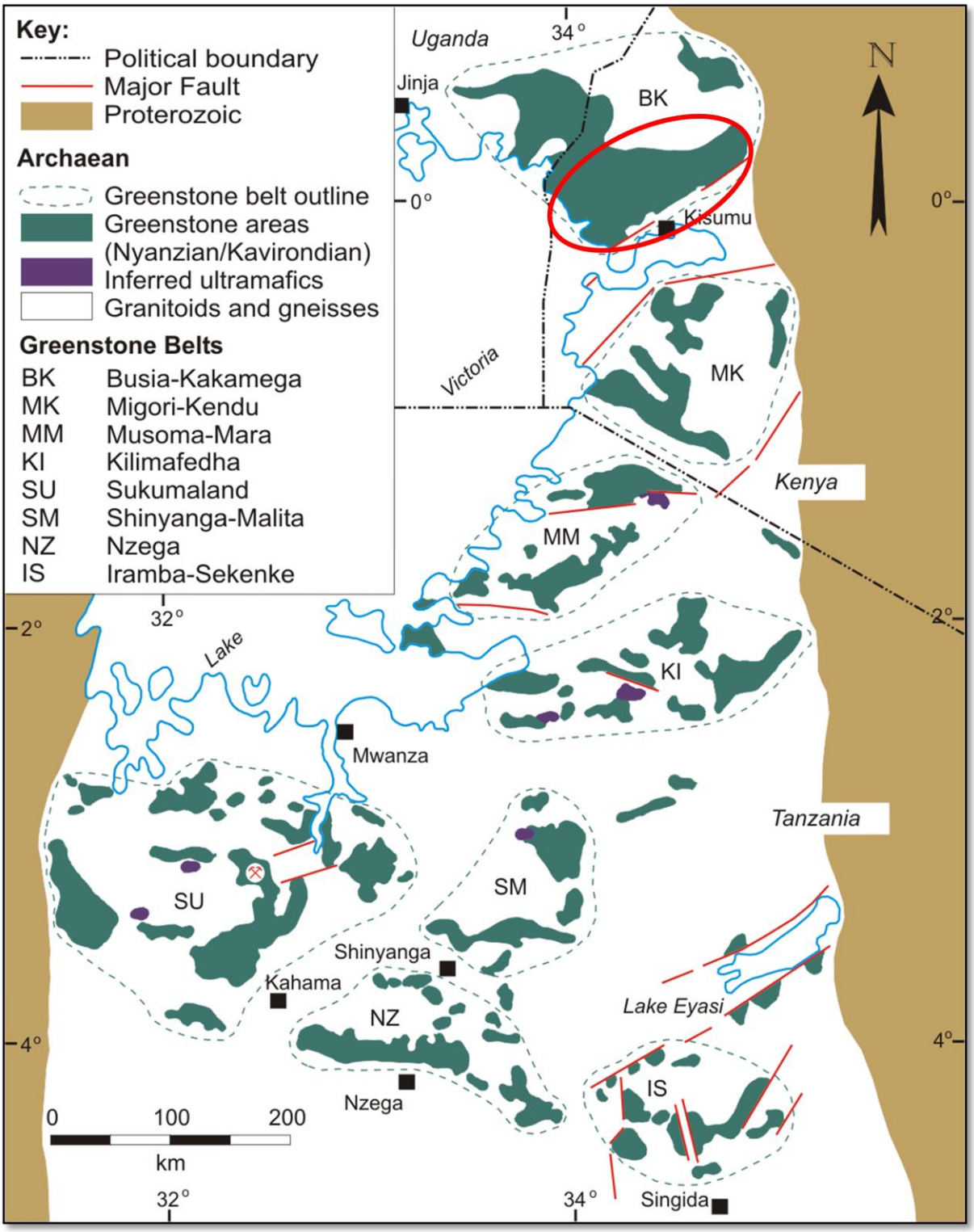

Figure 12. Distribution of greenstone belts within the Tanzania Craton of N and NW-Tanzania, W-Kenya and SE-Uganda (Chamberlain, 2003)**. The location of the Ndori Greenstone Belt is marked by the red ellipse.**

4.4 Structure

In the granite-greenstone terrane of the Tanzania Craton, structure is presumed the most important factor controlling the regional distribution, characteristics and geometry of orogenic gold deposits. The principal controlling mechanism have been permeability, provided by areas of low mean stress, fractures, shear zones, faults, folds and dykes (Borg, 1994).

Greenstone belts in the Tanzania Craton exhibit arcuate folding, most of which strike east-west. At least two principal phases of folding have affected rocks of these greenstone belts. A poorly documented first phase of deformation (D_1) culminated in thrusting and broad sinuous folding, causing repetition of Nyanzian strata. D_1 produced prominent open folds (wavelengths of 3-4 km) with approximately horizontal axes (Borg et al., 1990; Borg, 1994; Chamberlain, 2003).

A second phase of deformation (D_2) resulted in the development of large open and concentric folds with vertical to subvertical fold axes. Abundant flexures, S- and Z-structures are further manifestations of D_2. Interference patterns between parasitic folds of D_1 and D_2, together with a marked competency contrast between different units (BIF versus tuff) produced structurally complex high strain domains that contrast with terrains of relatively moderately deformed rocks (Borg et al., 1990; Chamberlain, 2003).

Later deformation produced numerous shear zones striking approximately WSW-ENE. The most recent deformation manifests in block faulting. Many of these fault structures are related to rifting of the East African subcontinent in Miocene to Recent times and faults can also be observed as vertical offsets in subrecent laterite covers (Borg et al., 1990).

4.5 Magmatism

Bell and Dodson (1981) delineated two events of granitoid magmatism from the Tanzania Craton: one at 2740 Ma and another at 2540 Ma, the younger being more widespread and accounting for extensive granitoid magmatism throughout large areas of Tanzania, western Kenya and southeastern Uganda. In western Kenya, the Mumias and the Maragoli Granites intrude both the Nyanzian and the Kavirondian Groups (Ichang'i and MacLean, 1991; Ngecu and

Gaciri, 1995; Opiyo-Akech et al., 1999). According to Gabert (1990), these granites are genetically related to gold mineralisation.

4.6 Metamorphism

Similar to other Archaean cratons, the Tanzania Craton can be subdivided into two main metamorphic terranes: the deformed, high grade metamorphic terrane of central Tanzania and the low grade granite-greenstone terrane of northern Tanzania, south western Kenya and south eastern Uganda (Clifford, 1970; Manya and Maboko, 2003; Manya et al., 2006). In Tanzania, the high grade metamorphic terrane is locally referred to as the Dodoman Belt where rocks have been metamorphosed to granulite facies. The low grade granite-greenstone terrane represents the Nyanzian and the Kavirondian Groups which occur in the area south and east of Lake Victoria. Rocks of the Nyanzian and the Kavirondian Groups have been metamorphosed to greenschist facies and locally to the amphibolite facies in the thermal aureoles of large granitic intrusions (Manya et al., 2006; Boniface and Mruma, 2012). Observations from throughout the world's preserved Archaean greenstone belts indicate a strong association of gold and greenschist facies rocks (Groves et al., 1998).

4.7 Crustal evolution and gold mineralisation

Dating of rocks of the Dodoman Group and various syn- and post-orogenic granitoids provided constraints on the timing of key geological events in the evolution of the Tanzania Craton (Bell and Dodson, 1981; Borg and Krogh, 1999). Distinct tectono-magmatic events are apparent and Chamberlain (2003) summarised these events along with other notable tectonic and metamorphic events as shown in Table 4 and schematically as illustrated in Figure 13.

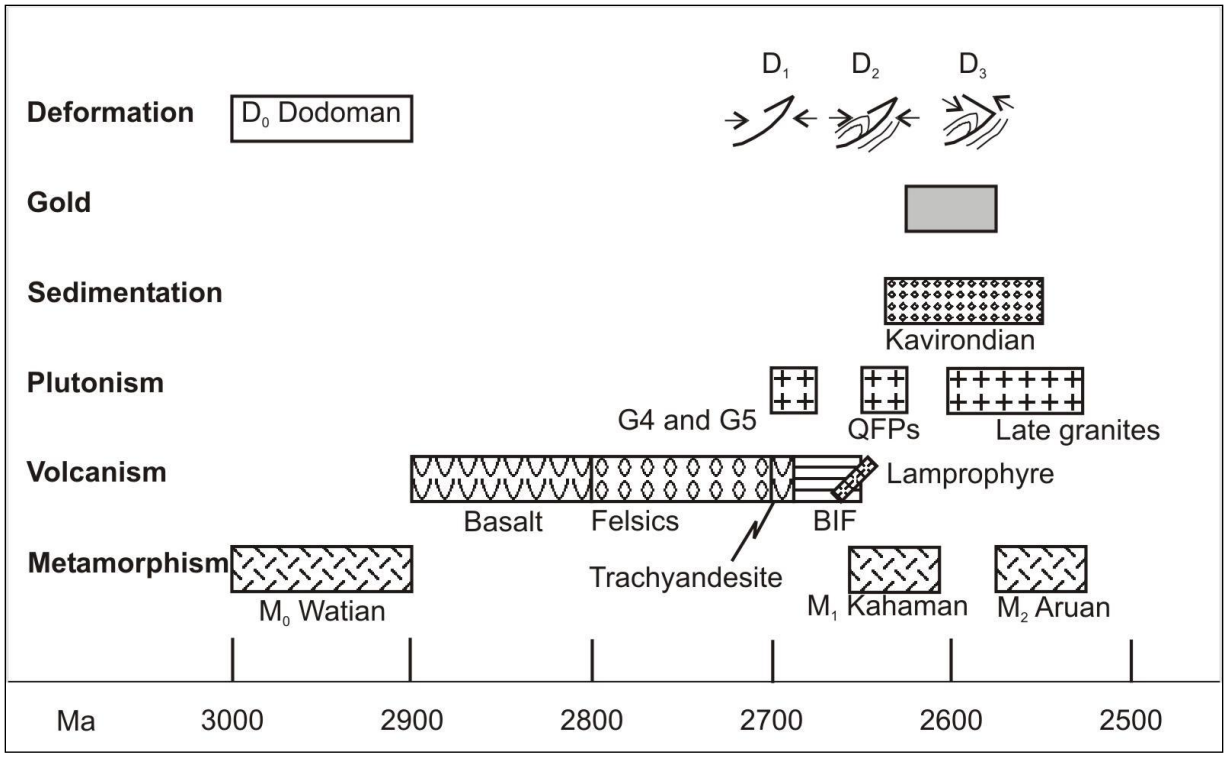

Figure 13. Schematic diagram illustrating the key accretion, intrusive, metamorphic and deformation events in the Tanzania Craton (Chamberlain, 2003)**.**

Table 4. Summary of geochronological stratigraphic and tectonothermal events of the Tanzania Craton (TC). ? Unreliable data, * due to excess Ar, considered unrealistically old; SGB, Sukumaland Greenstone Belt; BK, Busia-Kakamega Greenstone Belt; UBG, Uganda Basement Gneisses (Chamberlain, 2003)

Tectonothermal event and system	Rock type, Relationship	Relative age	Reference	Method	Age (Ma)
Syn- and post-Nyanzian/Kavirondian intrusions: 2550-2300 Ma					
Maragori Granite, N.Kenya	Post-Kavironian granite	Aruan	Cahen & Snelling, 1966	K/Ar	2495-2577
Mumias Granite, N. Kenya	Post-Kavirondian	Aruan	Dodson *et al*., 1975	Rb/Sr	2504±48
Pre-Kavirondian granite, Migori	Pre-Kavirondian granite	Aruan	Bell & Dodson, 1981	Rb/Sr	2740±120
Post-Nyanzian granite	Granite (Cahen *et al*., 1984: iii)	Aruan	Dodson *et al*., 1975	Rb/Sr	2472±62
Post-Nyanzian granite	Granite (Cahen *et al*., 1984: ii)	Aruan	Rammlmair *et al*., 1990	Rb/Sr	2530±30
Post-Nyanzian granite	Granite (Cahen *et al*., 1984: ii)	Aruan	Rammlmair *et al*., 1990	Rb/Sr	2540±70
Post-Nyanzian & Kavirondian granite	Granite (Cahen *et al*., 1984: i)	Aruan	Old & Rex, 1971	Rb/Sr	2555±73
Post-Nyanzian granite	Granite (Cahen *et al*., 1984: i)	Aruan	Cahen & Snelling, 1966	Rb/Sr	2550
Mineralization constraints: 2674-2644 Ma					
Post-Nyanzian – Kenya	Auriferous veining	Mineralization	Coomer, 1971	Pb-isotope	2674 ?
Post-Nyanzian: SGB, Geita	Lamprophyre dyke	Pre-mineralization	Borg & Shackleton, 1997	U/Pb	2644±3
Nyanzian: SGB, Geita	BIF – mineralized	Pre-mineralization	Walraven *et al*., 1994	Pb-isotope	2721+198-230
Nyanzian construction: 2654-2808 Ma					
Nyanzian: distal from Geita	Barren BIF - isotopically re-set	Kibaran	Walraven *et al*., 1994	Pb-isotope	1788+400-548
Nyanzian: SGB, Geita	BIF - unmineralized	Nyanzian	Walraven *et al*., 1994	Pb-isotope	2696+127-140
Nyanzian: southern SGB	Rhyolite	Nyanzian	Borg & Krogh, 1999	U/Pb	2654±15
Nyanzian: SGB, Geita	Trachyandesite within BIF	Nyanzian	Borg & Shackleton, 1997	U/Pb	2699±9
Nyanzian: BK, Kenya	Rhyodacite, pre-Kavirondian	Nyanzian	Yanagi & Suwa, 1981	Rb/Sr	2710±34
Nyanzian: southern SGB	Rhyolite	Nyanzian	Borg & Krogh, 1999	U/Pb	2780±3
Nyanzian: southern SGB	Rhyolite	Nyanzian	Borg & Krogh, 1999	U/Pb	2808±3
Aruan metamorphism: 2700-2570 Ma					
TC: south, Iringa	Migmatitic gniesses	Aruan	Cahen & Snelling, 1966	Rb/Sr	2600
TC: north, Kahama	Migmatitic gniesses	Aruan	Rammlmair *et al*., 1990	Rb/Sr	2570±50
TC: north, Kahama	Migmatitic gniesses	Aruan	Borg & Shackleton, 1997	U/Pb	2680±3
TC: basement gniess	Amphibolitic gneisses	Aruan	Wendt *et al*., 1972	Rb/Sr	2578±72
TC: pre-Kavirondian granite	Migori Granite	Aruan	Dodson *et al*., 1975	Rb/Sr	2741±222
UBG construction and Watian metamorphism: pre-2900 Ma					
UBG: pre-Nyanzian granite	Masaba Granite	Watian	Old & Rex, 1971	Rb/Sr	2998±182
UBG: basement gneiss	Granulite facies gneisses	Watian	Leggo, 1974	Rb/Sr	2900
TC: UBG dyke	Truncating non-foliated granites	UBG	Ueda *et al*., 1975	K/Ar	3118 ?*
UBG	Gneisses	UBG Model age	Lavreau, 1980		3349

The oldest rocks in East Africa that predate the Dodoman ages are the Uganda Basement Gneisses. These rocks were affected by a succession of Archaean tectono-metamorphic events referred to as the Watian, Aruan and Mirian (Chamberlain, 2003) as illustrated in Figure 14.

Event	Age (Ma)
Mirian gneisses (Kibaran metamorphism)	~950
Intrusive granites in the Tanzania Craton	1780 ± 60
Metamorphism of Proterozoic fold belts (Usagaran–Ubendian and Buganda–Toro systems)	~1900 (2000–1800)
Metamorphism, magmatism (Aruan metamorphism)	2500 ± 60 (2550)
Kavirondian System Nyanzian System	2700–2500
Metamorphism (Watian metamorphism	~2900 (2880)
Tanzania Craton (Dodoman, Nyanzian and Kavirondian systems):	
Dodoman System	> 2500
Uganda Craton (Uganda Basement Complex; Watian, Aruan and Mirian gneisses):	
Watian granulites	> 2900

Figure 14. Tectono-stratigraphic events of the Tanzania Craton, Uganda Craton and surrounding mobile belts (Gabert, 1990)**.**

The granulite facies metamorphism of the Watian gneisses is the earliest recorded event and occurred at ca. 2900 Ma (Leggo, 1974; Cahen et al., 1984; Gabert, 1990). A later metamorphic event, the Aruan, has been dated at ca. 2550 Ma (Leggo, 1974). The Aruan metamorphism coincided with a period of intense and widespread migmatisation and granitoid magmatism at 2600 – 2500 Ma in the Tanzania Craton (Bell and Dodson, 1981). This high-grade metamorphic

event was primarily responsible for the remobilisation of the syngenetic gold mineralisation which was genetically related to volcanic processes and had originally been formed in the greenstone host rocks. This widespread remobilisation might have caused the formation of gold-sulphide bearing quartz veinlets in the greenstone host rocks, as well as the formation of the majority of epigenetic-hydrothermal auriferous quartz veins and reefs (Gabert, 1990).

The high grade metamorphic rocks of the Dodoman Group were possibly formed by an event comparable to the oldest metamorphic event (the Watian event) that affected the Uganda Basement Gneisses (Gabert, 1990). Isotopic data suggest that an early metamorphic event occurred at ca. 2650 Ma to 2700 Ma (Walraven et al., 1994). This age is consistent with a date of 2680 ± 3 Ma obtained by Borg and Shackleton (1997) from the palaeosome of migmatitic basement gneisses that are presumed to be of Dodoman affinity. A younger age of 2570 ± 3 Ma was also obtained from dating the migmatitic gneisses (Rammlmair et al., 1990). This younger date correlates with the Aruan amphibolite facies event in the Uganda Basement Gneisses, which retrogressively overprinted Watian peak metamorphism assemblages (Chamberlain, 2003).

Ages of the Nyanzian stratigraphy range from 2808 ± 3 Ma to 2654 ± 15 Ma. An extrusive trachyandesite is dated at 2699 ± 9 Ma. Metamorphism of the Nyanzian and underlying gneisses is presumed to have commenced around 2680 Ma toward the end of the period of greenstone belt construction. A lamprophyre and related dykes intruded at ca. 2644 Ma, prior to hydrothermal mineralisation. Dating of various syn- and post-tectonic granitoids indicated a minimum age limit of ca. 2500 Ma for the Nyanzian and the Kavirondian Groups. At least two significant tectono-thermal events affected the stratigraphy after the Watian event, and prior to the Mirian: the Kahaman, between ca. 2650 – 2700 Ma; and the Aruan, between ca. 2590 – 2600 Ma. Gold mineralisation is associated with these two events (Gabert, 1990; Chamberlain, 2003).

CHAPTER 5 NDORI GREENSTONE BELT

5.1 Introduction

The Ndori Greenstone Belt (NGB), shown in Figure 12, forms part of the larger Busia-Kakamega Greenstone Belt in western Kenya. It is a predominantly east-northeast trending trough that extends about 90 km from the shores of Lake Victoria in the west to its termination against basement gneisses exposed in the Nandi escarpment in the east. The belt reaches its maximum width of about 50 km in the west tapering to about 20 km width in the east (Grant, 2006).

5.2 Stratigraphy

The geology of the NGB has been mapped and described by several authors (Hitchen, 1936; Pulfrey, 1946; Saggerson, 1952; Ngecu and Gaciri, 1995; Mason, 2010). It comprises mainly two rock groups, the older Nyanzian Group which is unconformably overlain by the relatively younger Kavirondian Group (Hitchen, 1936; Mathu and Davies, 1996). Estimated ages range from 3100 Ma for the base of the Nyanzian to 2500 Ma for the conclusion of the Kavirondian sedimentation (Grant, 2006). Both the Nyanzian Group and the Kavirondian Group were intruded by the Mumias and the Maragoli Granites.

The northeast portion of NGB falls largely within SPL213 (Siaya) and is dominantly composed of clastic sediments of the Kavirondian Group with Nyanzian Group volcanic rocks filling the cores of some anticlines. The southwest portion of the belt falls largely within SPL213 (Ndori) and is mostly composed of basaltic, andesitic, dacitic and occasionally rhyolitic volcanic rocks of the Nyanzian Group (Grant, 2006). The detailed and most recent map of the NGB by Mason (2010) has been adopted in this thesis. This map is illustrated in Figure 15.

5.2.1 Nyanzian Group volcanics

The Nyanzian volcanics, previously known as the Pre-Kavirondo Andesitic Suite (Hitchen, 1936), are the oldest rocks in the NGB (Pulfrey, 1946). Pulfrey (1946) suggests that the more basic volcanics occur at the top of the sequence while Shackleton (1950), Saggerson (1952) and Huddleston (1954) suggest that the Nyanzian volcanics become more acid towards the top of the sequence (Pulfrey, 1946; Shackleton, 1950; Saggerson, 1952; Huddleston, 1954).

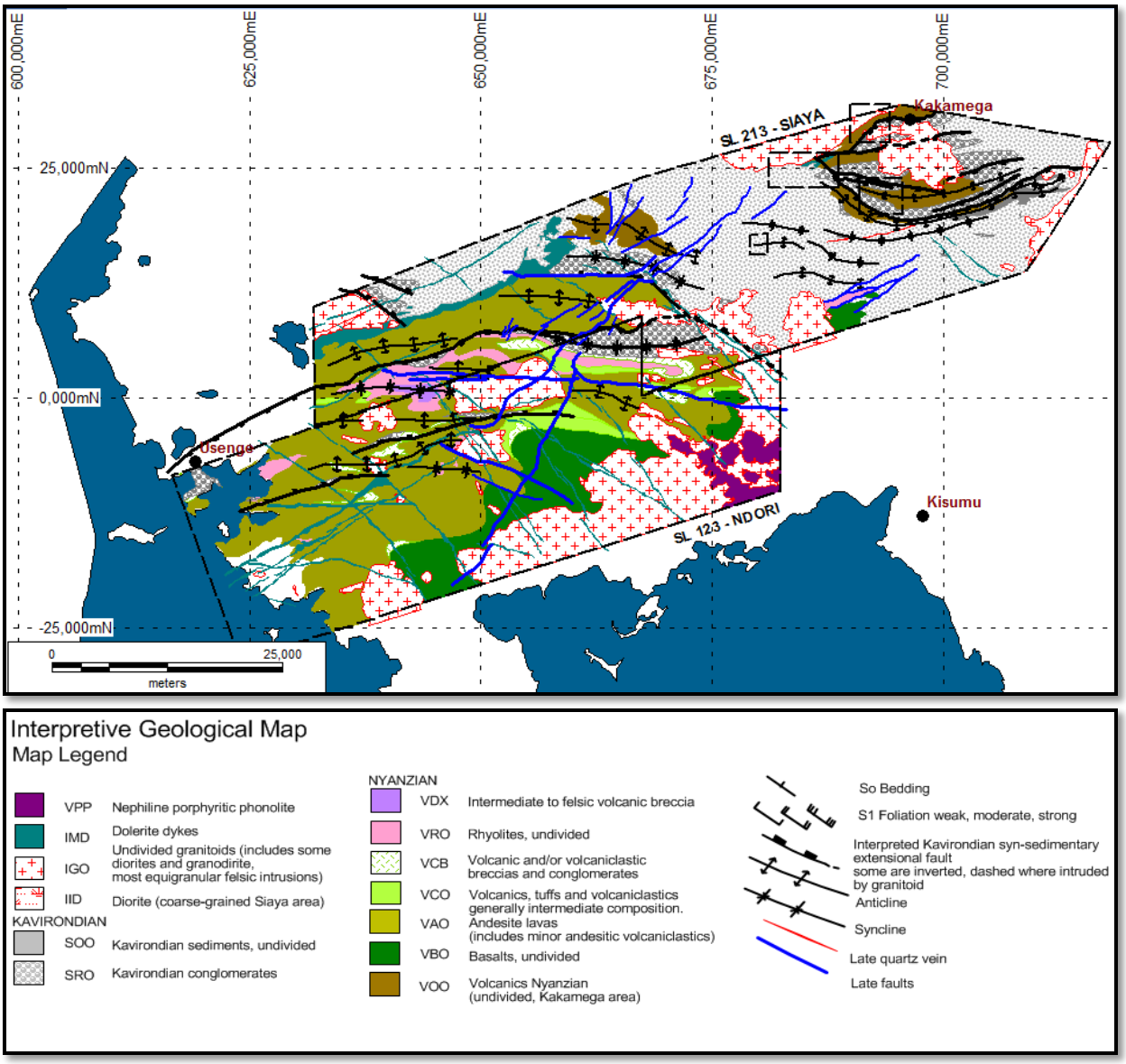

Figure 15. Regional geological map of the Ndori Greenstone Belt (modified after Mason, 2010).

Although no definite stratigraphic order of the volcanic rocks could be determined, Pulfrey (1946) proposed the following succession: rhyolites; major tuff development with some breccias and agglomerates; conglomerate; andesites; minor tuffs; and basalts. Pulfrey (1946) postulated that some of the rhyolites, if unaltered, would probably prove to be rhyodacites or even dacites. Mason (2010) also could not discriminate a unique stratigraphic sequence due to a lack of younging data. However, a common lithological sequence encountered by Mason (2010) from south to north is in sharp contrast with Pulfrey (1946) but supports observations by later

researchers: basalt; andesite and porphyritic andesite; various interpreted volcaniclastics and/or tuffs that include volcanic breccias and some volcaniclastic conglomerates; and rhyolite.

The area south and west of Luanda demonstrates the type section through the Nyanzian volcanics into the Kavirondian as illustrated in Figure 16. This section confirms the sequence proposed by Mason (2010): from basalts in the south, through andesites with or without volcaniclastics and tuffs, into volcaniclastics and tuffs of intermediate to felsic composition, then into the rhyolites that are overlain by the Kavirondian sediments (Mason, 2010). No sedimentary material of Nyanzian age, such as cherts and banded ironstones, found in the Migori Greenstone Belt, has been noted in association with the Nyanzian rocks of the NGB (Huddleston, 1954).

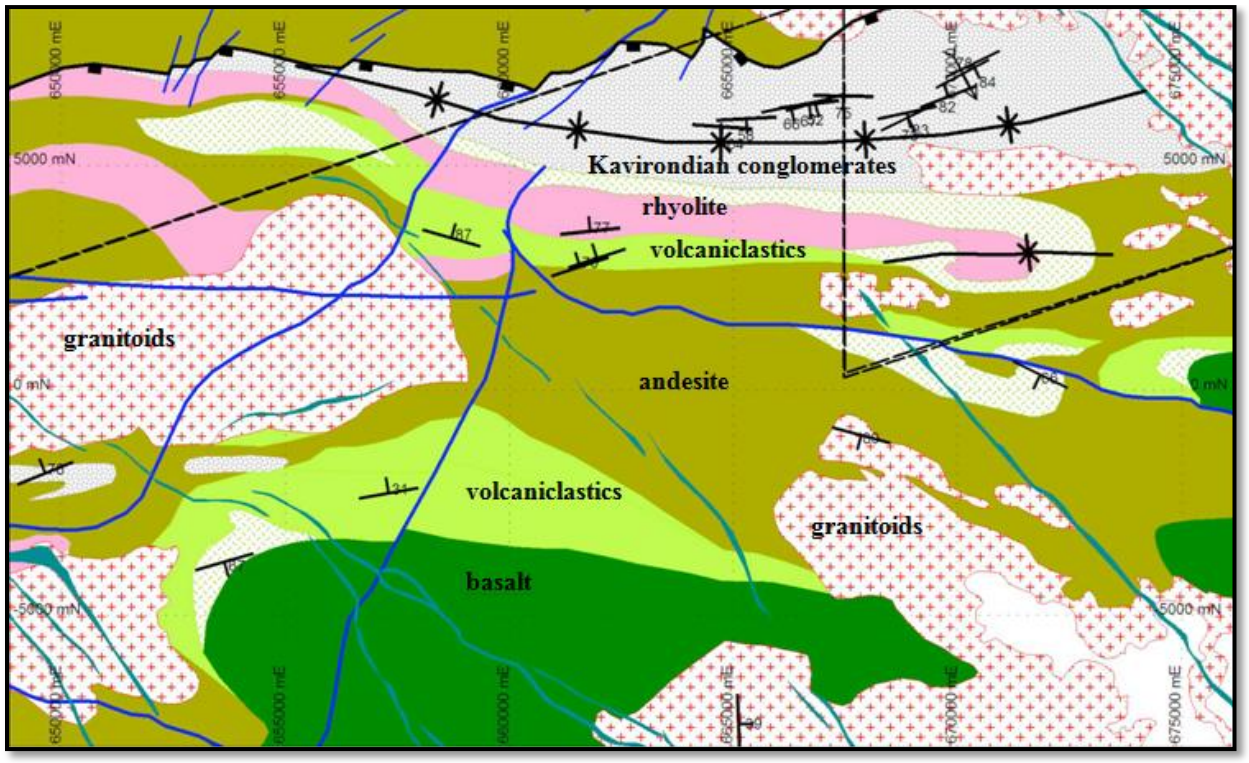

Figure 16. The area southwest of Luanda illustrating a type section through the Nyanzian volcanics into the base of the Kavirondian sediments (modified after Mason, 2010).

5.2.2 Kavirondian Group sediments

The thick group of sediments which overlies the Nyanzian volcanics has been previously named the Kavirondo Series (Hitchen, 1936) or the Kavirondian System (Stockley, 1943; Pulfrey, 1946;

Huddleston, 1954), but is now referred to as the Kavirondian Group (Ichang'i and MacLean, 1991; Ngecu and Gaciri, 1995). The Kavirondian Group occupies a sedimentary basin which is flanked on both sides by granitic intrusions and volcanic rocks as illustrated in Figure 17.

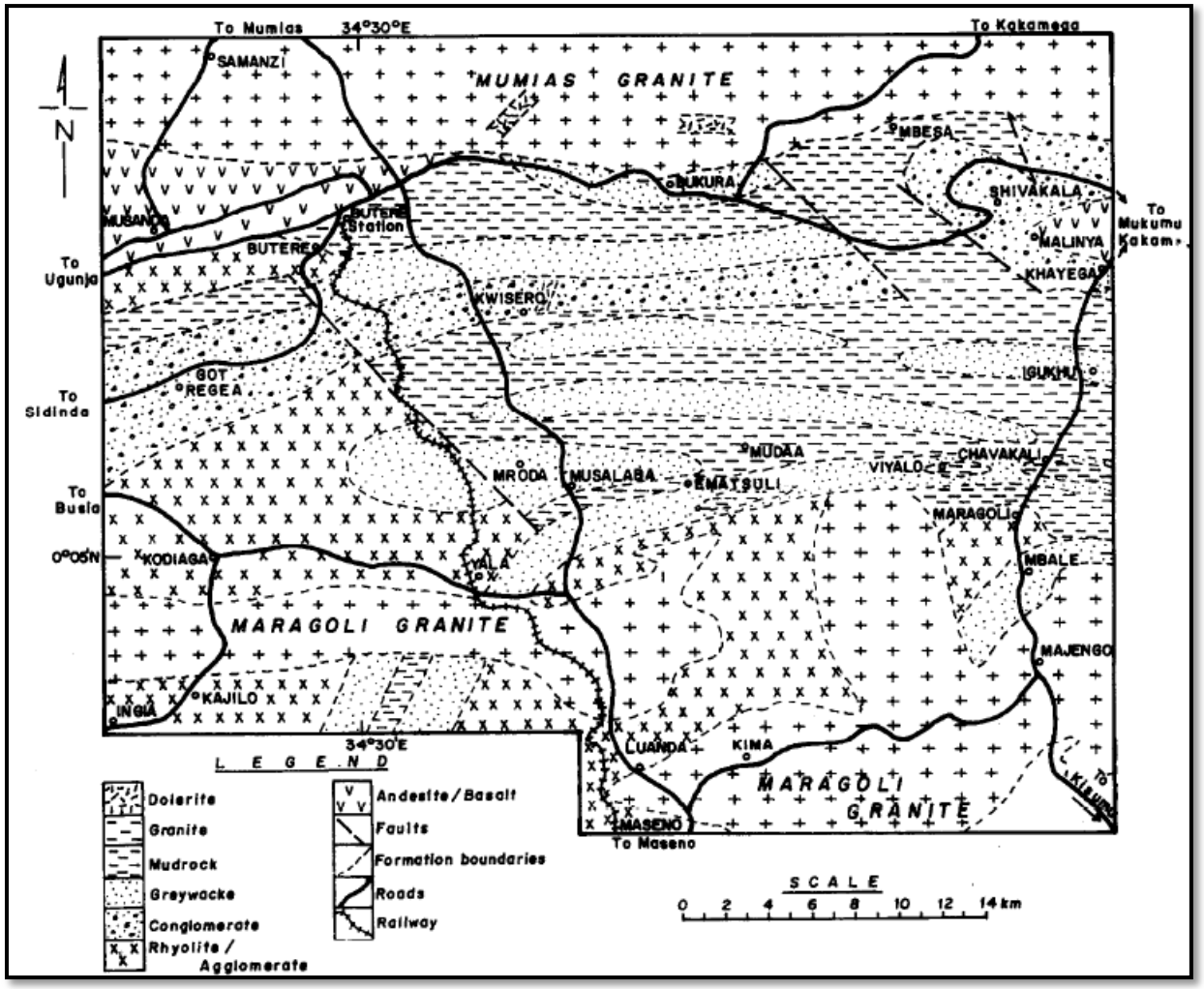

Figure 17. Geological map of the Kavirondian sedimentary basin in western Kenya (Ngecu and Gaciri, 1995)**.**

Conglomerates, grits and mudstones are the main members of the sequence (Huddleston, 1954). Various propositions have been made regarding the order of deposition of the sediments some of which are discussed below.

Combe (1927) interprets the succession as:

3. Upper Division of shales and phyllites with interbedded argillaceous sandstones
2. Middle Division of feldspathic sandstones, quartzites and grits, grading into arkoses, and containing conglomerate
1. Lower Division of shales and phyllites

Hitchen (1937) suggests a somewhat different succession:

3. Upper Division of feldspathic grits with pebble bands
2. Middle Division of slates and mudstones
1. Lower Division of feldspathic grits and conglomerates

Pulfrey (1946) suggests that as no constant datum horizons had been found no useful attempt could be made to split up the sedimentary sequence into subdivisions. Huddleston (1954) agrees with Pulfrey (1946) but acknowledges that the evidence just south of Kakamega does rather suggest a basal section which is predominantly conglomeratic followed by an alternating series of grits and mudstones.

Based on lithostratigraphic correlation of some of the formations in six water boreholes, Ngecu and Gaciri (1995) subdivided the Kavirondian Group into three formations: the Shivakala Formation; the Igukhu Formation; and the Mudaa Formation.

The Shivakala Formation is composed of polymictic conglomerates and unconformably overlies the volcanic rocks of the Nyanzian Group. Principal pebbles of the Shivakala conglomerate include basalt, andesite, dacite, rhyolites, granite and rare chert, presumably derived from the underlying Nyanzian formations (Chamberlain, 2003; Ngecu and Gaciri, 1995). In places, basal and intercalated conglomerates carry detrital gold derived most probably from the Nyanzian rocks or from intraformational gold-bearing strata (Gabert, 1990).

The Igukhu Formation conformably overlies the Shivakala Formation and the contact between these two formations is generally sharp. It is composed of greywacke with quartz as the most abundant mineral constituent of the greywacke (Ngecu and Gaciri, 1995). The Mudaa Formation is the youngest in the Kavirondian Group and has a gradational basal contact with the underlying

Igukhu Formation. It is essentially composed of laminated shales and mudstones, commonly interbedded with thin bands of sandstone.

Based on observations from mapping, Mason (2010) constructed a composite, interpreted stratigraphic column shown in Figure 18. The unconformity indicated is suggested by earlier workers and is consistent with the clast composition of the conglomerates (Mason, 2010).

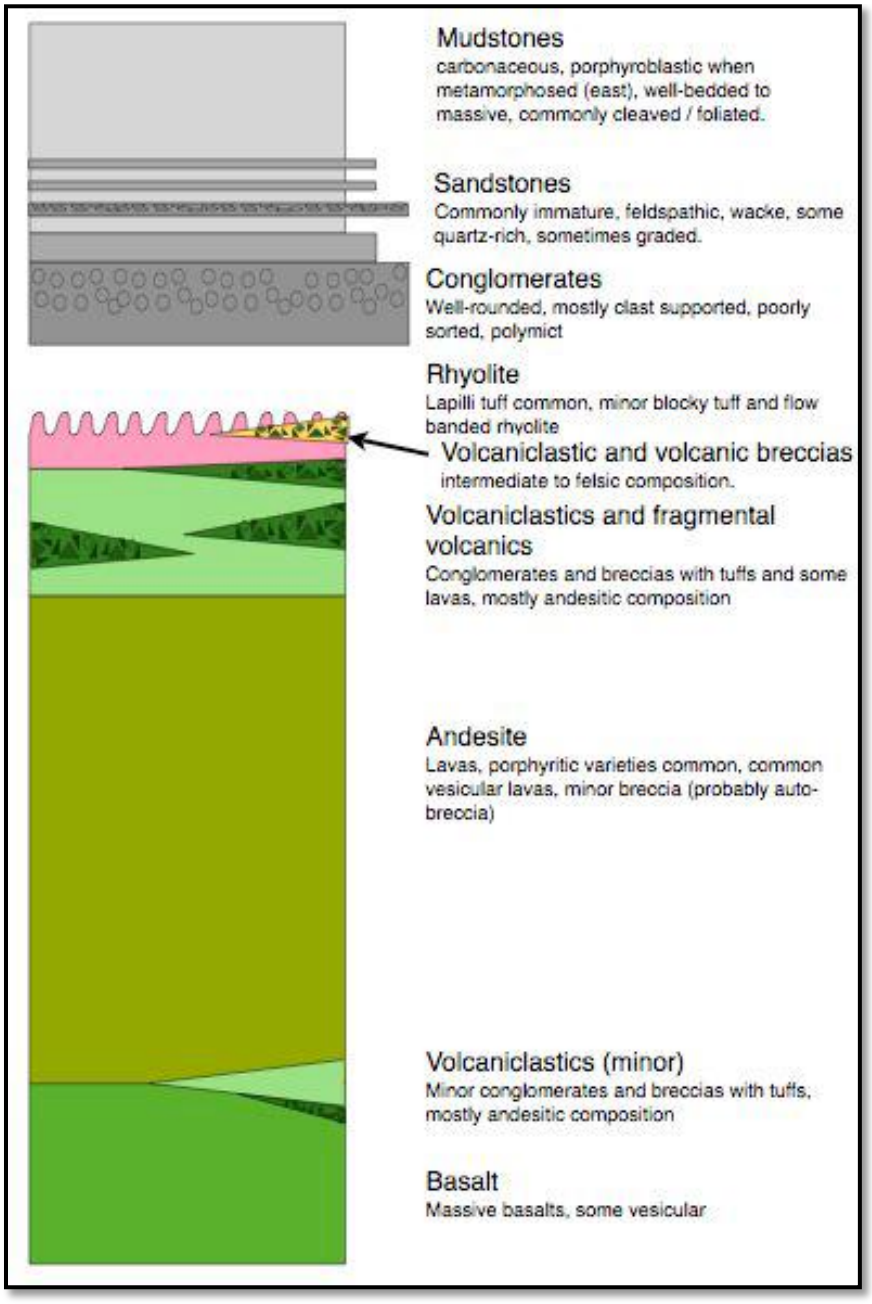

Figure 18. Composite stratigraphic column for the Ndori Greenstone Belt (Mason, 2010)**.**

5.3 Structure

Subsequent to the deposition of the volcano-sedimentary sequence, the geological evolution involves the intrusion of granitoid bodies with associated deformation (Mason, 2010). Pulfrey (1946) and Huddleston (1954) recognised two major periods of deformation. In the first period the Nyanzian rocks were folded prior to the deposition of the Kavirondian sediments on their upturned edges. The denudation of the up-lifted Nyanzian volcanics contributed largely to the make-up of the coarser-grained members of the Kavirondian sequence. In the second period the Kavirondian itself was then infolded with the Nyanzian and thrown into a series of generally broad folds the axes of which follow an almost east-west direction. Dips of both the Nyanzian and the Kavirondian rocks are generally high, ranging from 65° to vertical (Huddleston, 1954).

Based on the mapping by Mason (2010), the western part of the NGB is devoid of deformation features. To some extent this can be attributed to the abundance of mafic to intermediate lavas; mafic to intermediate lavas at low metamorphic grade have internal strain highly partitioned such that large areas of essentially internally undeformed rock are cut by relatively narrow high strain zones that commonly exhibit strong flattening fabrics and collectively accommodate bulk strain of the deformed rock mass. Conversely, sedimentary rocks, abundant in the eastern part of the belt, have strain evenly distributed throughout so deformation features are common. Nonetheless, Mason (2010) interpreted the geological evolution including deformation history and possible tectonic setting as outlined below:

- An extended period of bimodal volcanism resulted in the accumulation of a major sequence of volcanic and related rocks. The tectonic environment was probably a back-arc region.
- Uplift and erosion caused denudation of the upper part of the volcanic pile and may have signified arc collision.
- Continued extension without attendant volcanism formed the Kavirondian sedimentary basin whose source region included areas outside the back-arc volcanic terrane and may have included original basement to the Nyanzian volcanics. In any case a significant felsic granitoid contributed sediment to the Kavirondian sediment. It is during this time that syn-sedimentary extensional faults formed and thick sequences of coarse conglomerates were deposited proximal to these structures.

- Continental collision and concomitant cessation of subduction probably caused the onset of significant tectonism. This is the beginning of contractional deformation which is responsible for most of the deformation features observed in the NGB.
- Initial contractional (shortening) deformation probably caused inversion of suitably oriented, earlier formed Kavirondian syn-sedimentary structures although several of these early structures have not been inverted.
- Ongoing contraction and steepening of inverted extensional structures caused shortening to be accommodated less by inversion and more by folding. Tightening of folds and general deformation of the rock mass to accommodate shortening was responsible for widespread foliation development.
- Shortening also resulted in concomitant thickening of the crust and regional metamorphism to greenschist facies.
- As a consequence of inversion of extensional structures, the structural or mechanical architecture left would have considerably influenced subsequent contractional deformation. Early extensional structures would have been the locus of strong contractional deformation.
- Fold attenuation, particularly adjacent to early extensional structures, would have accommodated much of the remaining shortening.
- During crustal shortening, concomitant thickening of the crust resulted in the partial melting of the lower crust and the transient intrusion of significant volumes of granite (and related intrusive rocks) into shallower crustal levels. A lack of foliation development in granitic rocks attests to their intrusion late in the contractional deformation history. The granites are also cut by late stage faults also indicating a late- but not post-deformation intrusion.

5.4 Magmatism

Massive granitic plutons intruded the volcano-sedimentary successions of the Nyanzian Group and the Kavirondian Group. These plutons are feldspar-porphyritic, but hornblende bearing, and locally contain mafic enclaves (Opiyo-Akech et al., 1999). Three major plutons in the NGB have been identified by different names by different authors: the names Mumias (Pulfrey, 1946; Huddleston, 1954; Opiyo-Akech et al., 1999), Kitoshi (Sanders, 1965; Klver, 1975) or Kakamega (Ngecu and Gaciri, 1995; Mason, 2010) Granite refer to one pluton, the Maragoli

(Pulfrey, 1946; Huddleston, 1954; Opiyo-Akech et al., 1999), Kisian (Patel and Raja, 1979) or Maseno (Ödman, 1929) Granite refer to another, and Asembo or Bondo (Opiyo-Akech et al., 1999) Granite refer to the third pluton. In this thesis the names Mumias, Maragoli and Asembo have been adopted to refer to the three major granitic intrusions. Figure 19 shows the distribution of these major granitic intrusions in western Kenya.

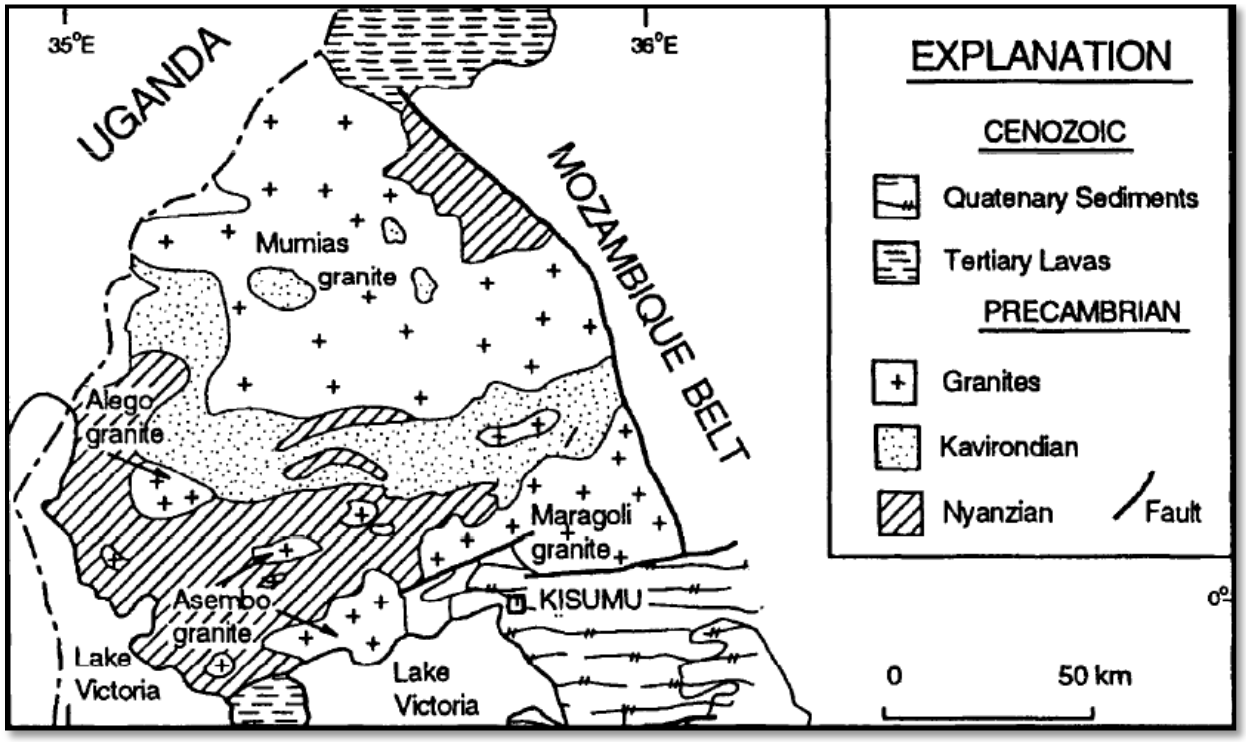

Figure 19. Sketch map showing the distribution of the major granitic intrusions in western Kenya (Opiyo-Akech et al., 1999)**.**

The Mumias Granite outcrops in the northern section of the NGB and is the most extensive granite body in the greenstone belt. From around the town of Mumias, it extends westwards into Uganda and eastwards beyond the town of Kakamega. The Maragoli Granite has a wide development in the southern section of the belt where it extends from Maragoli to Kamuga Bay (Huddleston, 1954; Opiyo-Akech et al., 1999). The Asembo Granite extends from west of Kombewa, westwards through Asembo Bay into Uyoma (Opiyo-Akech et al., 1999). According

to Opiyo-Akech (1999), the Mumias and the Maragoli Granites are characterised by large tors that dominate the landscape, while the Asembo Granite has a more gentle landscape.

5.5 Metamorphism

Thermal or contact metamorphism due to the intrusion of the major granite masses is responsible for most of the metamorphic changes exhibited by the rocks of the Nyanzian and the Kavirondian Group in western Kenya (Pulfrey, 1946; Saggerson, 1952; Huddleston, 1954; Sanders, 1965). The metamorphism produced greenschist facies mineral assemblages that grade into amphibolites facies at the margins of the major granitic intrusions (Ichang'i and MacLean, 1991). The greenschist facies mineral assemblage is characterised by the development of chlorite, epidote, albite, sericite and less frequently actinolite and biotite (Saggerson, 1952).

5.6 Geochronology

The Nyanzian volcanics in the NGB were dated, using the Rb/Sr method, at 2710 ± 340 Ma while granitic pebbles in the Kavirondian conglomerates were dated at 2611 ± 311 Ma. The Mumias and the Maragoli granites, which intrude both the volcanic and sedimentary successions, were both dated but using different methods. The Mumias granite was dated using the Rb/Sr method at ca. 2504 ± 48 Ma (Ngecu and Gaciri, 1995) while the Maragoli granite was dated using the K/Ar method at 2495 – 2577 Ma (Cahen and Snelling, 1966).

CHAPTER 6 MASUMBI AU-CU PROSPECT

6.1 Introduction

The Masumbi Au-Cu Prospect is situated in the Siaya District of the Nyanza Province, West Kenya approximately 50 km west of the town of Kisumu and near the northern boundary of SPL123. It is located near the Nyarodi granite on the north flank of the Maragoli Granite (Grant, 2006). Access to the prospect can be gained by taking the main national bitumen Kisumu-Luanda-Siaya road and branching to the south at a T-junction that is 300 m after the Ngiya Business Centre. The Masumbi Prospect is approximately 2 km from this junction. A locality map for Masumbi is illustrated in Figure 20.

6.2 Geological setting

The Masumbi Prospect is associated with a series of altered intermediate to felsic volcanics that have been significantly intruded by a series of rocks that include granodiorite, diorite, felsic porphyry dykes and granitic rocks (Mason, 2011). The geology of the area surrounding the Masumbi Prospect is illustrated in Figure 21.

6.3 Lithology

The lithological units at the Masumbi Prospect are all igneous and are grouped into volcanic and intrusive rocks. The volcanic rocks are largely dacites that are considerably more veined and altered than the felsic intrusive rocks. The dacites are glassy plagioclase-phyric and aphyric lavas in which the glass devitrified before the lava pile was intruded by a least one and probably more suites of dioritic to granodioritic intrusives.

The intrusive rocks are fine- to medium-grained diorites and granodiorites with a wide range of grain sizes and textures. A generalised modal mineral composition of these felsic intrusive rocks is illustrated in Figure 22. These rocks are presumed to be from relatively thin, sheet-like intrusive units rather than pluton-scale intrusive bodies as they are finer-grained compared to standard ‘batholithic’ diorites and granodiorites (Crawford, 2011).

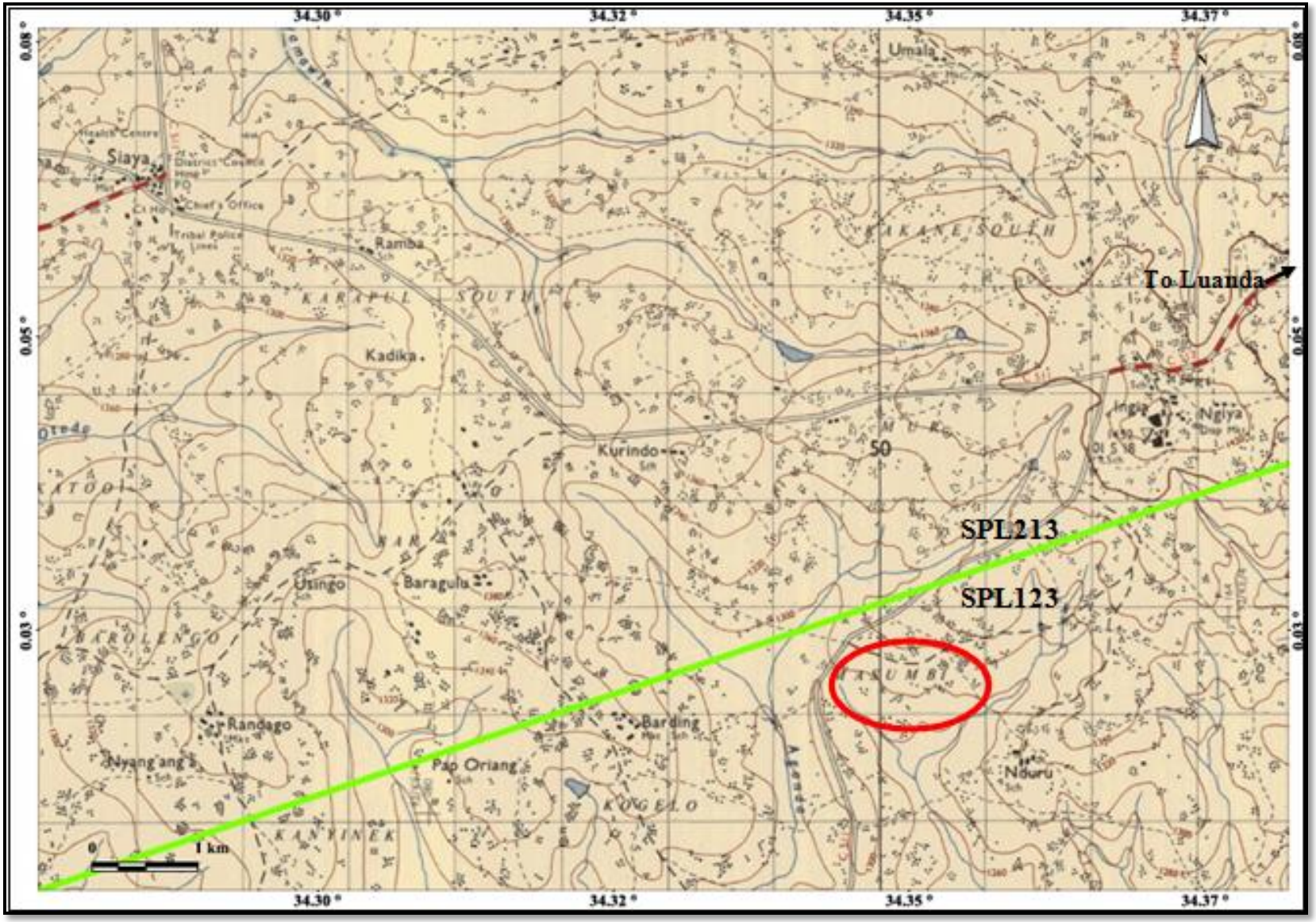

Figure 20. Locality map for the Masumbi Au-Cu Prospect.

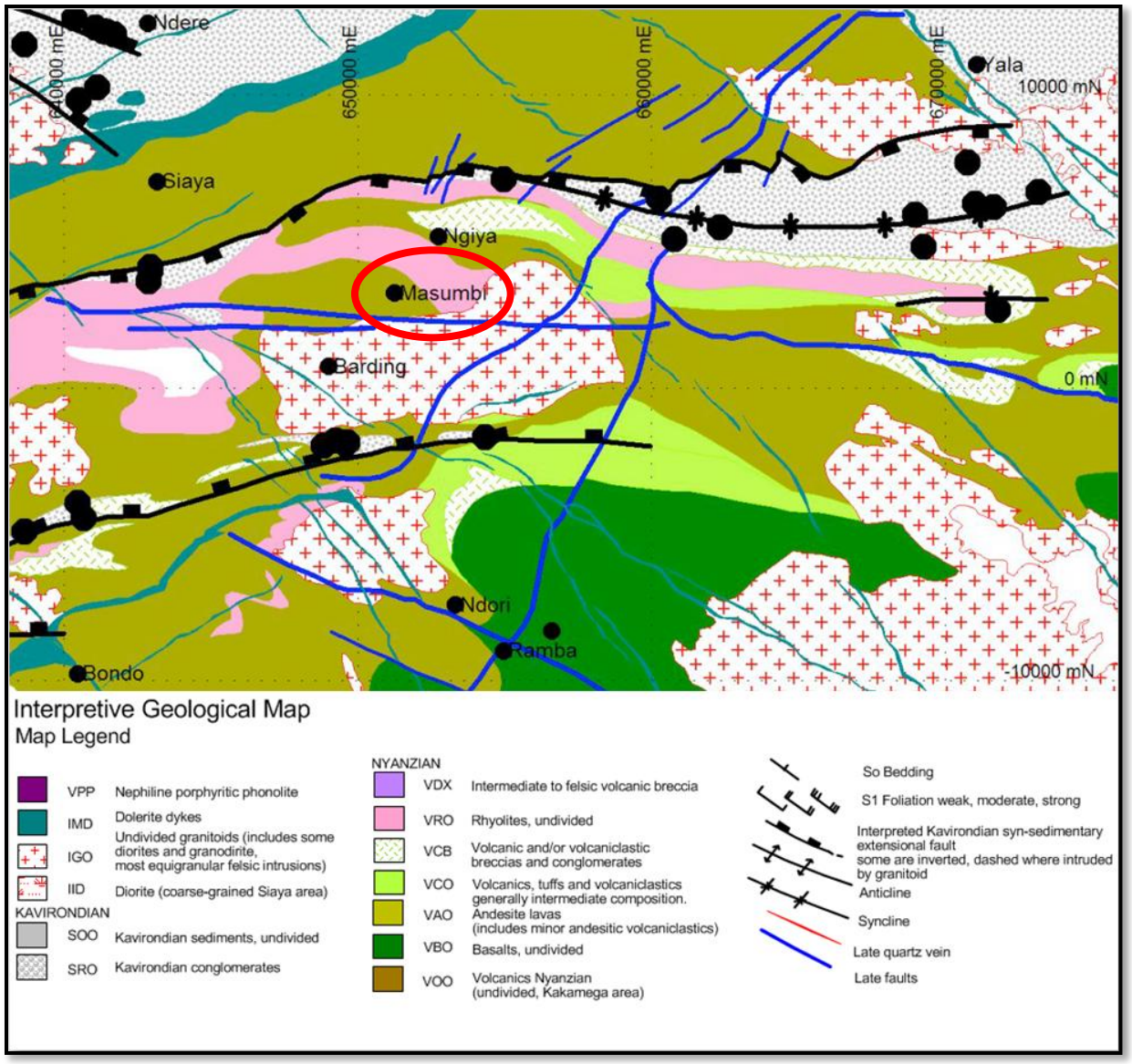

Figure 21. Geological map of the area surrounding the Masumbi Au-Cu Prospect shown by the red ellipse (Modified after Mason, 2010).

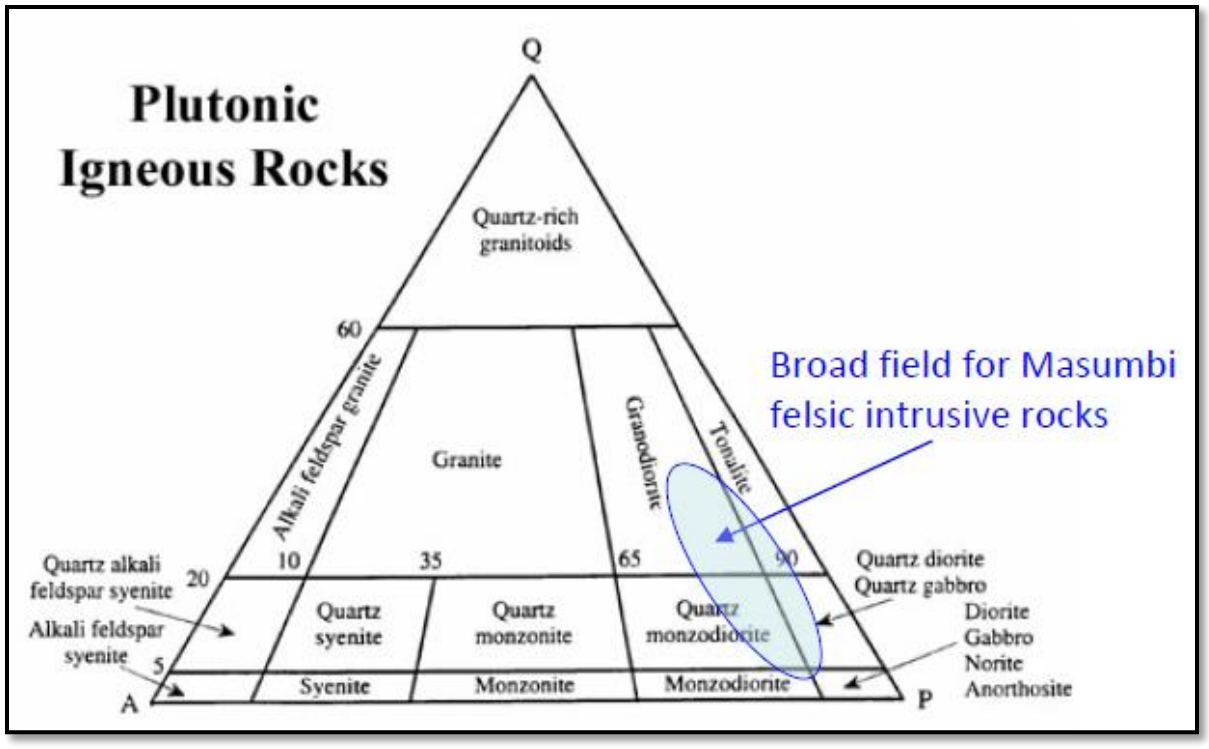

Figure 22. Generalised modal mineral classification of Masumbi Prospect felsic intrusive rocks (Crawford, 2011)**.**

6.4 Structure

Deformation features are dominantly brittle and comprise fractures and veins. No penetrative foliations are developed thereby indicating a low-strain deformation environment (Mason, 2011). The mineralisation at Masumbi trends north-south to north-northwest-south-southeast and Grant (2006) postulates that this trend defines shear zones striking north-northwest and dipping to the east at shallow to steep angles. Mason (2010) recognises that the mineralisation trend at Masumbi is similar to that at Ramba Lumba. Ramba Lumba is spatially associated with one or more regionally extensive, interpreted late stage fault zones and comprises remarkably straight, planar, similarly oriented veins indicative of low-strain, high differential stress fracturing (Mason, 2010).

6.5 Alteration

An understanding of the characteristics and patterns of wallrock alteration associated with mineralisation has proved to be an effective guide to ore targeting in many types of mineral deposits (Bakken, 1990). Wallrock alteration at Masumbi is in the form of silicification, propylitisation, sericitisation, chloritisation, epidotisation and biotitisation (Grant, 2006; Crawford, 2011; Mason, 2011; Tomkinson, 2012).

An early stage alteration assemblage in both the volcanic and intrusive rocks comprises chlorite + epidote + magnetite ± biotite ± amphibole with zones of murky and ill-defined silicification which does not show any clear fracture control in the granitoid host. This alteration may be related to early copper mineralisation but was not gold-bearing and suggests the involvement of a magmatic hydrothermal system. This early Fe-rich (magnetite-bearing) alteration may have been critical in localising the later gold mineralising event through sulphidation reactions (Tomkinson, 2012).

A late stage alteration assemblage comprises pyrite ± chalcopyrite ± muscovite commonly found as centre, late fill of brittle micro-fractures. These micro-fractures have epidote ± chlorite selvages. The presence of epidote in the selvages to these fractures suggests some form of continuum with the earlier more widespread magnetite-bearing alteration. The alteration paragenesis and Au-Cu mineralisation at Masumbi is strongly reminiscent of the Wandoo orebody at Boddington mine in West Australia and this style of mineralisation has potential to produce very significant low grade but large tonnage Au-Cu deposits (Tomkinson, 2012).

6.6 Mineralisation

Mineralisation at Masumbi is associated with anastomosing silicified shear zones within haloes of silicified, propylitised and mylonitised granitoids (Grant, 2006). It is also related to strongly altered silicified volcanic rocks that appear pale due to the presence of fine sericite (Mason, 2011). Individual shears range in width from 1 m to more than 9 m, with alteration haloes extending in excess of 10 m into their hanging and footwalls (Grant, 2006).

Gold is spatially related with pyrite and chalcopyrite grains and aggregates localised along stringer veins and in disseminations within the more intensely silicified portions of the shears (Grant, 2006). The gold therefore occurs as part of a later overprint of fine fractures filled with pyrite ± chalcopyrite some of which have epidote-rich selvages and which contain free gold locally (Tomkinson, 2012). The main zone of gold mineralisation appears to be structurally controlled as it cross-cuts a number of different logged lithologies and is associated with the occurrence of pyrite and quartz veins (Gray and Jones, 2011).

CHAPTER 7 METHODOLOGY

7.1 Introduction

This chapter discusses the sampling criteria and petrological methods employed in this study. The samples were taken from diamond drill-holes. The location and distribution of these drill-holes are illustrated in Figure 23. Polished thin sections were prepared for petrographic examination and these were also investigated using the microprobe for mineral chemistry and for detection of very small inclusions in sulphides.

7.2 Drill-core sampling

Five diamond drill-holes (Figure 23) from the Masumbi Au-Cu Prospect were sampled.

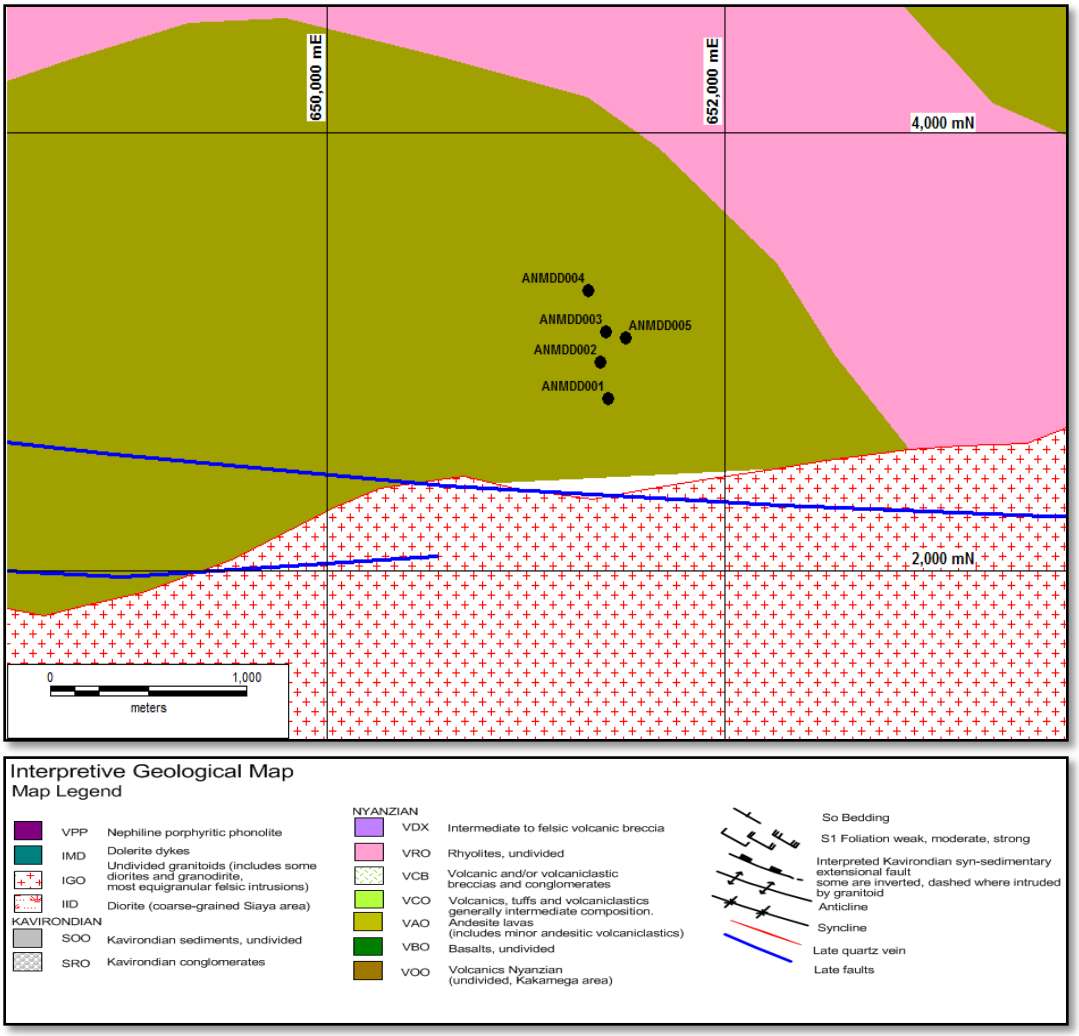

Figure 23. Location of Masumbi diamond drill-holes.

Twenty seven samples were carefully selected to represent major and some minor lithologies as well as alteration phenomena and sulphide mineralisation. These samples were selected from both gold-and/or-copper-mineralised sections and barren sections showing alteration. Table 5 shows the source location and distribution of the samples. Photographs of these samples are illustrated in Appendix A.

Table 5. Source location and distribution of samples

Drill-hole ID	Sample ID	Depth (m)	Lithology	Au (ppm)	Cu (ppm)
ANMDD001	TSM01	62.06	Granodiorite	0.156	**NR
ANMDD001	TSM02	68.32	Granodiorite	2.01	NR
ANMDD001	TSM03	71.86	Hbl* diorite	0.184	NR
ANMDD001	TSM04	95.64	Microgranodiorite	0.182	NR
ANMDD001	TSM05	171.36	Felsic dyke	0.003	NR
ANMDD002	TSM06	60.38	Granodiorite	0.231	1990
ANMDD002	TSM07	68.55	Dacite	1.205	825
ANMDD002	TSM08	71.29	Dacite	0.483	3610
ANMDD002	TSM09	82.17	Microdiorite	7.87	735
ANMDD002	TSM10	89.41	Hbl-quartz diorite	0.511	302
ANMDD002	TSM20	51	Dacite	0.371	4270
ANMDD002	TSM21	131.55	Diorite	0.927	NR
ANMDD003	TSM11	56.73	Diorite porphyry	0.007	0
ANMDD003	TSM12	58.6	Microdiorite	1.135	31
ANMDD003	TSM13	62.01	Granodiorite	0.186	106
ANMDD003	TSM14	107.15	Micromonzonite	0.485	1380
ANMDD003	TSM15	111.72	Basaltic dyke	0.105	214
ANMDD003	TSM16	112.87	Dacite	7.38	710
ANMDD003	TSM22	81.26	Diorite	0.656	790
ANMDD003	TSM23	172.36	Dacite	10.95	53
ANMDD004	TSM17	115.92	Microdiorite	0.091	78
ANMDD004	TSM18	119.28	Dacite	0.033	67
ANMDD004	TSM19	121.11	Microdiorite	0.016	0
ANMDD004	TSM24	51	Dacite	0.818	271
ANMDD005	TSM25	91.32	Dacite	2.73	2480
ANMDD005	TSM26	54.39	Granodiorite	2.18	NR
ANMDD001	TSM27	180.59	Microdiorite	11.2	NR

*hbl – hornblende; **NR – Not recorded

7.3 Petrological methods

7.3.1 Preparation of polished thin sections

Struers and Leco machines in the Rhodes Geology Department were utilised to prepare polished thin sections for microscopic examination in reflected and transmitted light. The procedure used to prepare the polished thin sections is described below.

- A specimen block is cut from the rock sample to fit on a standard glass slide measuring 26 mm x 48 mm.
- The specimen is ground to approximately 8mm thickness using 90 µm and 46 µm wheels on a Struers Accutom-50 machine.
- The specimen is mounted onto the glass slide in the vacuum impregnation unit CitoVac using EpoFix resin.
- Surplus specimen material is cut to a thickness of 0.5-2 mm using the Struers cut-off machine.
- The Struers Accutom-50 machine is also used to grind thin section to a thickness of 90 µm and 40 µm (section + resin).
- The mounted section is automatically lapped using a Leco polishing machine by means of an aluminium disc with a nylon lap.
- The thin section is automatically polished using the Leco polishing machine. The abrasives used are 6 µm and 3 µm diamond paste. The polishing is gradually reduced to 1 µm.
- The specimen is now finished with a thickness of 30 µm.

7.3.2 Petrography

Petrographical analysis was conducted using an optical microscope in the Department of Geology microscopy laboratory. Sulphide minerals in thin sections were examined using reflected light while silicate and carbonate minerals were examined using transmitted light. Microphotographs were taken with a Leica EC3 digital colour camera mounted on a Leica microscope. The camera has 3.1 Megapixel high-resolution imaging capability.

7.3.3 Electron probe micro-analyses

Electron Probe Micro-Analyses (EPMA) data acquisition was performed in the Department of Geology at Rhodes University. The JEOL™ JXA-8230 Superprobe was utilised to quantitatively analyse sample material which included silicate minerals, carbonate minerals, sulphide minerals and gold. The selected polished thin sections were coated with a fine layer of carbon to generate an electrically conductive surface. The analysing system uses four automated Wavelength Dispersive Spectrometers (WDS). Analytical conditions employed were: acceleration voltage 15 kV, probe current 20 nA, counting time 10 sec on peak and 5 sec on background and beam size spot <1 micron. Natural standards were used for measuring the characteristic X-rays. The ZAF matrix correction method was employed for quantification.

7.4 Structural analysis

Stereonet projections provide a powerful means to represent three-dimensional information on a two-dimensional surface (Knox-Robinson and Gardoll, 1998). Structural measurements for epidote veins and quartz-pyrite veins in drill-holes ANMDD001-004 were plotted on equal area projection, lower hemisphere stereonets using the GEOrient version 9.5.0 software.

7.5 Statistical analysis

The correlation coefficient describes the degree of relationship between two variables and the Pearson's correlation coefficient (r) is commonly used as a measure of the strength of a linear relationship between the two variables (Lee Rodgers and Nicewander, 1988). Gold and copper assays from the Masumbi diamond drill-holes were statistically analysed to establish whether a linear relationship exists between gold and copper mineralisation. Pearson's correlation coefficients were calculated and scatter plots were generated to show graphical relationships between gold and copper.

CHAPTER 8 RESULTS

8.1 Introduction

A total of twenty seven thin sections from drill cores were examined under the optical microscope for sulphides, silicates, carbonates and oxides. Seventeen of the thin sections examined represent medium- to coarse-grained dioritic to granodioritic felsic intrusive rocks. Figure 24 illustrates the range of grain sizes, textures and alterations of the felsic intrusive rocks. The remainder of the thin sections represent the largely dacitic volcanic rocks that are considerably more veined and altered than the felsic volcanic rocks. The textures and alteration of the volcanic rocks are illustrated in Figure 25. The petrographic results of selected thin sections are discussed in section 8.2. Eight thin sections were selected for examination using the EPMA and the results are discussed in section 8.3.

Structural data for quartz-pyrite veins, pyrite veins and epidote veins in drill-holes ANMDD001-004 were plotted on equal area, lower hemisphere stereonets using the GEOrient version 9.5.0 software. The software was utilised to calculate the mean principal orientations of the veins. Stereoplots for these veins are presented in subsection 8.4.1.

Gold and copper assays from drill-holes ANMDD002-004 were plotted on scatter plots and Pearson's correlation coefficients calculated. This calculation was undertaken to establish whether there is a linear relationship between gold and copper mineralisation or not. The scatter plots and the correlation coefficients are presented is subsection 8.4.2.

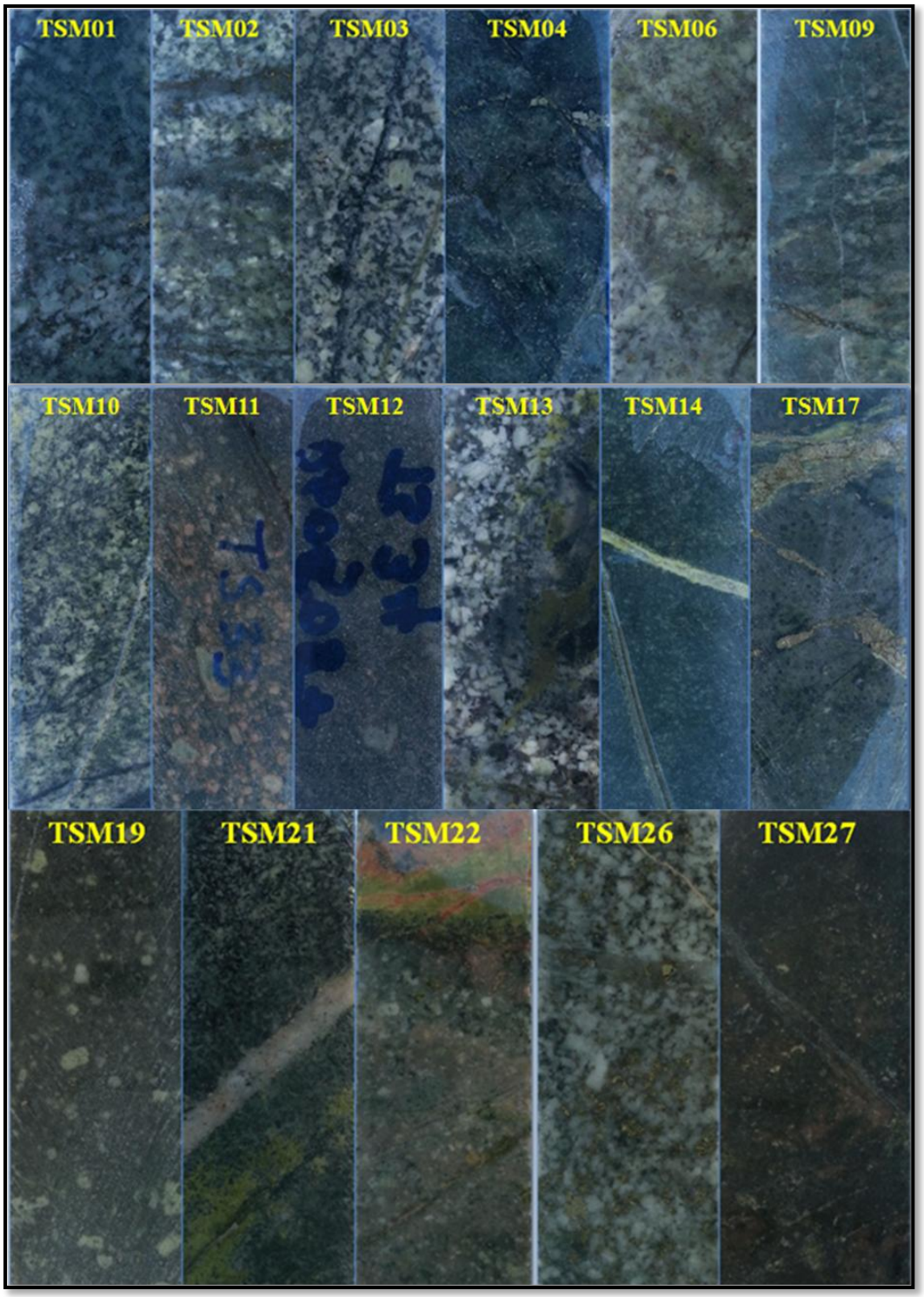

Figure 24. Texture, grain size and alteration of intrusive felsic rocks from the Masumbi Prospect as observed in quartered drill core specimens. Width of each specimen is 23.8 mm.

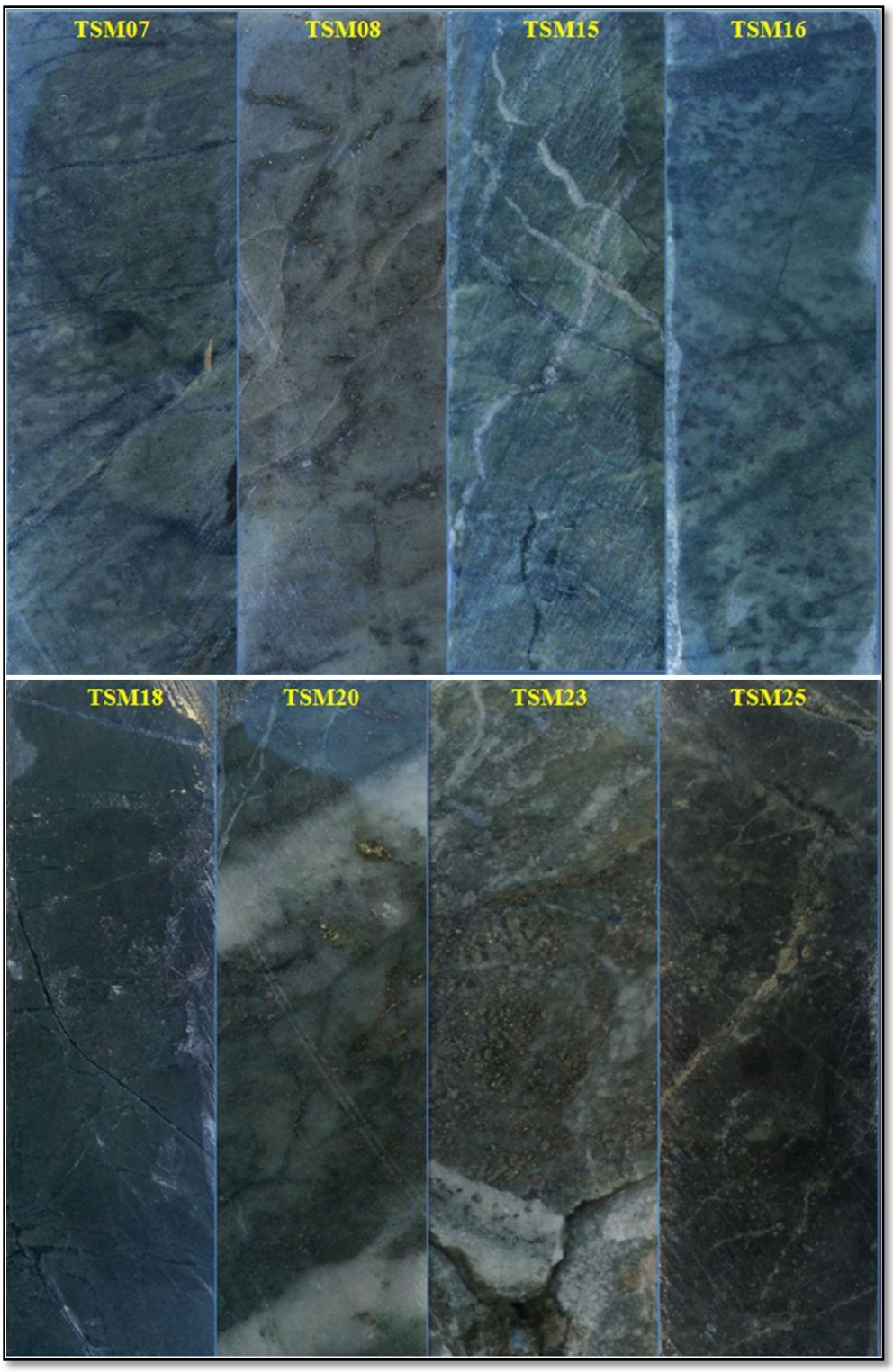

Figure 25. Texture, grain size and alteration of volcanic rocks from the Masumbi Prospect as observed in quartered drill core specimens. Width of each specimen is 23.8 mm.

8.2 Petrography

Results from petrographic examination have been subdivided into intrusive rocks and volcanics rocks. The intrusive rocks are felsic in composition and include tonalite, micro-tonalite, granodiorite, diorite and quartz-diorite. The volcanic rocks have been classified as dacites.

8.2.1 Intrusive rocks

- **Sample Number TSM02 (Tonalite)**

This sample comes from drill-hole ANMDD001 at a depth of 68.32 m. It is a medium to coarse grained and moderately altered intrusive felsic rock that has been classified as a tonalite. Gangue minerals present include quartz and plagioclase feldspar. Quartz is present as distinctive, rounded and euhedral crystals. The common secondary minerals are chlorite and sericite. Former biotite is being replaced by chlorite and plagioclase feldspar is being altered to sericite. The alteration of biotite to chlorite is shown in Figure 26 (a, b) and the alteration of plagioclase to sericite is shown in Figure 26 (c, d).

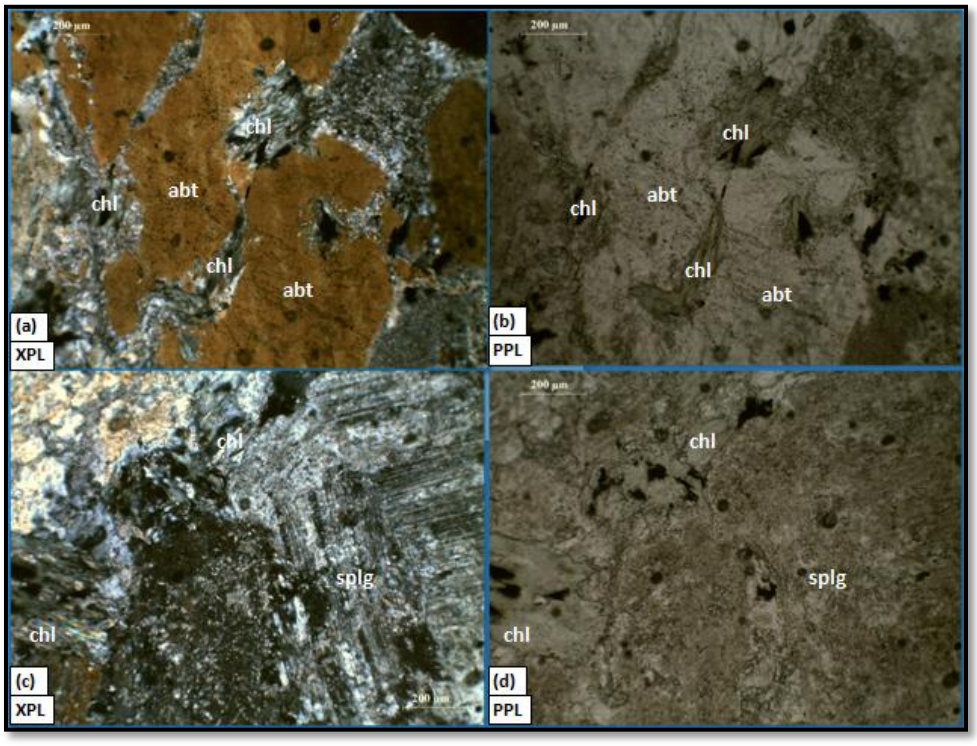

Figure 26. Microphotographs of TSM02 under transmitted light showing biotite altering to chlorite (a, b) and plagioclase altering to sericite (c, d); PPL=Plane Polarised Light, XPL=Crossed Polars, abt=altered biotite, chl=chlorite and splg=sericitised plagioclase.

- **Sample Number TSM04 (Micro-tonalite)**

Sample number TSM04 comes from drill-hole ANMDD001 at a depth of 95.64 m. It is finer grained than the tonalite represented by sample TSM02. This sample can be classified as a holocrystalline micro-tonalite that is dominated by tabular plagioclase and interstitial quartz. The plagioclase is intensely altered to sericite as illustrated in Figure 27 (a) and (b). There are several veinlets composed of euhedral pyrite and anhedral chalcopyrite occurring together with chlorite, muscovite and occasionally calcite. Figure 27 (c) and (d) illustrate veinlets of euhedral pyrite and anhedral chalcopyrite occurring with chlorite. Chalcopyrite also occurs as disseminations throughout the rock away from the veins.

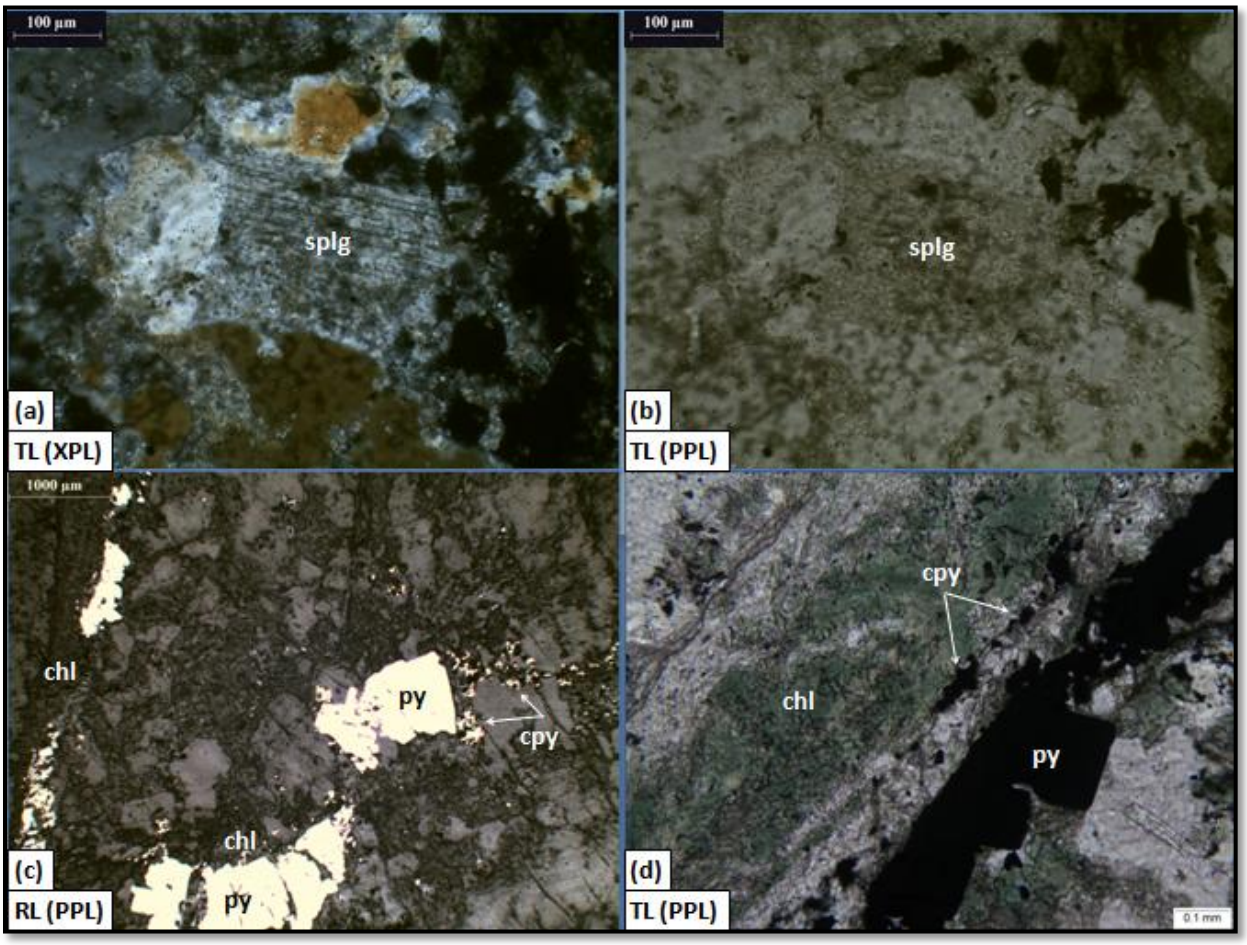

Figure 27. Microphotographs showing plagioclase altering to sericite (a, b) and veinlets composed of euhedral pyrite and anhedral chalcopyrite sulphides occurring with chlorite (c, d) in TSM04; RL=Reflected Light, TL=Transmitted Light, PPL= Plane Polarised Light, XPL= Crossed Polars, cpy=chalcopyrite, chl=chlorite, py=pyrite and splg=sericitised plagioclase.

- **Sample Number TSM06 (Granodiorite)**

Thin section sample TSM06 comes from drill-hole ANMDD002 at a depth of 60.38 m. It is a medium-grained granodiorite consisting of sericite-altered plagioclase and subhedral and anhedral quartz. The plagioclase altering to sericite is illustrated in Figure 28 (a, b, c). Chloritised biotite is a minor phase in this sample. This sample contains scattered euhedral pyrite and anhedral chalcopyrite grains as shown in Figure 28 (d).

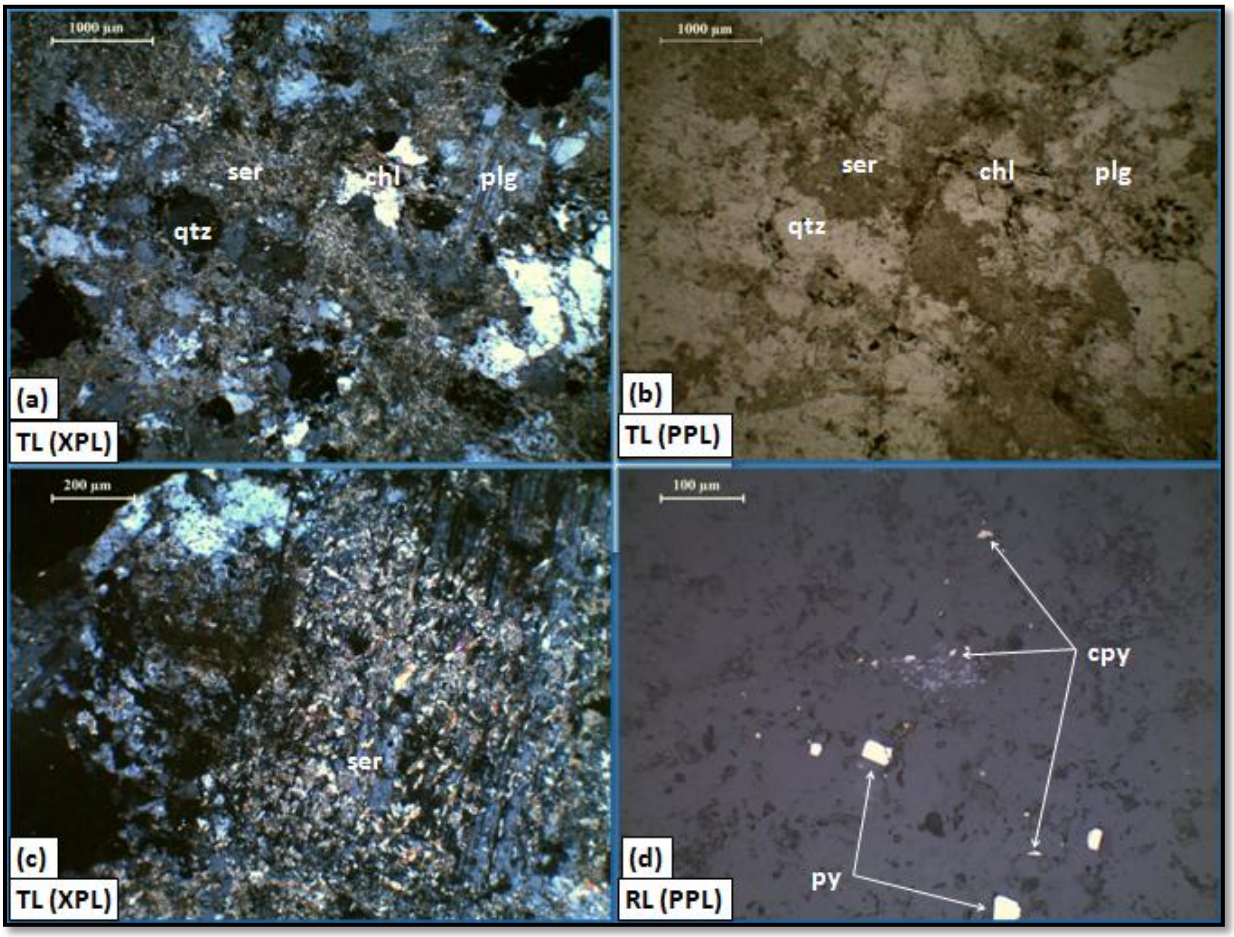

Figure 28. Microphotographs showing plagioclase altering to sericite (a, b, c) and scattered euhedral pyrite and anhedral chalcopyrite grains (b) in TSM06; TL=Transmitted Light, RL=Reflected Light, XPL=Crossed Polars,PPL=Plane Polarised Light, cpy=chalcopyrite, chl=chlorite, plg=plagioclase, py=pyrite, qtz=quartz, and ser=sericite.

- **Sample Number TSM10 (Quartz diorite)**

This thin section sample comes from drill-hole ANMDD002 at a depth of 89.41 m. It is a quartzo-feldspathic intrusive rock that can be classified as a quartz diorite. Feldspars occur as both occasional large crystals and interstitial material intergrown with quartz. Chlorite, epidote and occasional sericite are common alteration minerals. Scattered chalcopyrite is commonly associated with both chlorite and epidote alteration. Figure 29 (a) shows the chlorite alteration present in this thin section sample. Scattered chalcopyrite grains hosted in epidote are illustrated in Figure 29 (b), (c) and (d). High relief and anomalous interference colours typical of epidote are shown in Figure 29 (c) and (d) respectively.

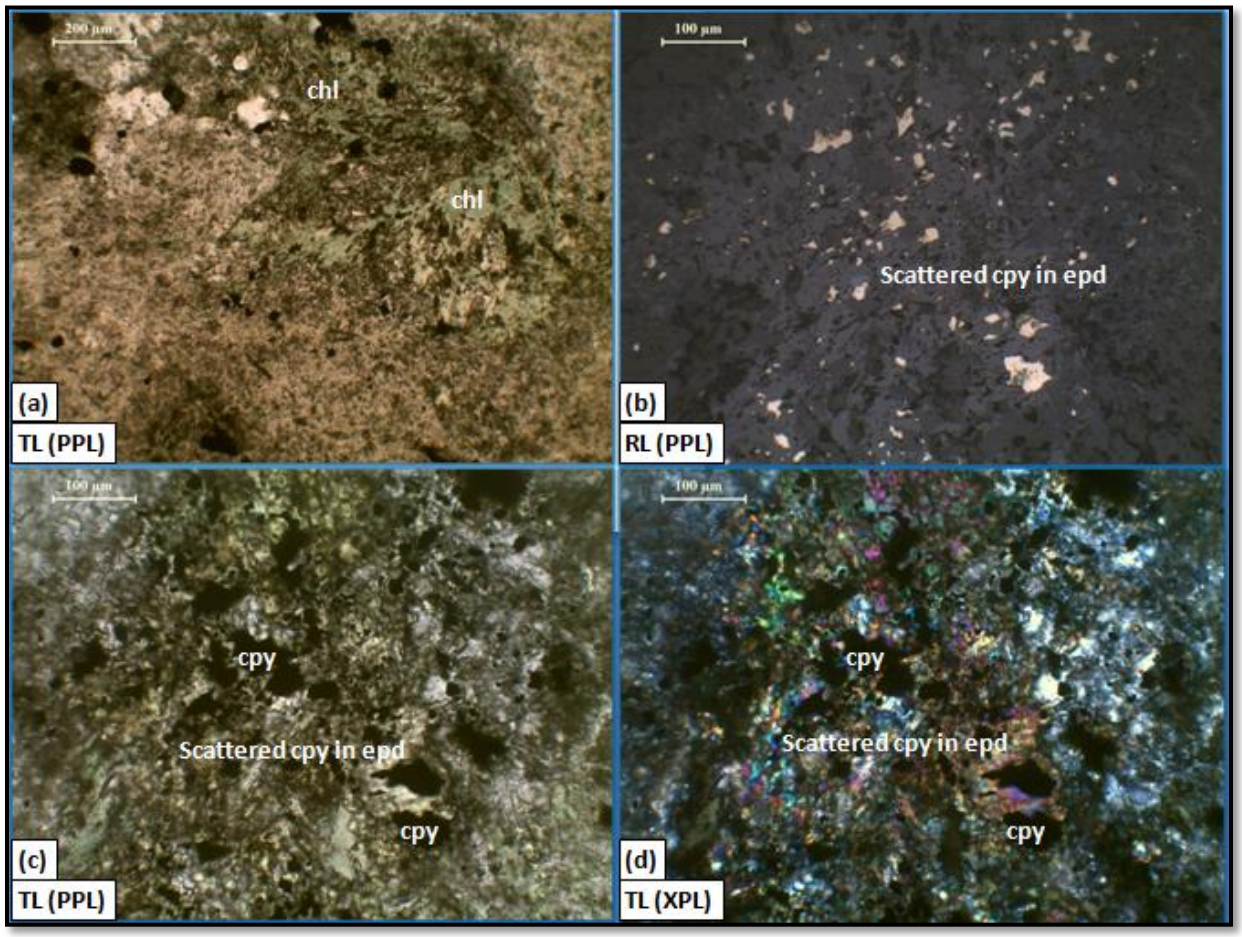

Figure 29. Micrographs showing chlorite alteration (a) and epidote alteration containing scattered chalcopyrite (b, c, d) in TSM10; TL=Transmitted Light, RL=Reflected Light, PPL=Plane Polarised Light, XPL=Crossed Polars, cpy=chalcopyrite, chl=chlorite, and epd=epidote.

- **Sample Number TSM11 (Felsic intrusive)**

Thin section sample TSM11 comes from drill-hole ANMDD003 at a depth of 56.73 m. It is a quartzo-feldspathic intrusive rock characterised by a porphyritic texture. Quartz and plagioclase phenocrysts occur in a finer-grained quartzo-feldspathic groundmass. Although pyrite grains are very sporadic, where they occur they have a preferred orientation as shown in Figure 30 (a). Sericite alteration is common as illustrated in Figure 30 (b).

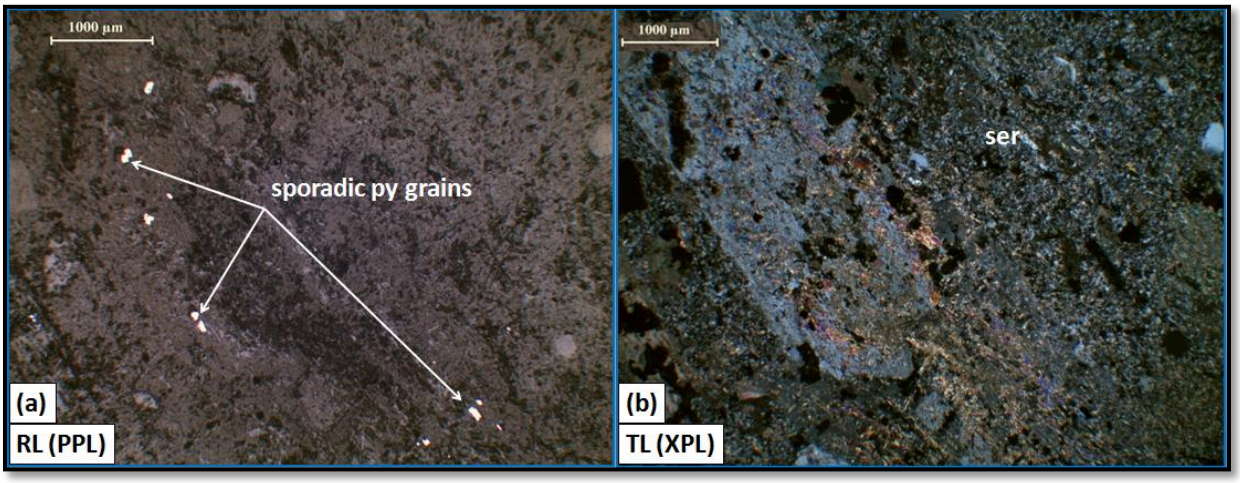

Figure 30. Microphotographs showing sporadic pyrite grains (a) and sericite alteration (b) in TSM11; RL=Reflected Light, TL=Transmitted Light, py=pyrite, ser=sericite.

- **Sample Number TSM22 (Diorite)**

This thin section comes from drill-hole ANMDD003 at a depth of 81.26 m. It is a medium-grained dioritic intrusive rock with ubiquitous epidote alteration. Hairline sulphide veinlets are common and concordant with epidote veins. Figure 31 (a) and (b) illustrate epidote alteration and veinlets of pyrite and chalcopyrite that are concordant with the epidote veins. There are quartz veins that crosscut epidote alteration as shown in Figure 31 (c) and (d).

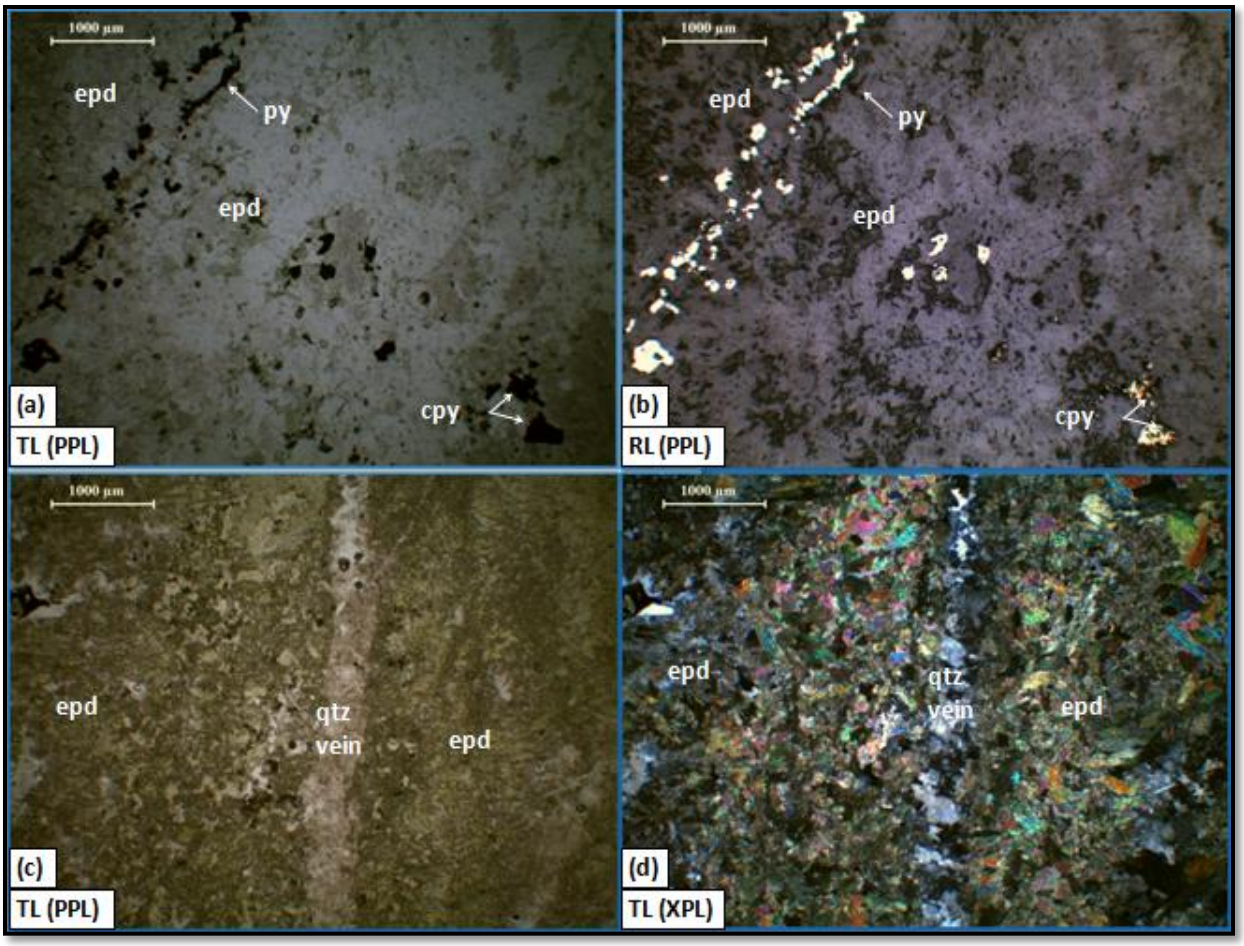

Figure 31. Microphotographs showing epidote alteration with concordant sulphide veinlets (a, b) and crosscutting quartz vein (c, d) in TSM22; TL=Transmitted Light, RL=Reflected Light, cpy=chalcopyrite, epd=epidote, and py=pyrite.

8.2.2 Volcanic rocks

- **Sample Number TSM07 (Dacite)**

This thin section sample comes from drill-hole ANMDD002 at a depth of 68.55 m. It is a dacitic volcanic rock with a heterogeneous texture, consisting of sericitised plagioclase and anhedral quartz grains. Veins are common and often include quartz, quartz-carbonate, and quartz-carbonate-chlorite. Chalcopyrite and pyrite grains are mostly associated with quartz-carbonate-chlorite veins. Figure 32 (a) and (b) illustrate a quartz vein containing chalcopyrite and pyrite.

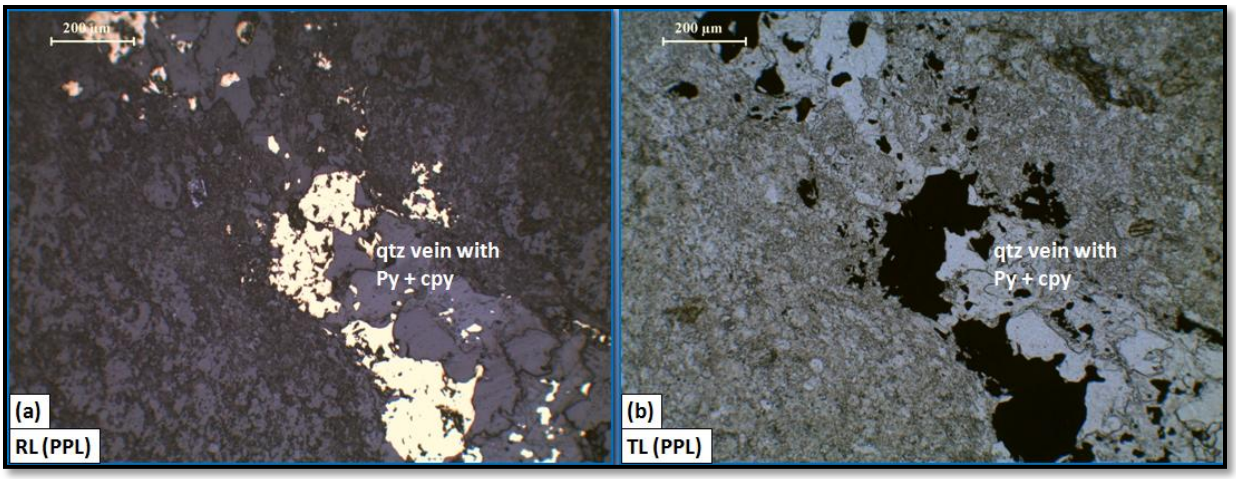

Figure 32. Microphotographs showing a quartz vein containing pyrite and chalcopyrite in TSM07; RL=Reflected Light, TL=Transmitted Light, PPL=Plane Polarised Light, cpy=chalcopyrite, py=pyrite, and qtz=quartz.

- **Sample Number TSM08 (Dacite)**

Thin section sample TSM08 also comes from drill-hole ANMDD002. It is a fine-grained dacitic volcanic rock that hosts several subparallel quartz veinlets containing pyrite and chalcopyrite as illustrated in Figure 33 (a) and (b). There are later sulphide-free quartz veins that obliquely transect the mineralised veins. Chalcopyrite is interstitial between pyrite grains as shown in Figure 33 (c) and also occurs as inclusions in pyrite as shown in Figure 33 (d). Scattered chalcopyrite grains are common in the groundmass.

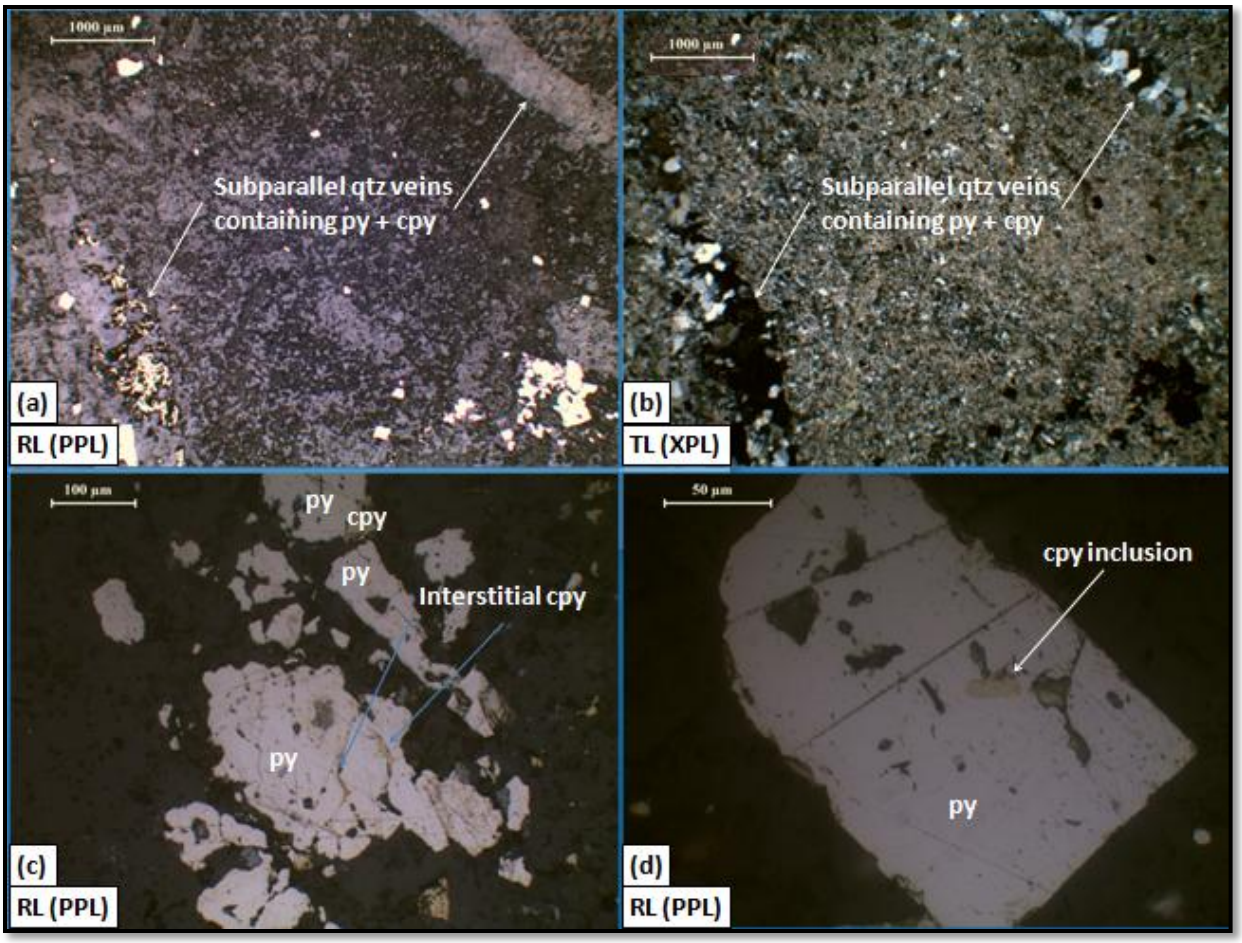

Figure 33. Microphotographs showing subparallel quartz veins containing pyrite and chalcopyrite as well as interstitial chalcopyrite and chalcopyrite inclusion in TSM08; RL=Reflected Light, TL=Transmitted Light, cpy=chalcopyrite and py=pyrite.

- **Sample Number TSM16 (Dacite)**

Thin section TSM16 comes from drill-hole ANMDD003 at a depth of 112.87 m. It is a siliceous fine-grained dacitic rock. This sample consists of heterogeneous texture. Figure 34 (a) shows a contact between a finer-grained matrix and a coarser-grained matrix. Veinlets containing quartz and sulphides crosscut the sample. These veinlets are commonly associated with pale green chlorite illustrated in Figure 34 (b), (c) and (d). Carbonate-alteration is also common in this sample.

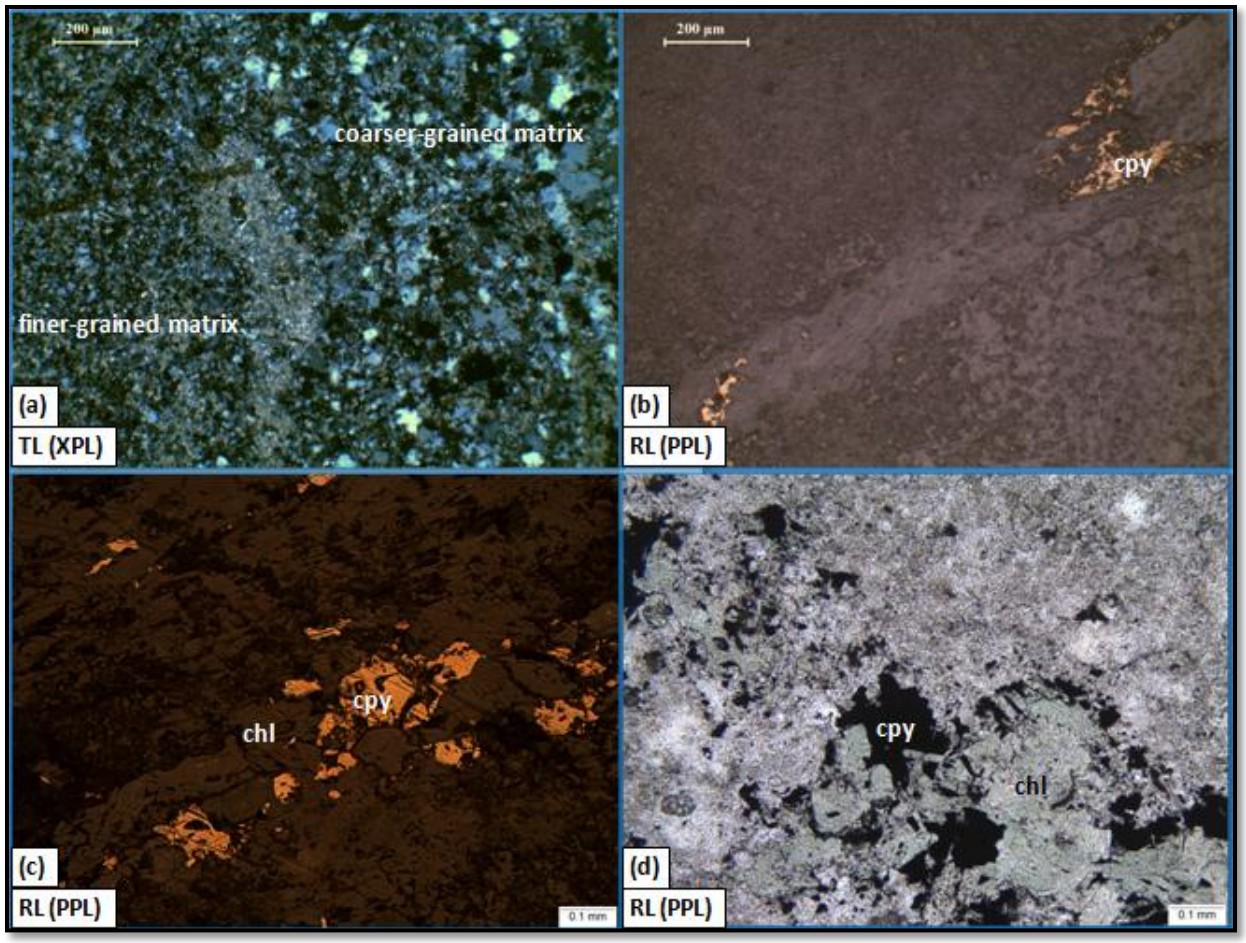

Figure 34. Microphotographs showing heterogeneous texture (a) chalcopyrite in chlorite-rich veinlets (b, c, d) in TSM16; TL=Transmitted Light, RL=Reflected Light, chl=chlorite, cpy=chalcopyrite.

8.3 Electron probe micro-analyses (EPMA)

Results from the EPMA have been subdivided into intrusive rocks and volcanic rocks. The intrusive rocks examined include micro-tonalite, micro-diorite, diorite and granodiorite. The volcanics rocks are all classified as dacites. Respective gold assay values have been included in order to relate to mineral chemistry where grains of gold were identified.

Due to the small size (close to or less than 1 micron) of the inclusions measured, composition of the inclusions could not be measured accurately. The compositions of most of these inclusions were estimated using the facility of semi-quantitative analysis attached to the WDS software. As the measured inclusion is less than the measuring spot, the measured composition frequently includes a part of the host sulphide.

8.3.1 Intrusive rocks

- **Sample Number TSM04 (Micro-tonalite, 0.182 ppm Au)**

Thin section sample TSM04 was examined using the EPMA. Anhedral chalcopyrite is present as interstitial material between pyrite grains. Figure 35 illustrates a high resolution and high contrast backscatter EPMA image showing anhedral chalcopyrite interstitial between pyrite grains.

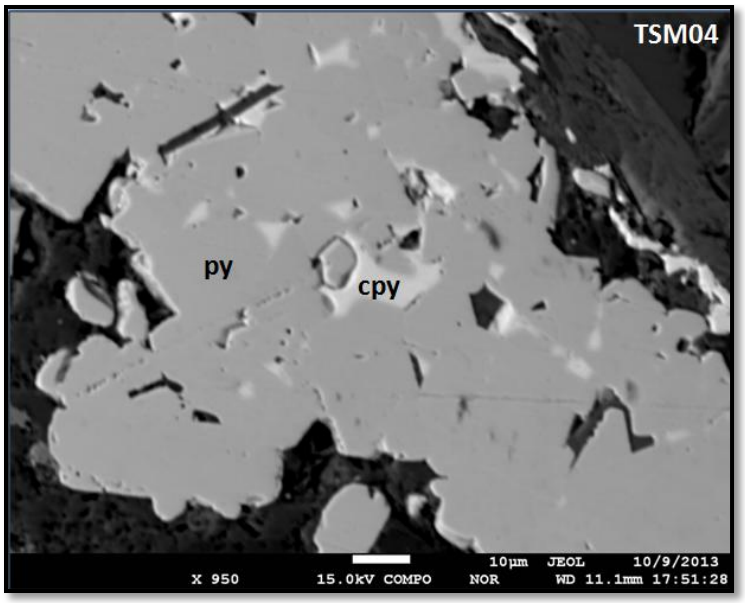

Figure 35. High contrast backscatter EPMA image showing anhedral chalcopyrite grains interstitial between pyrite grains; py=pyrite and cpy=chalcopyrite.

There are high-density minerals included in some pyrite grains of thin section sample TSM04 as shown in Figure 36. Microprobe determination of elemental concentration of these inclusions shows enrichment in Ag, Te and Se. According to the WDS semi-quantitative calculations, the inclusions are close to kurilite (Ag_8Te_3Se) composition. Figure 37 shows the elemental concentrations of the possible kurilite in the pyrite grains. The high S and Fe contents in the spectrum are attributed to the influence of the host pyrite grains.

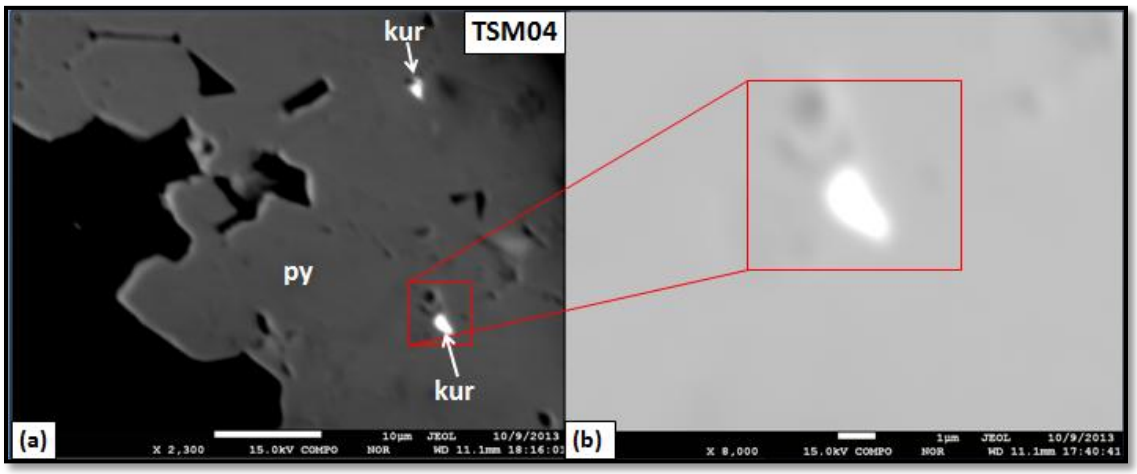

Figure 36. High resolution backscatter EPMA image of high-density inclusions in pyrite grains (a) and an enlarged image of one of the inclusions (b); kur=kurilite (Ag_8Te_3Se) and py=pyrite.

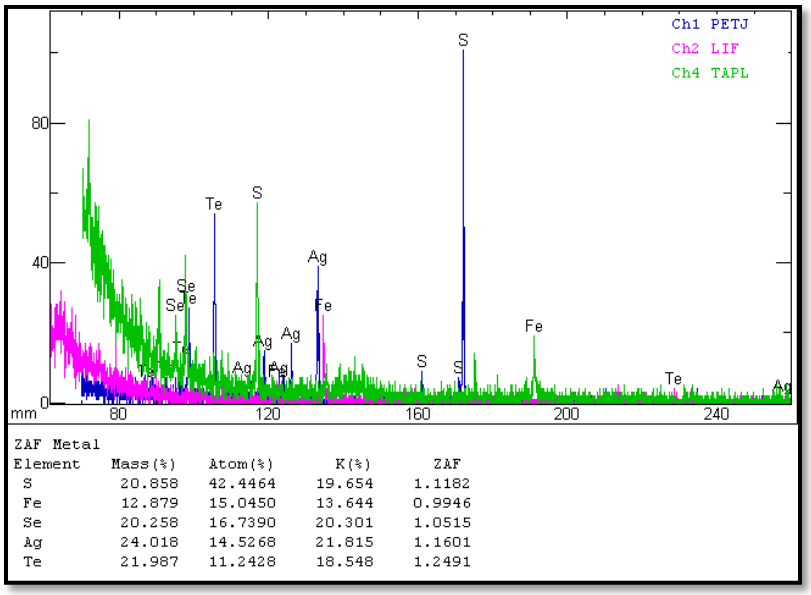

ZAF Metal

Element	Mass(%)	Atom(%)	K(%)	ZAF
S	20.858	42.4464	19.654	1.1182
Fe	12.879	15.0450	13.644	0.9946
Se	20.258	16.7390	20.301	1.0515
Ag	24.018	14.5268	21.815	1.1601
Te	21.987	11.2428	18.548	1.2491

Figure 37. Elemental concentrations in one of the kurilite (Ag_8Te_3Se) inclusions in pyrite grains.

- **Sample Number TSM09 (Micro-diorite, 7.87 ppm Au)**

Thin section sample TSM09 comes from drill-hole ANMDD002 at a depth of 82.17 m. It is a finely holocrystalline micro-diorite with occasional pyrite-chalcopyrite-bearing veins dominated by quartz and chlorite. Examination of this thin section using EPMA identified a grain of gold and a silver-bismuth-tellurium mineral inclusion in pyrite host. According to the WDS semi-quantitative calculations, the Ag-Bi-Te mineral inclusion is close to volynskite ($AgBiTe_2$) composition. The gold grain inclusion is illustrated in Figure 38 (a) while the possible volynskite inclusion is illustrated in Figure 38 (b).

The elemental composition of the gold grain was determined using WDS and the results are shown by means of a spectrum illustrated in Figure 39. This spectrum confirms that the gold is associated with silver. The Fe and S peaks in the spectrum can be attributed to the host pyrite. Figure 40 illustrates the spectrum showing elemental compositional of the possible volynskite inclusion.

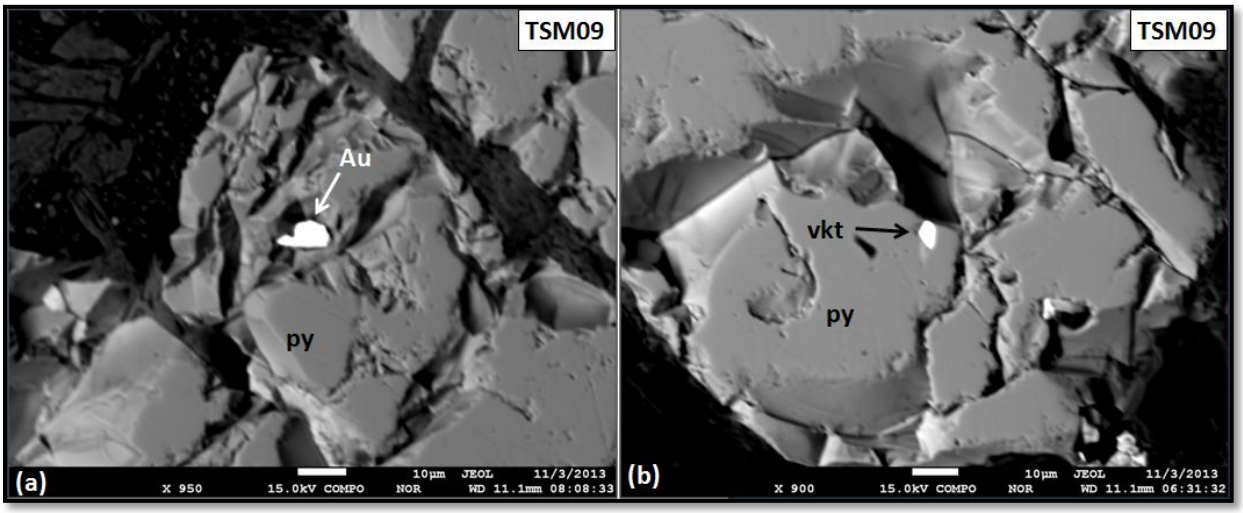

Figure 38. High contrast and high resolution backscatter EPMA images showing a gold inclusion (a) and a volynskite inclusion (b) in pyrite host in thin section sample TSM09; Au=gold, py=pyrite, vkt=volynskite ($AgBiTe_2$).

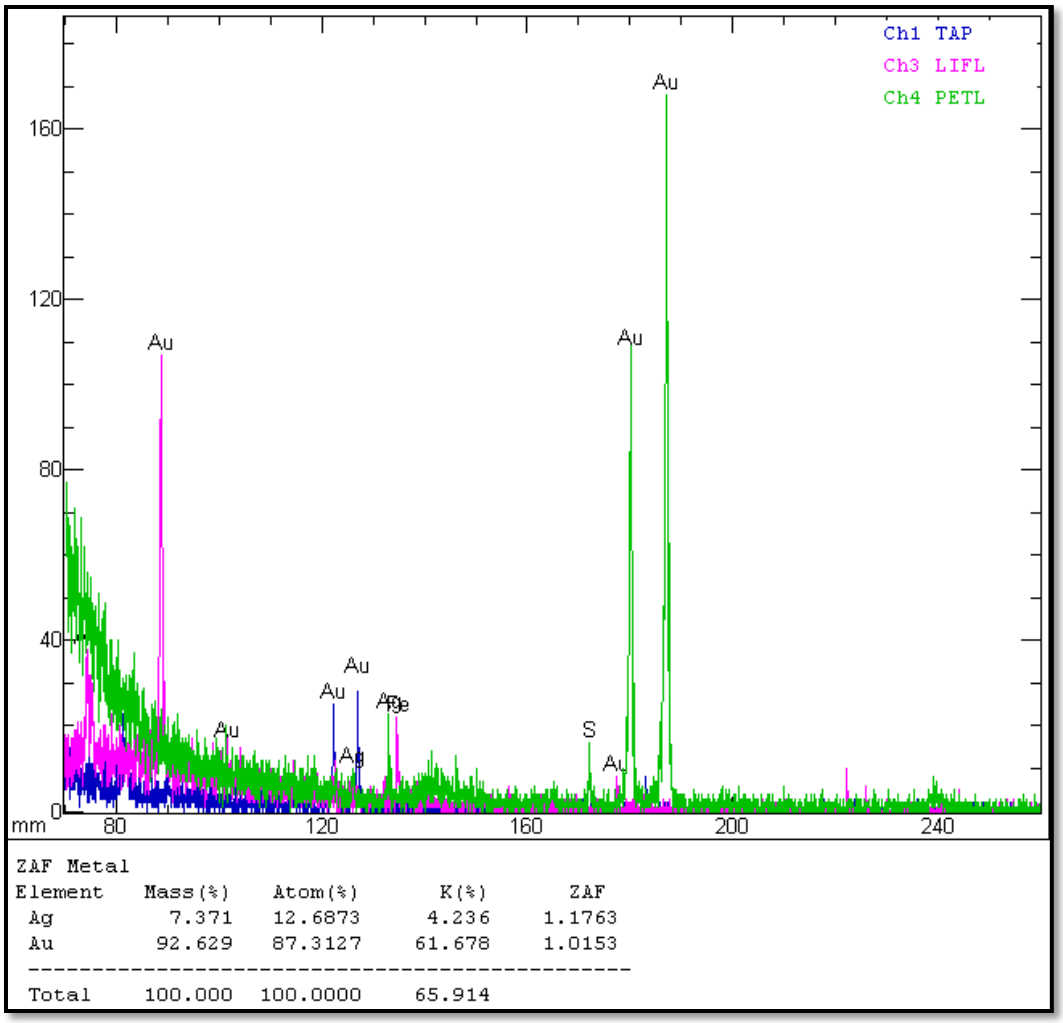

ZAF Metal

Element	Mass(%)	Atom(%)	K(%)	ZAF
Ag	7.371	12.6873	4.236	1.1763
Au	92.629	87.3127	61.678	1.0153
Total	100.000	100.0000	65.914	

Figure 39. Spectrum showing elemental concentrations of a gold grain included in a pyrite grain in thin section sample TSM09.

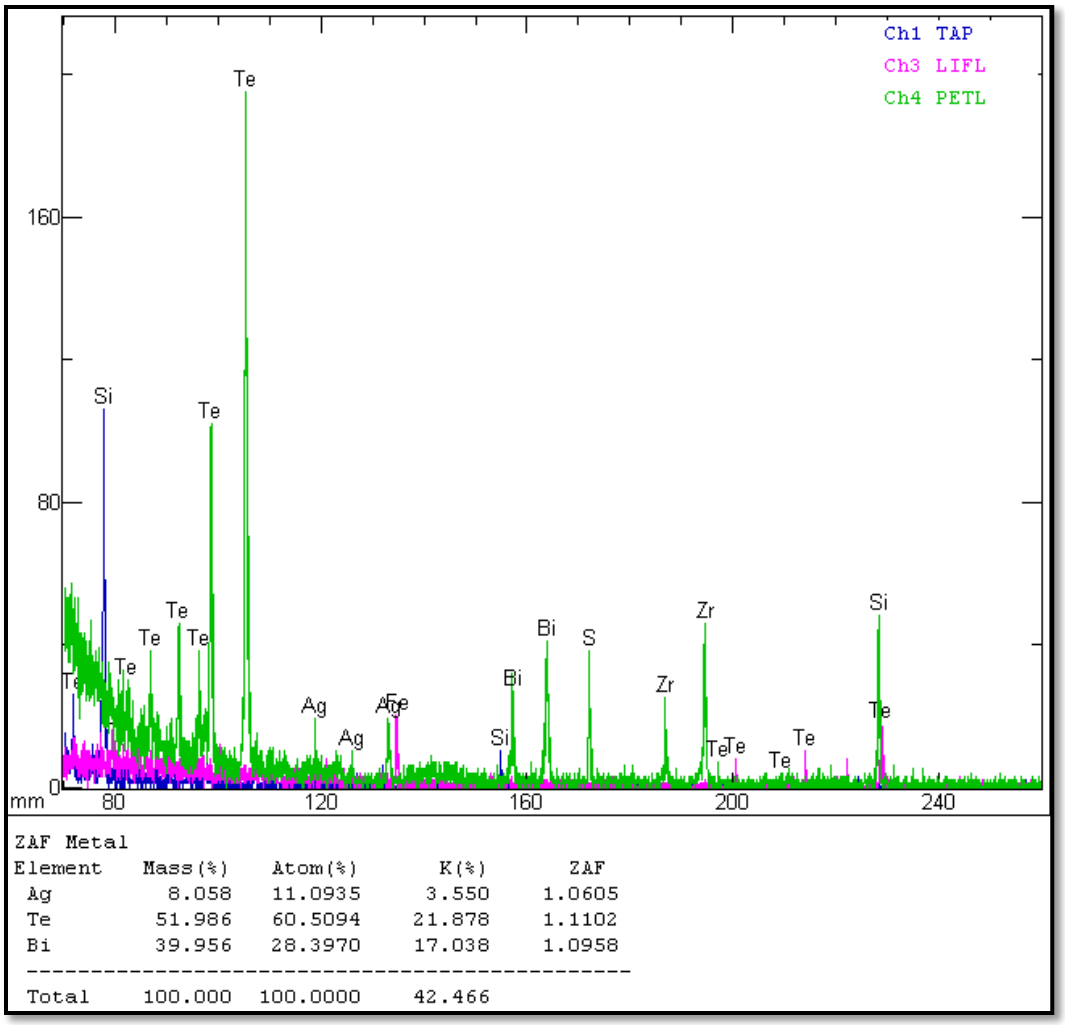

ZAF Metal

Element	Mass(%)	Atom(%)	K(%)	ZAF
Ag	8.058	11.0935	3.550	1.0605
Te	51.986	60.5094	21.878	1.1102
Bi	39.956	28.3970	17.038	1.0958
Total	100.000	100.0000	42.466	

Figure 40. Spectrum showing elemental concentrations of a volynskite ($AgBiTe_2$) included in a pyrite in thin section sample TSM09.

Further examination of TSM09 identified several bismuth telluride mineral inclusions in the pyrite host as illustrated in Figure 41 (a) and (b). Figure 41 (b) is an enlargement of the area enclosed by a red rectangle in Figure 41 (a). According to the WDS semi-quantitative calculations, the Bi-Te mineral inclusion is close to tellurobismuthite (Bi_2Te_3) composition. A Spectrum showing elemental concentrations of one of the tellurobismuthite inclusions is illustrated in Figure 42.

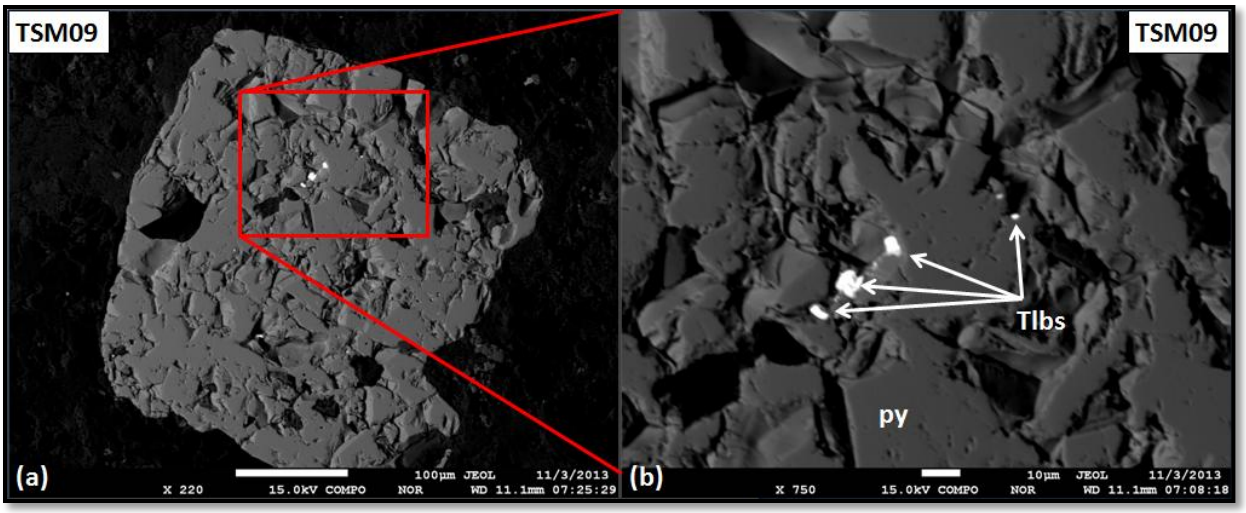

Figure 41. High contrast and high resolution backscatter images showing tellurobismuthite inclusions in a pyrite host; py=pyrite, Tlbs=tellurobismuthite (Bi_2Te_3).

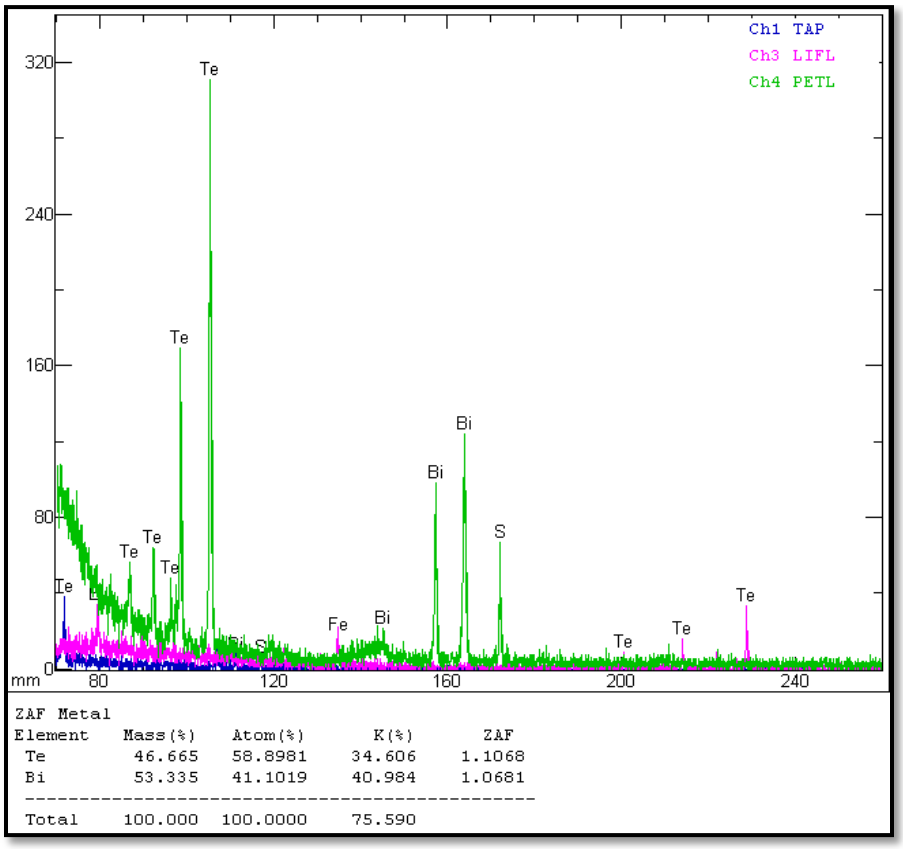

Figure 42. Spectrum showing elemental concentrations of one of the tellurobismuthite (Bi_2Te_3) inclusions in the pyrite host in thin section sample TSM09.

- **Sample Number TSM21 (Diorite, 0.927 ppm Au)**

Examination of thin section TSM21 using the EPMA under high resolution identified an approximately 3 µm long gold inclusion in a porous pyrite grain as illustrated in Figure 43 (a) and (b); Figure 43 (b) is an enlargement of an area enclosed by a red box in Figure 43 (a).

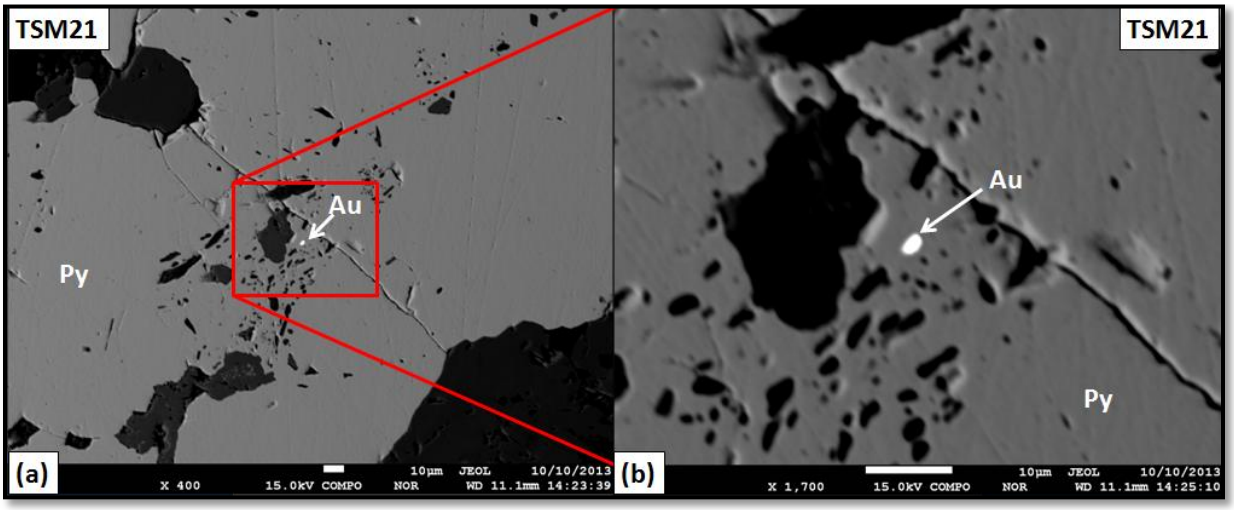

Figure 43. High contrast and high resolution backscatter EPMA images showing a gold inclusion in a porous pyrite grain in thin section sample TSM21; Au=gold, Py=pyrite.

The gold grain contains minor silver as shown by the elemental concentration spectrum in Figure 44. Fe and S peaks in the spectrum are attributed to the pyrite hosting the gold grain.

Also included in the pyrite grains in thin section sample TSM21 are grains of a mineral containing elements tellurium and bismuth. According to the WDS semi-quantitative calculations, the inclusion is close to tellurobismuthite (Bi_2Te_3) composition. Figure 45 illustrates the possible tellurobismuthite grains included in the pyrite grain while Figure 46 shows the elemental concentration of the tellurobismuthite grains. The Fe and S peaks shown in the spectrum are a result of the influence of the hosting pyrite grain.

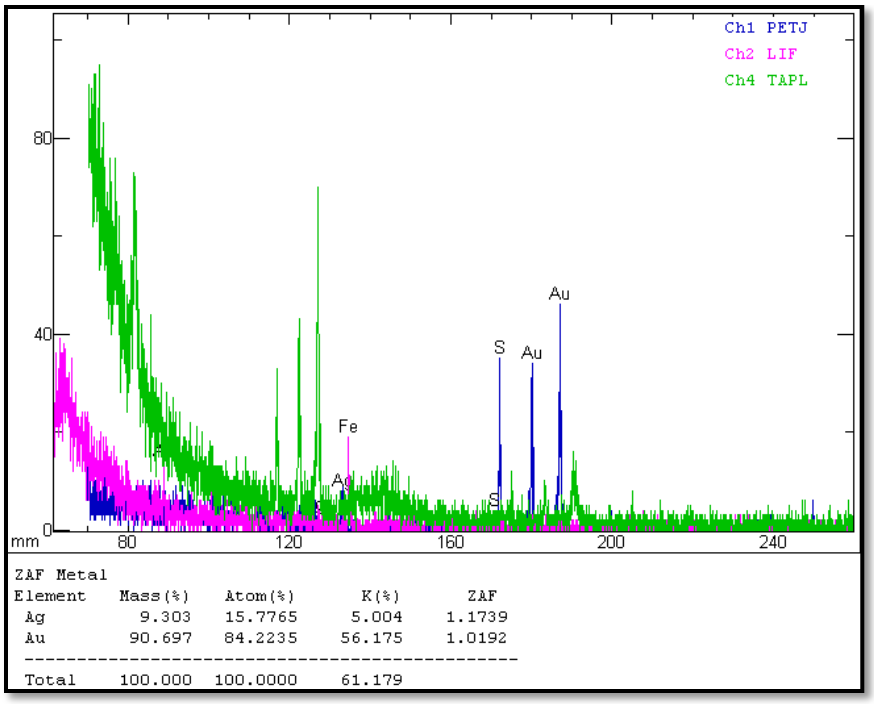

Figure 44. Spectrum showing elemental concentration of a gold grain included in a pyrite grain in this section sample TSM21.

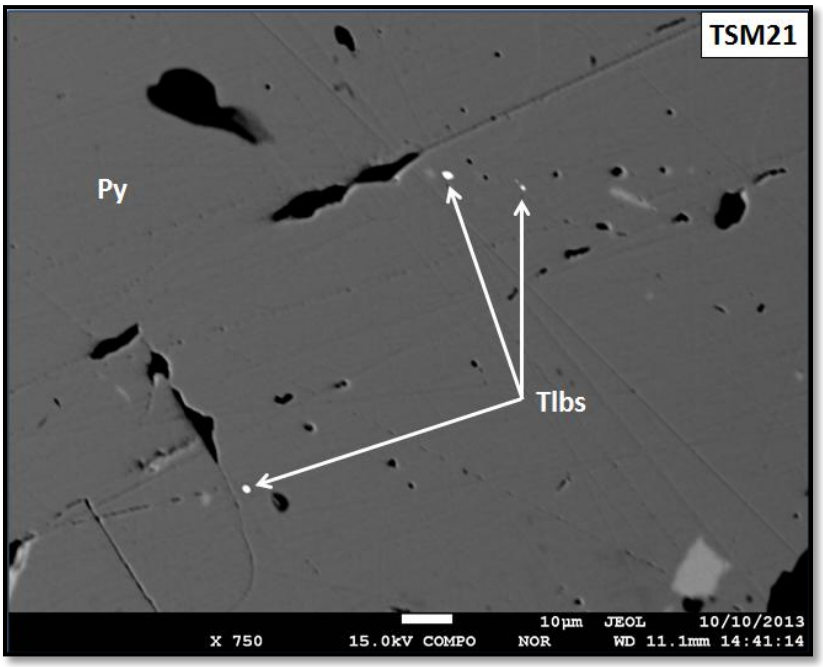

Figure 45. High resolution backscatter EPMA image showing tellurobismuthite inclusions in a pyrite grain in thin section sample TSM21; Py=pyrite, Tlbs=tellurobismuthite (Bi_2Te_3).

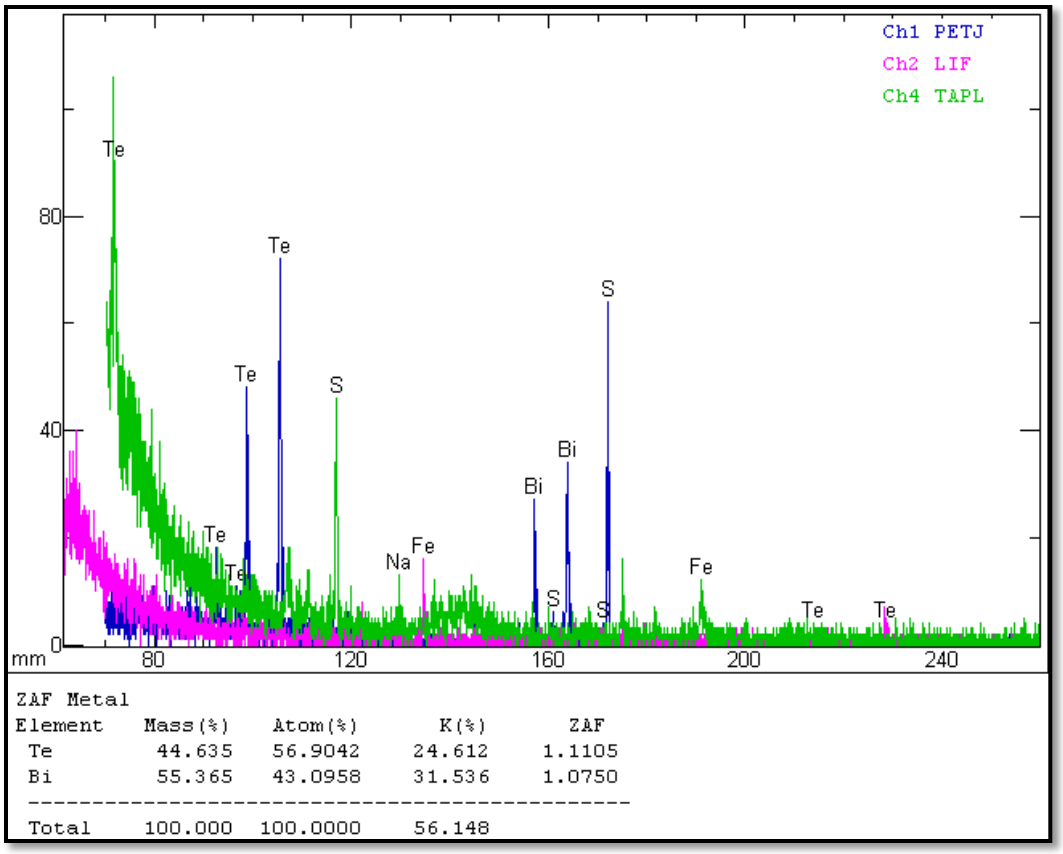

Figure 46. Spectrum showing the elemental concentrations of tellurobismuthite (Bi_2Te_3) grains included in a pyrite grain in thin section sample TSM21.

- **Sample Number TSM26 (Granodiorite, 2.18 ppm Au)**

EPMA was utilised to examine points selected from thin section sample TSM26. Elongate gold grains were identified as inclusions in pyrite grains. The gold grains appear to follow vein-like preferred orientations as illustrated in Figure 47 (a) and (b); Figure 47 (b) is an enlargement of the area marked by a red box in Figure 47 (a). Two distinct orientations that are oblique to each other are apparent.

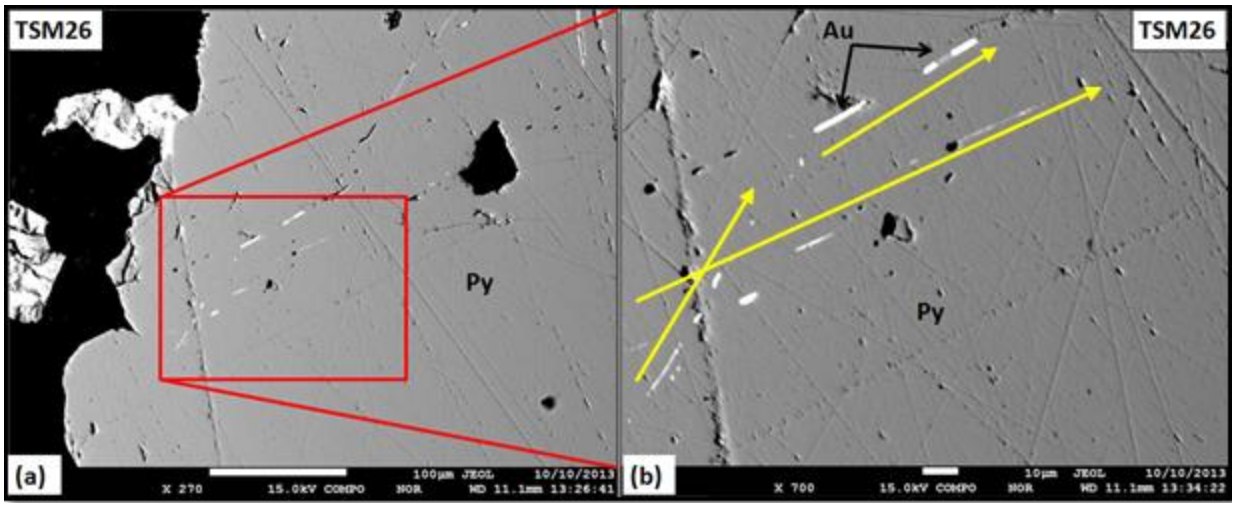

Figure 47. High resolution and high contrast EPMA images showing elongate gold grains included in pyrite grains in thin section sample TSM26; Py=pyrite, Au=gold. The two distinct orientations of gold grains are shown by the yellow arrows in (b).

The elemental compositions of the gold grains were determined using WDS and the results are shown by means of a spectrum illustrated in Figure 48. This spectrum confirms that the gold is associated with silver approximately in equal proportions. The Fe and S peaks in the spectrum can be attributed to the host pyrite.

Further examination of the points selected from thin section sample TSM26 showed that not all inclusions of high-density minerals in the pyrite grains are gold and silver. One such inclusion contained tellurium and bismuth and was identified as possible tellurobismuthite. Another inclusion contained bismuth, tellurium, selenium and sulphur and was identified as possibly kawazulite, $Bi_2(Te, Se, S)_3$. Figure 49 illustrates the tellurobismuthite and kawazulite inclusions in a pyrite grain in thin section sample TSM26. Similar to the gold and silver grains, these inclusions are elongate in shape. Elemental compositions of the tellurobismuthite and kawazulite grains were estimated based on the WDS and the results are represented by spectrums illustrated in Figure 50 and Figure 51 respectively. The Fe and S peaks in Figure 50 can be attributed to the host pyrite. However, the S peak in Figure 51 can be attributed to a combination of both the host pyrite and the kawazulite inclusion.

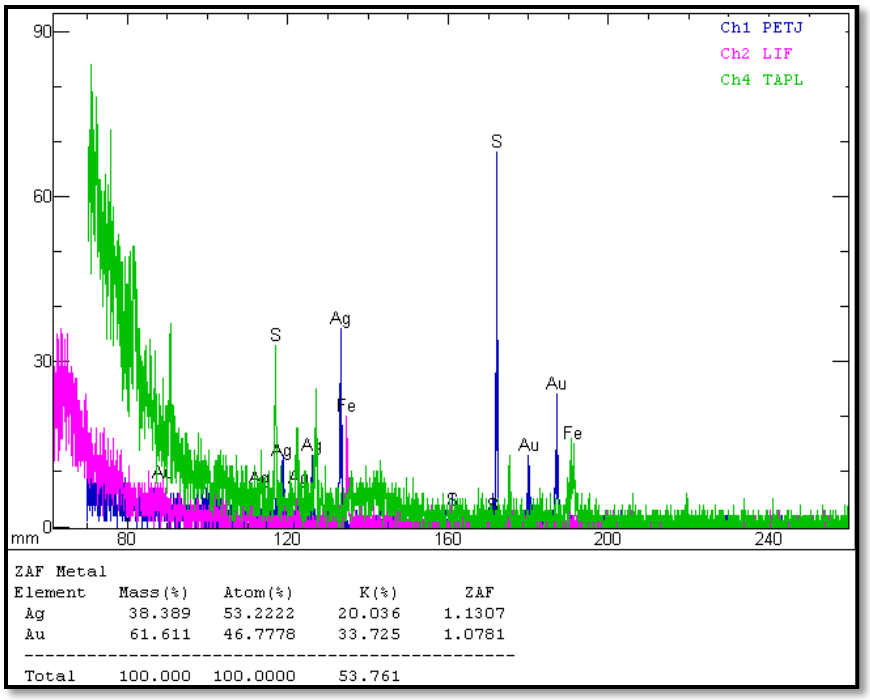

Figure 48. Spectrum showing elemental concentrations for a gold grain included in a pyrite grain in thin section sample TSM26.

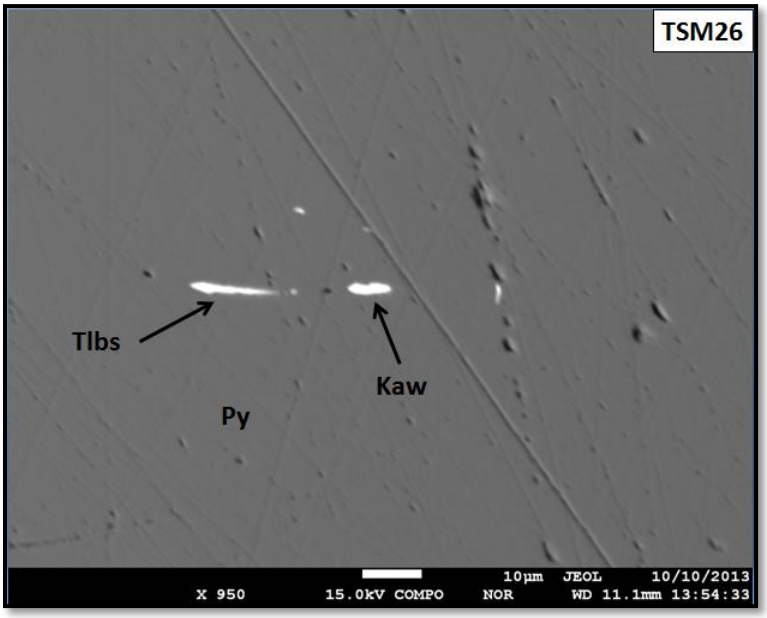

Figure 49. High resolution and high contrast EPMA image showing tellurobismuthite and kawazulite inclusions in a pyrite grain in thin section sample TSM26; Tlbs=tellurobismuthite (Bi_2Te_3), Kaw=kawazulite [$Bi_2(Te, Se, S)_3$], Py=pyrite.

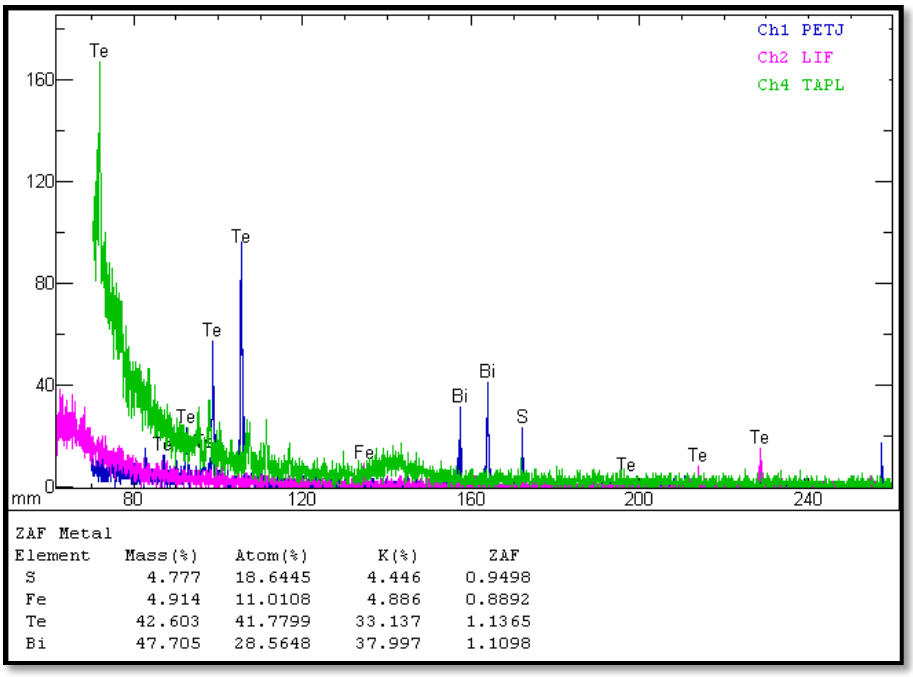

ZAF Metal

Element	Mass(%)	Atom(%)	K(%)	ZAF
S	4.777	18.6445	4.446	0.9498
Fe	4.914	11.0108	4.886	0.8892
Te	42.603	41.7799	33.137	1.1365
Bi	47.705	28.5648	37.997	1.1098

Figure 50. Spectrum showing elemental concentrations for tellurobismuthite (Bi_2Te_3) inclusion in a pyrite grain in thin section TSM26.

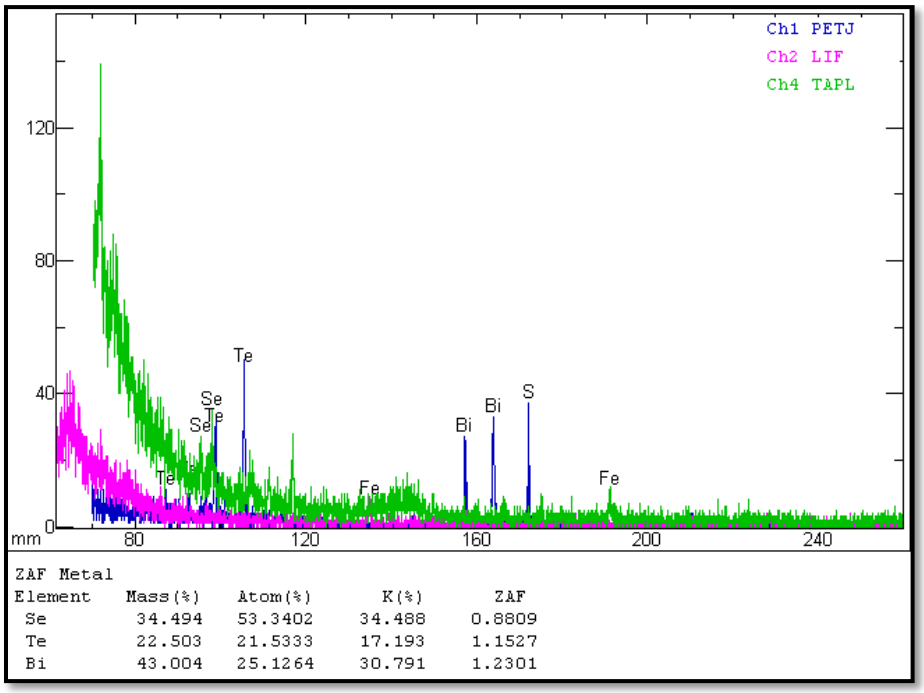

ZAF Metal

Element	Mass(%)	Atom(%)	K(%)	ZAF
Se	34.494	53.3402	34.488	0.8809
Te	22.503	21.5333	17.193	1.1527
Bi	43.004	25.1264	30.791	1.2301

Figure 51. Spectrum showing elemental concentrations for kawazulite [Bi_2(Te, Se, S)$_3$] inclusion in a pyrite grain in thin section sample TSM26.

- **Sample Number TSM27 (Micro-diorite, 11.20 ppm Au)**

Examination of thin section sample TSM27 by the EPMA identified anhedral chalcopyrite and euhedral magnetite inclusions in chlorite as illustrated in Figure 52. Although this sample contains a high gold assay value no grains of gold could be found using the EPMA.

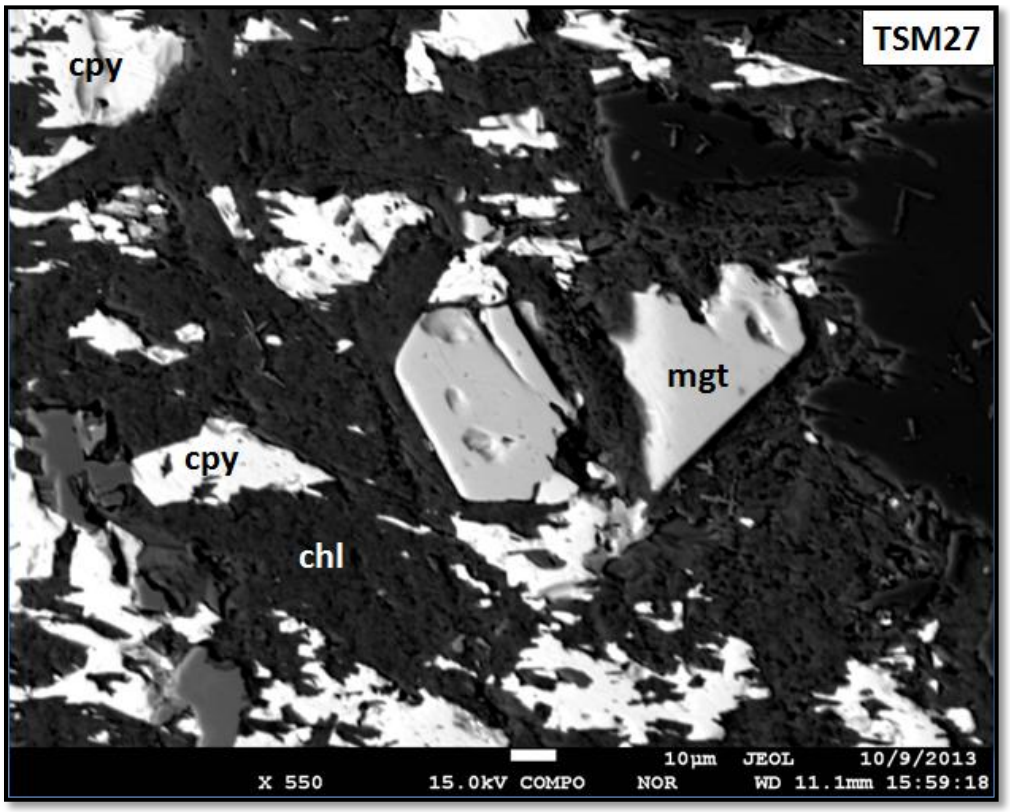

Figure 52. High resolution and high contrast EPMA image showing anhedral chalcopyrite and magnetite inclusions in chlorite in thin section TSM27; cpy=chalcopyrite, chl=chlorite, mgt=magnetite.

8.3.2 Volcanic rocks

- **Sample Number TSM08 (Dacite, 0.483 ppm Au)**

A few points on thin section sample TSM08 were selected for examination by the EPMA. Pyrite grains appear porous and host various inclusions that include sulphides and silicates. Figure 53 illustrates high resolution and high contrast backscatter EPMA images of the various inclusions

hosted in pyrite grains. Sulphide inclusions are galena and chalcopyrite. Silicate inclusions include sericite and sphene. A high-density mineral containing Pb, Bi, Se and S (possibly wittite, $Pb_3Bi_4S_6Se_3$) was also found as an inclusion in the pyrite grains.

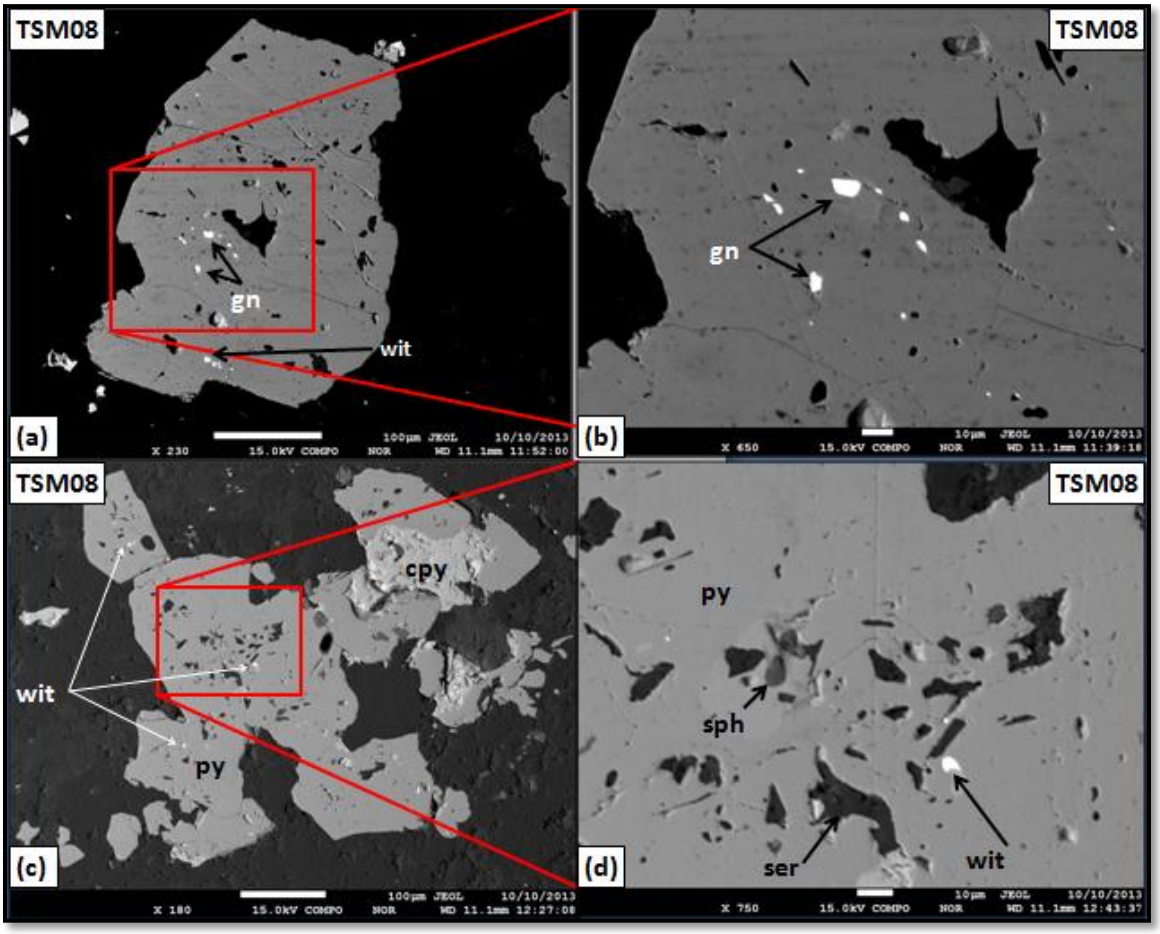

Figure 53. High resolution backscatter EPMA images showing inclusions in porous pyrite grains: galena in (a) and (b), wittite in (a), (c) and (d), chalcopyrite in (c), sphene in (d) and sericite in (c) and (d); cpy=chalcopyrite, gn=galena, py=pyrite, ser=sericite, sph=sphene, wit=wittite ($Pb_3Bi_4S_6Se_3$)

The elemental concentrations of the possible wittite in thin section sample TSM08 are shown in Figure 54.

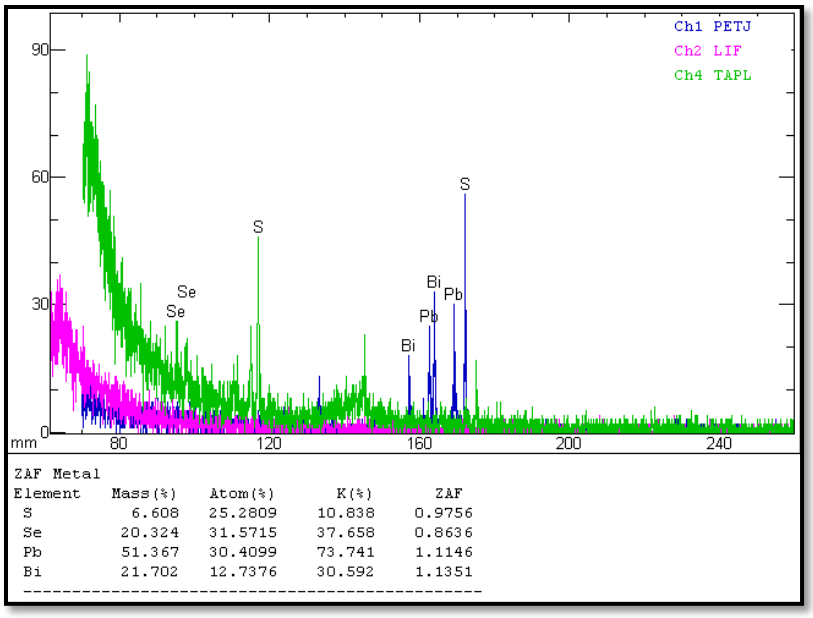

ZAF Metal

Element	Mass(%)	Atom(%)	K(%)	ZAF
S	6.608	25.2809	10.838	0.9756
Se	20.324	31.5715	37.658	0.8636
Pb	51.367	30.4099	73.741	1.1146
Bi	21.702	12.7376	30.592	1.1351

Figure 54. Spectrum showing elemental concentration of wittite ($Pb_3Bi_4S_6Se_3$) included in a pyrite grain in thin section sample TSM08.

Monazite was also found as an inclusion in pyrite grains of thin section TSM08 as illustrated in Figure 55. The elemental concentration of the monazite is shown in Figure 56.

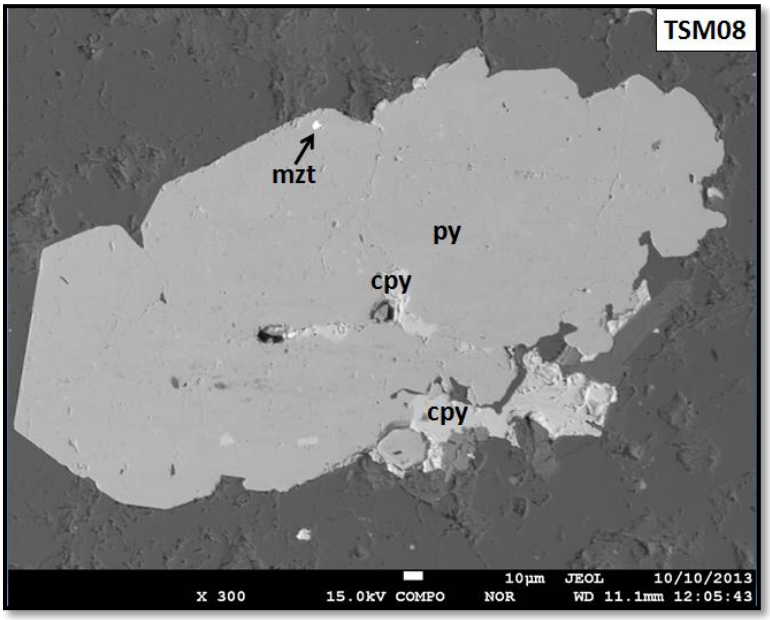

Figure 55. Backscatter EPMA image showing monazite and chalcopyrite inclusions in a pyrite grain in thin section sample TSM08; cpy=chalcopyrite, mzt=monazite, py=pyrite.

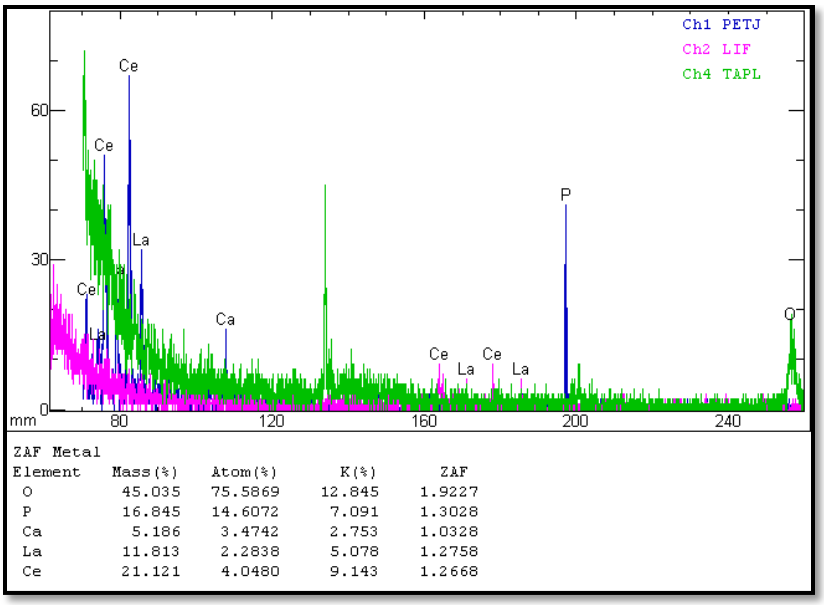

ZAF Metal

Element	Mass(%)	Atom(%)	K(%)	ZAF
O	45.035	75.5869	12.845	1.9227
P	16.845	14.6072	7.091	1.3028
Ca	5.186	3.4742	2.753	1.0328
La	11.813	2.2838	5.078	1.2758
Ce	21.121	4.0480	9.143	1.2668

Figure 56. Elemental concentrations for monazite inclusion in a pyrite grain in thin section TSM08.

- **Sample Number TSM23 (Dacite, 10.95 ppm Au)**

TSM23, from drill-hole ANMDD003 at a depth of 172.36 m, is a dacitic volcanic rock. Examination by EPMA identified tellurobismuthite inclusions in pyrite grains as illustrated in Figure 57. The elemental spectrum for one of the inclusions is illustrated in Figure 58. Although the sample has a high gold assay value, no grains of gold were found in this sample.

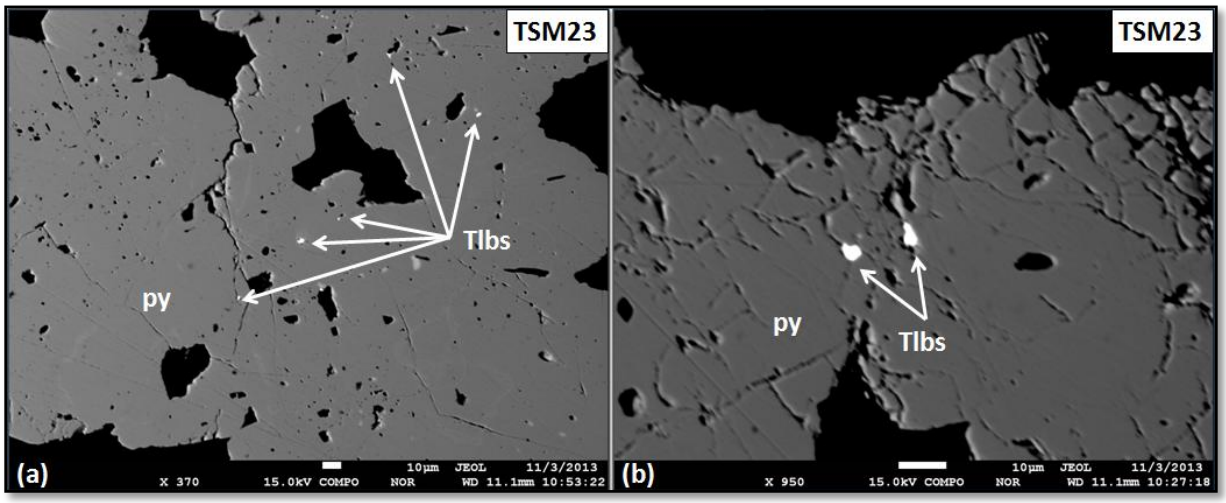

Figure 57. High contrast and high resolution backscatter EPMA images showing tellurobismuthite inclusions in pyrite grains in TSM23; py=pyrite, Tlbs=tellurobismuthite (Bi_2Te_3).

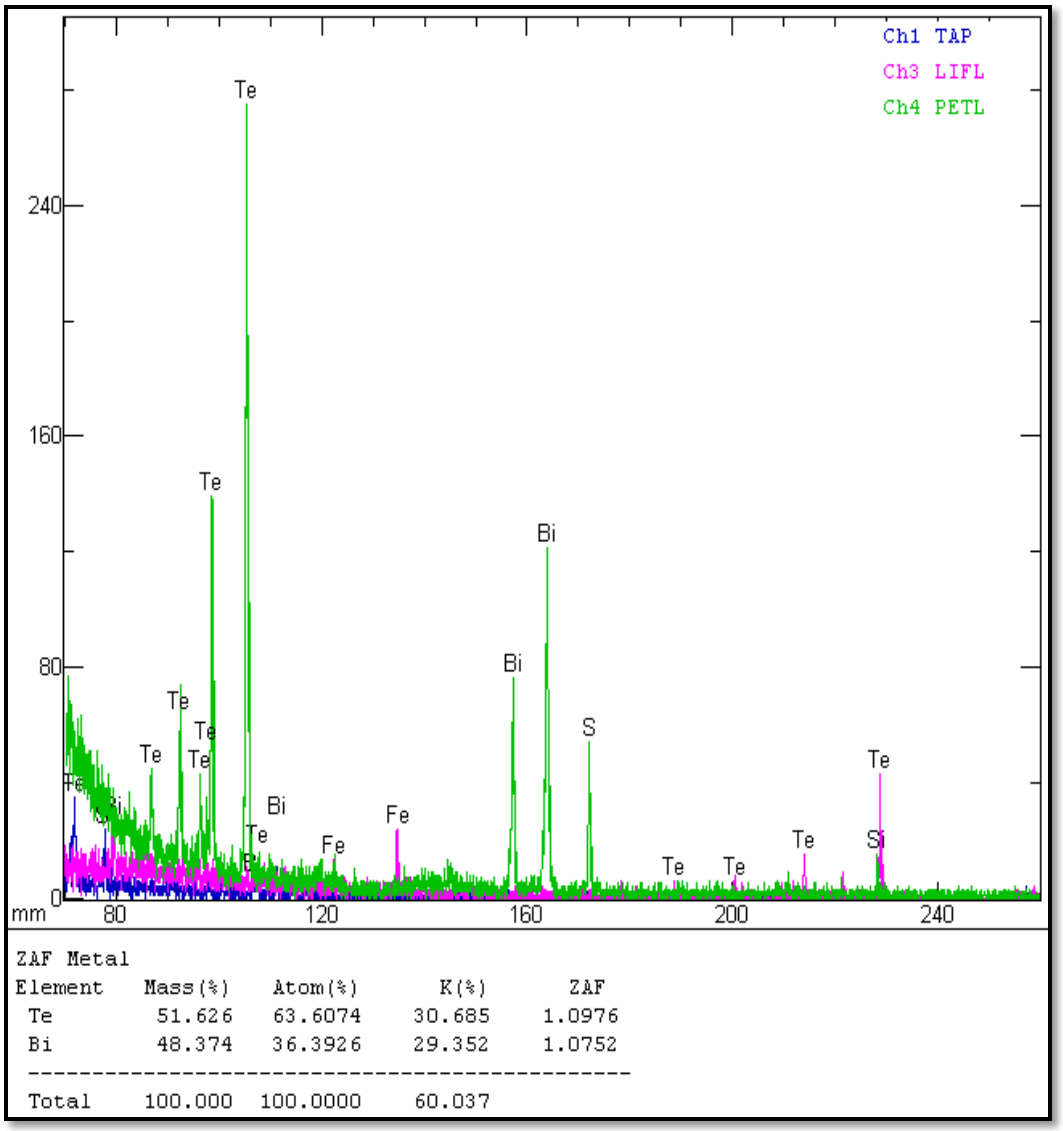

Figure 58. Spectrum showing elemental concentrations of one of the tellurobismuthite.

- **Sample Number TSM25 (Dacite, 2.73 ppm Au)**

Thin section sample TSM25 was examined using EPMA. Anhedral chalcopyrite grains were identified interstitial between epidote and quartz grains as illustrated by the high resolution backscatter EPMA image in Figure 59. WDS was utilised to determine elemental composition of the anhedral chalcopyrite and the epidote. Spectrums showing elemental concentrations of the anhedral chalcopyrite and the epidote identified in this thin section sample are shown in Figure 60 and Figure 61 respectively.

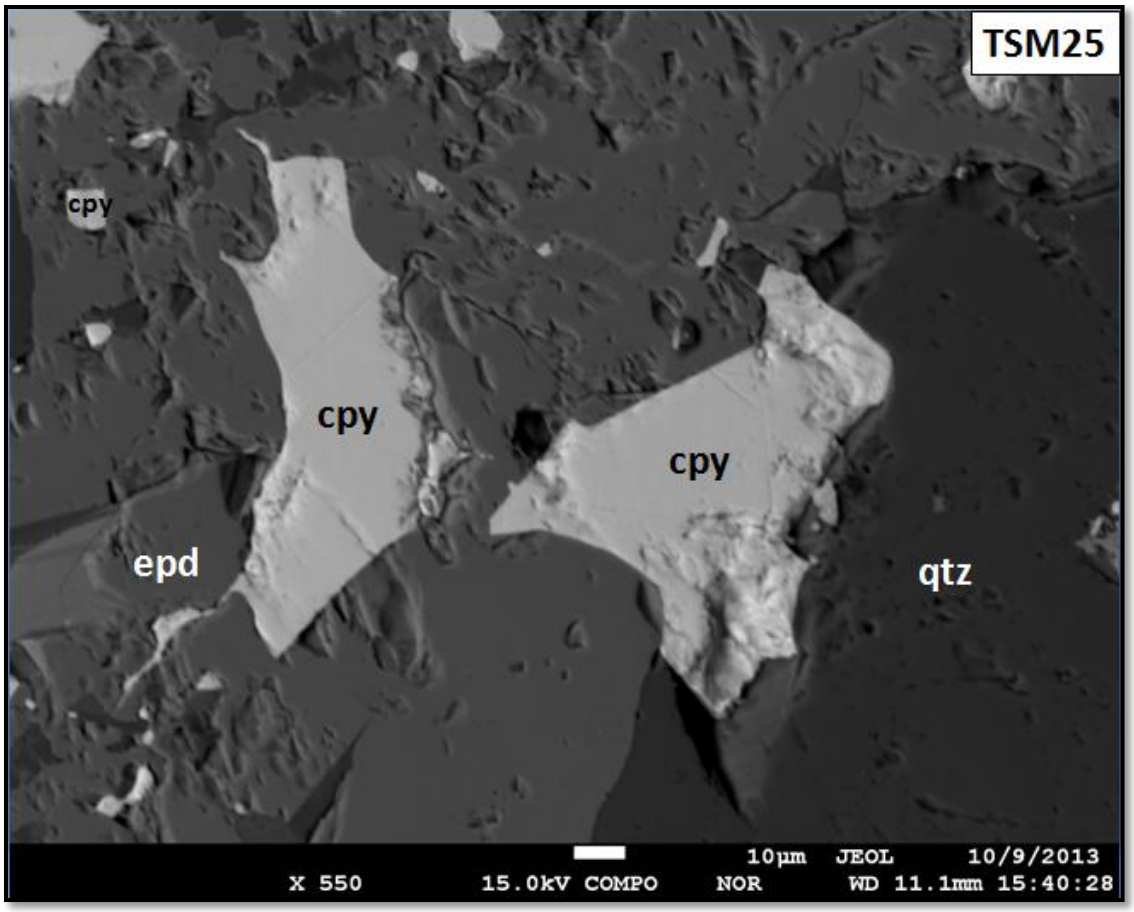

Figure 59. High contrast and high resolution backscatter EPMA image showing anhedral chalcopyrite grains interstitial between epidote and quartz grains; cpy=chalcopyrite, epd=epidote, qtz=quartz.

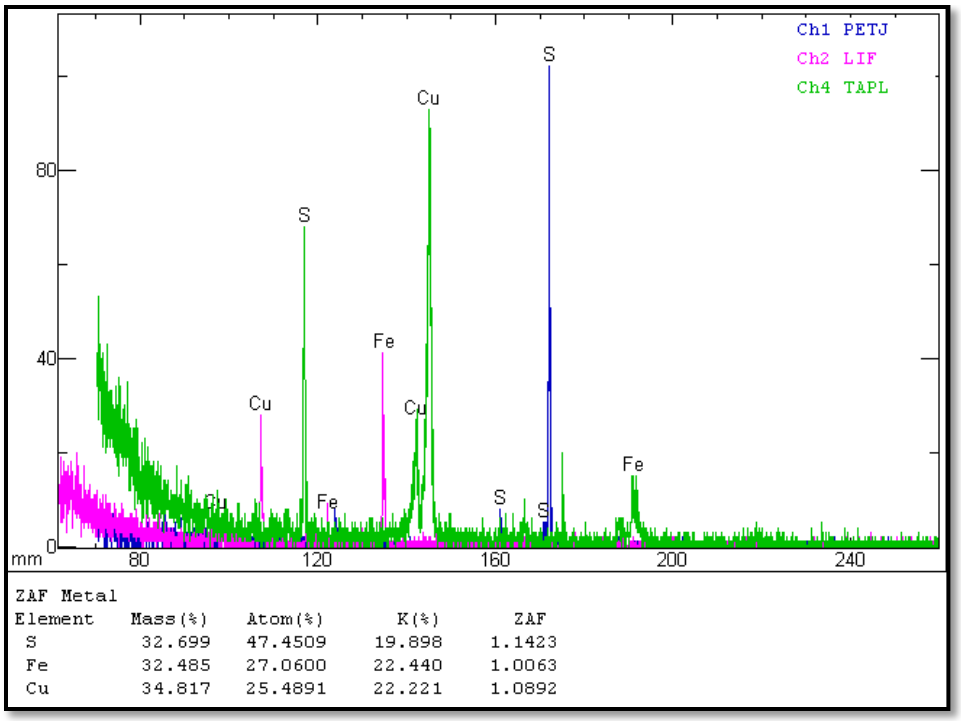

ZAF Metal

Element	Mass(%)	Atom(%)	K(%)	ZAF
S	32.699	47.4509	19.898	1.1423
Fe	32.485	27.0600	22.440	1.0063
Cu	34.817	25.4891	22.221	1.0892

Figure 60. Spectrum showing elemental concentrations for anhedral chalcopyrite interstitial between epidote and quartz grains.

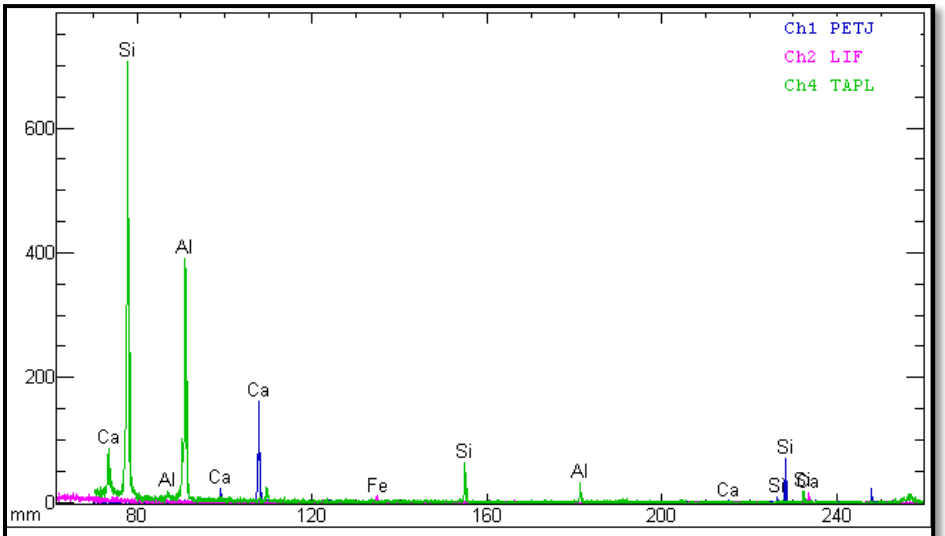

ZAF Metal

Element	Mass(%)	Atom(%)	K(%)	ZAF
Al	12.235	16.2349	4.959	1.3245
Si	21.745	27.7154	9.104	1.2822
Ca	54.434	48.6224	28.141	1.0384
Fe	11.587	7.4273	5.472	1.1367

Figure 61. Spectrum of elemental concentration for epidote identified in thin section sample TSM25

8.4 Structural analysis

Stereonet projections were employed to represent composite structural readings for quartz-pyrite veins, pyrite veins and epidote veins in drill-holes ANMDD001-004. The structural readings for the veins are presented in strike/dip notation and the stereoplots were generated in equal area projection and in lower hemisphere.

Structural measurements for the quartz-pyrite veins are shown in Table 6 and the corresponding equal area, lower hemisphere stereoplot is illustrated in Figure 62. The mean principal orientation of the quartz-pyrite veins is 304/54.

Table 6. Structural readings for quartz-pyrite veins in Masumbi drill-holes ANMDD001-004

HOLEID	Strike	Dip	HOLEID	Strike	Dip	HOLEID	Strike	Dip
ANMDD001	277	71	ANMDD002	283	70	ANMDD003	288	74
ANMDD001	306	47	ANMDD002	133	84	ANMDD003	282	57
ANMDD001	278	67	ANMDD002	306	84	ANMDD003	280	70
ANMDD001	314	89	ANMDD002	273	68	ANMDD003	304	72
ANMDD001	310	46	ANMDD002	298	57	ANMDD004	108	11
ANMDD001	315	42	ANMDD002	275	67	ANMDD004	358	61
ANMDD001	32	20	ANMDD002	133	85	ANMDD004	2	38
ANMDD001	302	51	ANMDD002	98	89	ANMDD004	343	51
ANMDD001	279	76	ANMDD002	274	52	ANMDD004	305	16
ANMDD001	301	71	ANMDD002	288	61	ANMDD004	324	32
ANMDD001	303	76	ANMDD002	279	63	ANMDD004	323	63
ANMDD001	294	50	ANMDD002	302	44	ANMDD004	299	64
ANMDD001	282	43	ANMDD002	284	59	ANMDD004	1	36
ANMDD001	275	45	ANMDD002	280	63	ANMDD004	338	32
ANMDD001	308	48	ANMDD002	254	15	ANMDD004	348	27
ANMDD002	302	70	ANMDD002	38	15	ANMDD004	358	31
ANMDD002	285	58	ANMDD002	319	67	ANMDD004	6	37
ANMDD002	305	23	ANMDD002	310	62	ANMDD004	346	27
ANMDD002	212	88	ANMDD002	308	63	ANMDD004	322	45
ANMDD002	319	83	ANMDD002	317	73	ANMDD004	311	36
ANMDD002	302	86	ANMDD003	324	41	ANMDD004	321	39
ANMDD002	291	67	ANMDD003	304	72	ANMDD004	326	38
ANMDD002	130	89	ANMDD003	323	53	ANMDD004	316	38
ANMDD002	301	66	ANMDD003	312	52			
ANMDD002	132	81	ANMDD003	308	55			

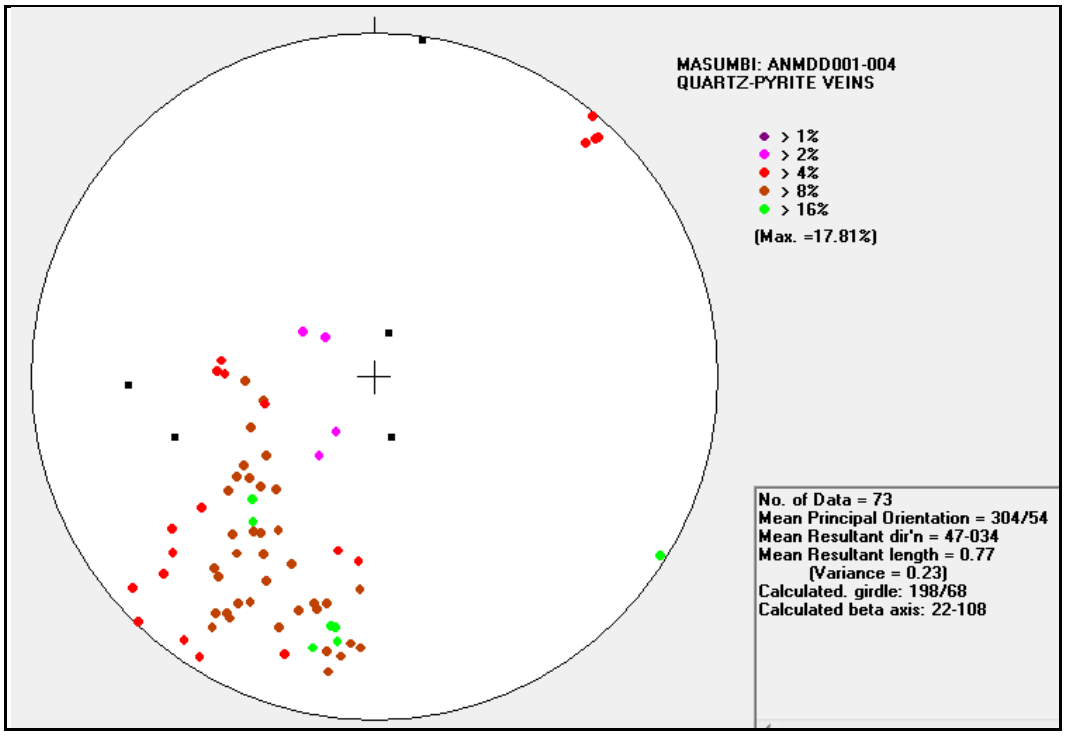

Figure 62. Equal area projection, lower hemisphere stereoplot for quartz-pyrite veins in ANMDD001-004.

Table 7 and Figure 63 show structural measurements for the pyrite veins and the corresponding equal area, lower hemisphere stereoplot respectively. The mean principal orientation of the pyrite veins is 322/46. Structural readings for the epidote veins are shown in Table 8 and illustrated in Figure 64. The mean principal orientation of the epidote veins is 308/68.

Table 7. Structural readings for pyrite veins in Masumbi drill-holes ANMDD001-004

HOLEID	Strike	Dip	HOLEID	Strike	Dip
ANMDD001	352	59	ANMDD003	333	21
ANMDD001	294	50	ANMDD003	351	48
ANMDD001	280	62	ANMDD003	343	67
ANMDD001	336	45	ANMDD003	339	50
ANMDD001	320	55	ANMDD003	335	48
ANMDD001	294	75	ANMDD003	299	54
ANMDD002	303	28	ANMDD004	331	11

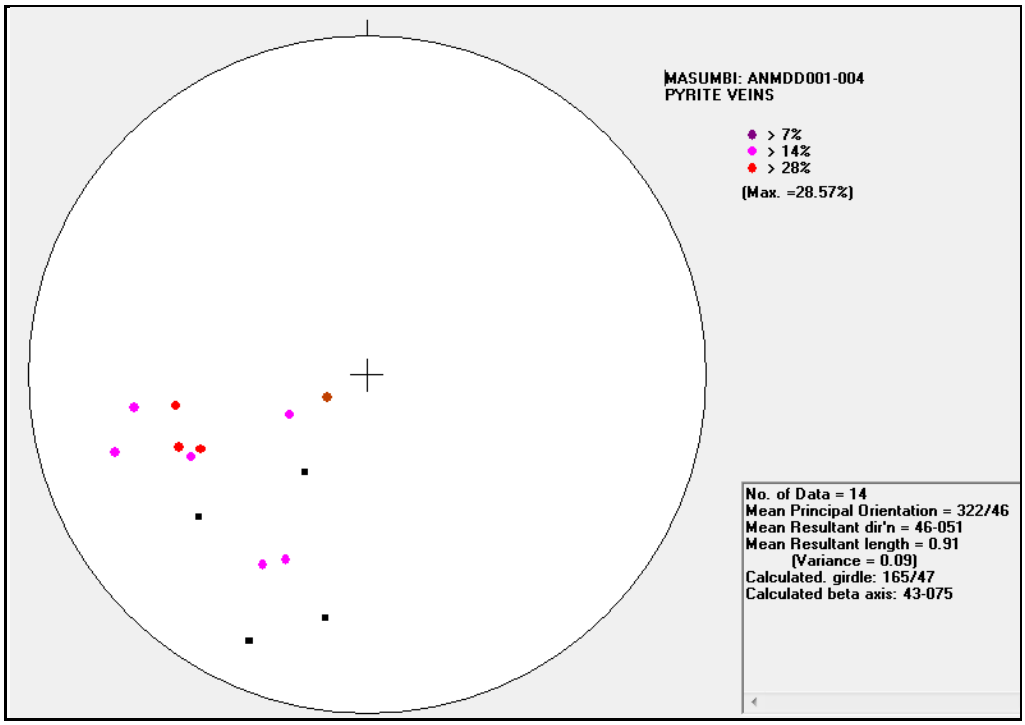

Figure 63. Equal area projection, lower hemisphere stereoplot for pyrite veins in ANMDD001-004.

Table 8. Structural readings for epidote veins in Masumbi drill-holes ANMDD001-004

HOLEID	Strike	Dip	HOLEID	Strike	Dip	HOLEID	Strike	Dip
ANMDD001	284	67	ANMDD002	311	84	ANMDD004	10	84
ANMDD001	172	33	ANMDD002	292	74	ANMDD004	10	21
ANMDD001	282	59	ANMDD002	150	76	ANMDD004	98	50
ANMDD001	138	84	ANMDD002	304	80	ANMDD004	345	51
ANMDD001	280	83	ANMDD002	305	72	ANMDD004	202	79
ANMDD001	281	74	ANMDD002	296	79	ANMDD004	316	63
ANMDD001	292	60	ANMDD002	142	75	ANMDD004	328	50
ANMDD001	313	83	ANMDD002	292	79	ANMDD004	190	14
ANMDD002	278	75	ANMDD003	256	69	ANMDD004	304	76
ANMDD002	301	88	ANMDD003	91	27	ANMDD004	304	61
ANMDD002	239	59	ANMDD003	47	58	ANMDD004	331	31
ANMDD002	307	63	ANMDD003	41	38	ANMDD004	324	78
ANMDD002	148	68	ANMDD004	248	88	ANMDD004	347	64
ANMDD002	316	65	ANMDD004	208	89	ANMDD004	353	58
ANMDD002	307	85	ANMDD004	237	89	ANMDD004	344	44
ANMDD002	304	61	ANMDD004	39	53	ANMDD004	77	89
ANMDD002	17	70	ANMDD004	359	46	ANMDD004	262	29

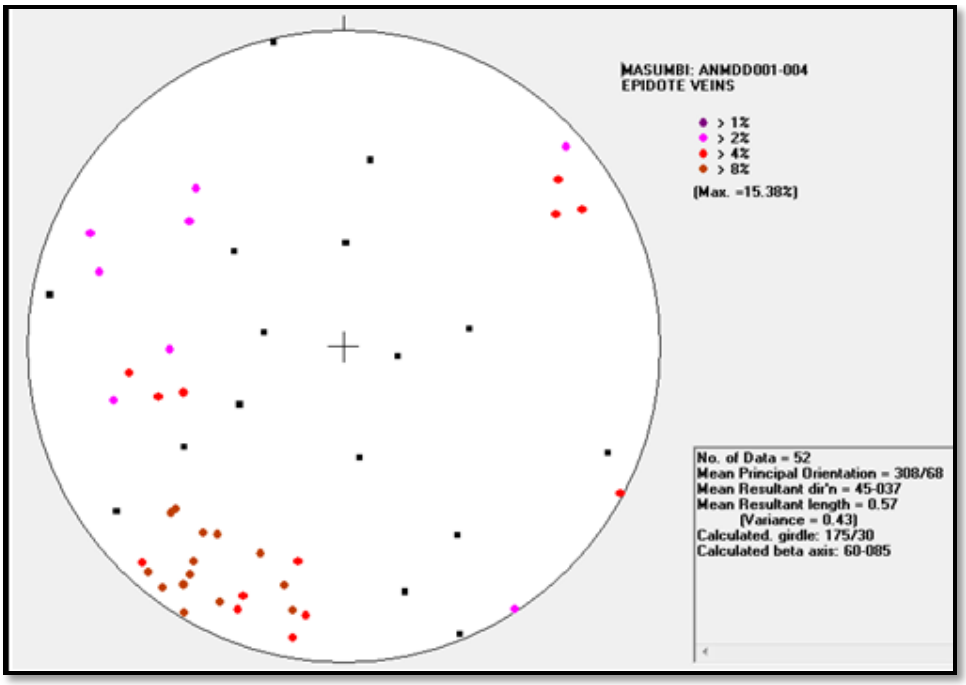

Figure 64. Equal area, lower hemisphere stereoplot for epidote veins in ANMDD001-004.

8.5 Correlation of ore elements

Based on the distribution of assays in drill-holes ANMDD002-004 as illustrated in Figure 65, there is a correlation between copper and gold. The complete assays are illustrated in strip logs in Appendix B. In order to determine whether there is temporal correlation between gold and copper mineralisation or not, scatter plots were generated and Pearson's correlation coefficients calculated for the three drill-holes that have both gold and copper assays: ANMDD002, ANMDD003 and ANMDD004. Table 9 shows the calculated Pearson's correlation coefficients (r) for each drill-hole and for the combined drill-holes. The scatter plots for the three drill-holes are illustrated in Figures 66 - 68. Figure 69 shows the scatter plot for all the three drill holes.

Table 9. Correlation between gold and copper mineralisation in drill-holes ANMDD002-004

Drill-hole ID	Correlation (r)
ANMDD002	0.082
ANMDD003	0.119
ANMDD004	0.771
ANMDD002, 3 & 4	0.189

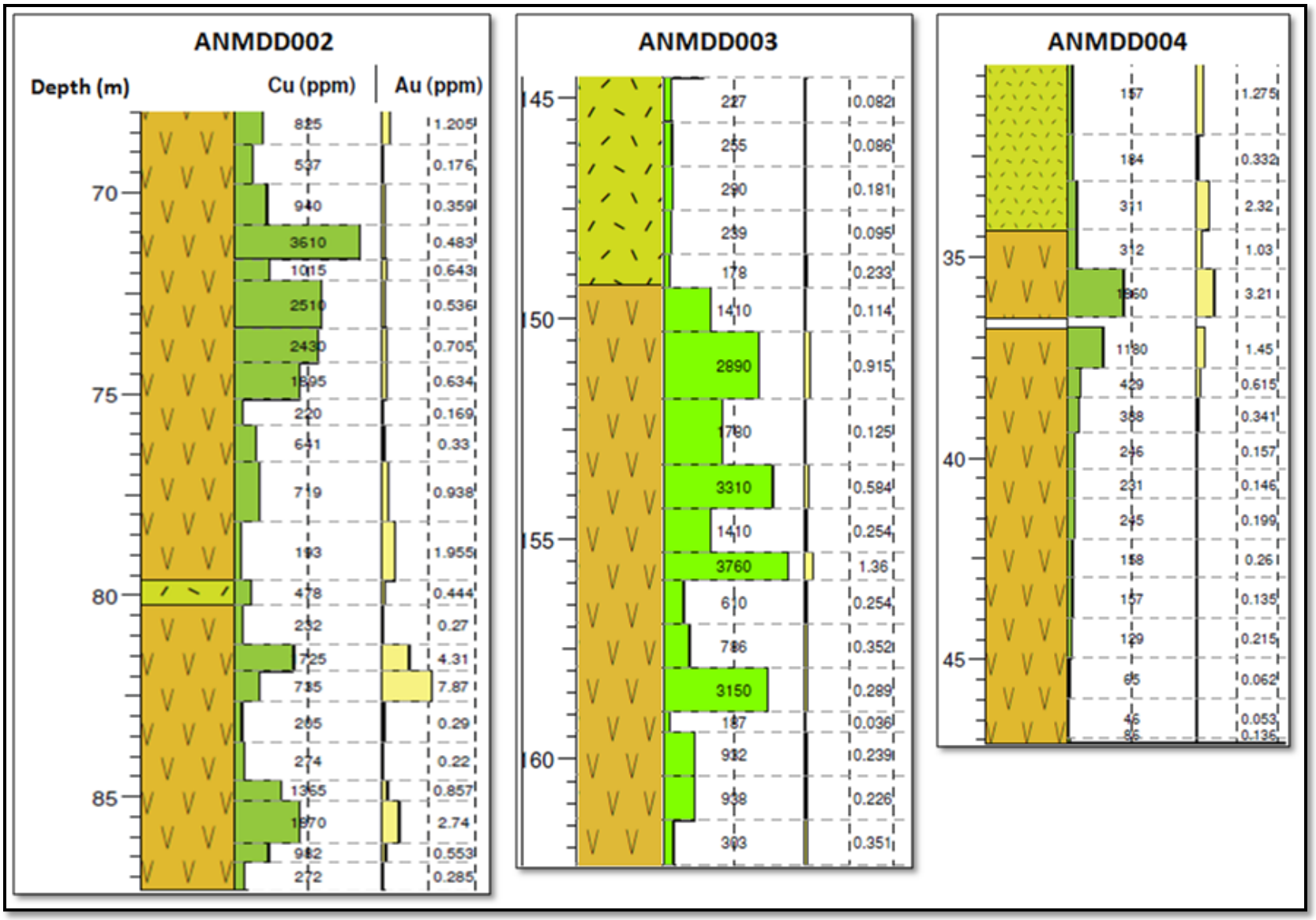

Figure 65. Association of copper and gold over mineralised intervals in drill-holes ANMDD002, 3 and 4.

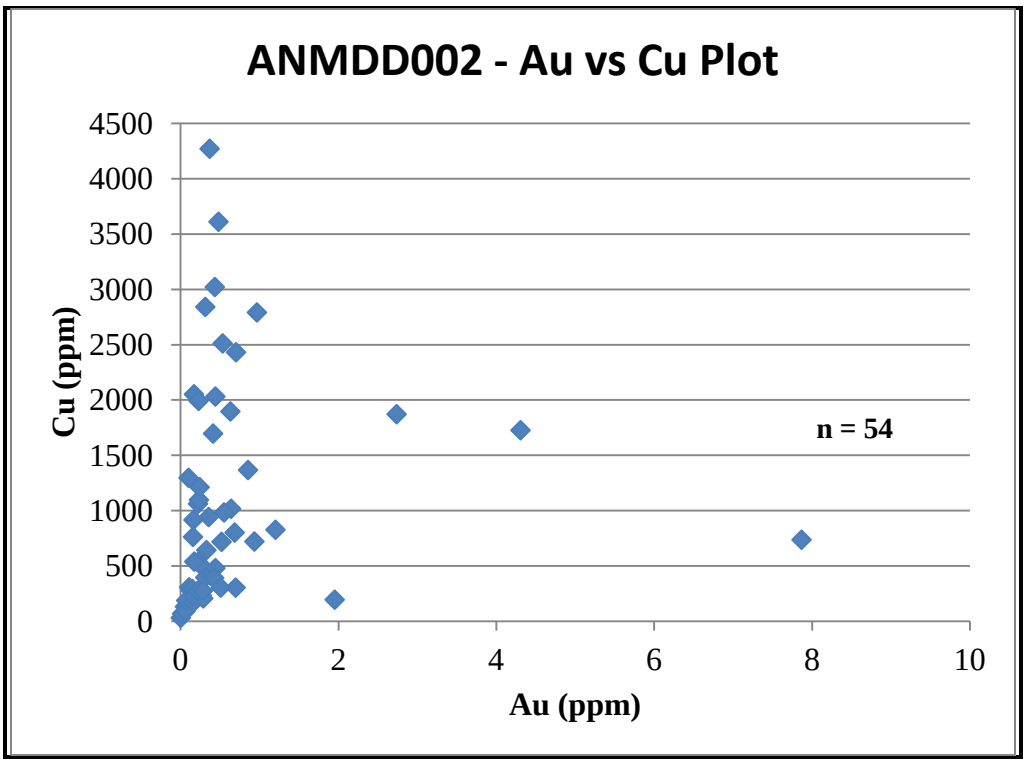

Figure 66. Scatter plot showing correlation between gold and copper mineralisation in ANMDD002

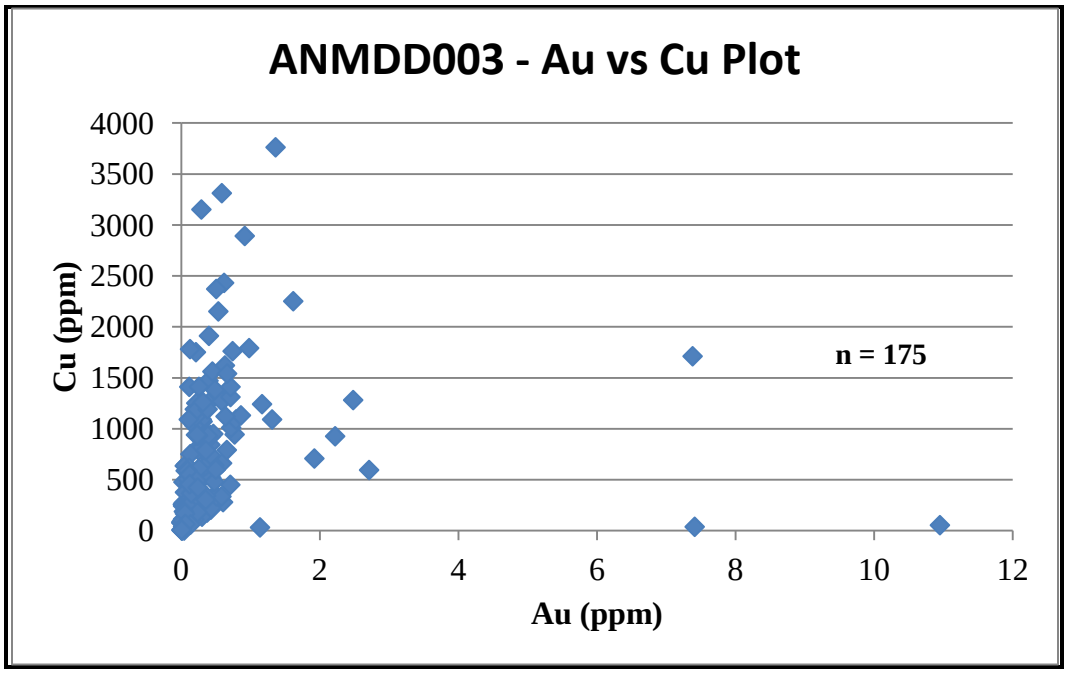

Figure 67. Scatter plot showing correlation between gold and copper mineralisation in ANMDD003.

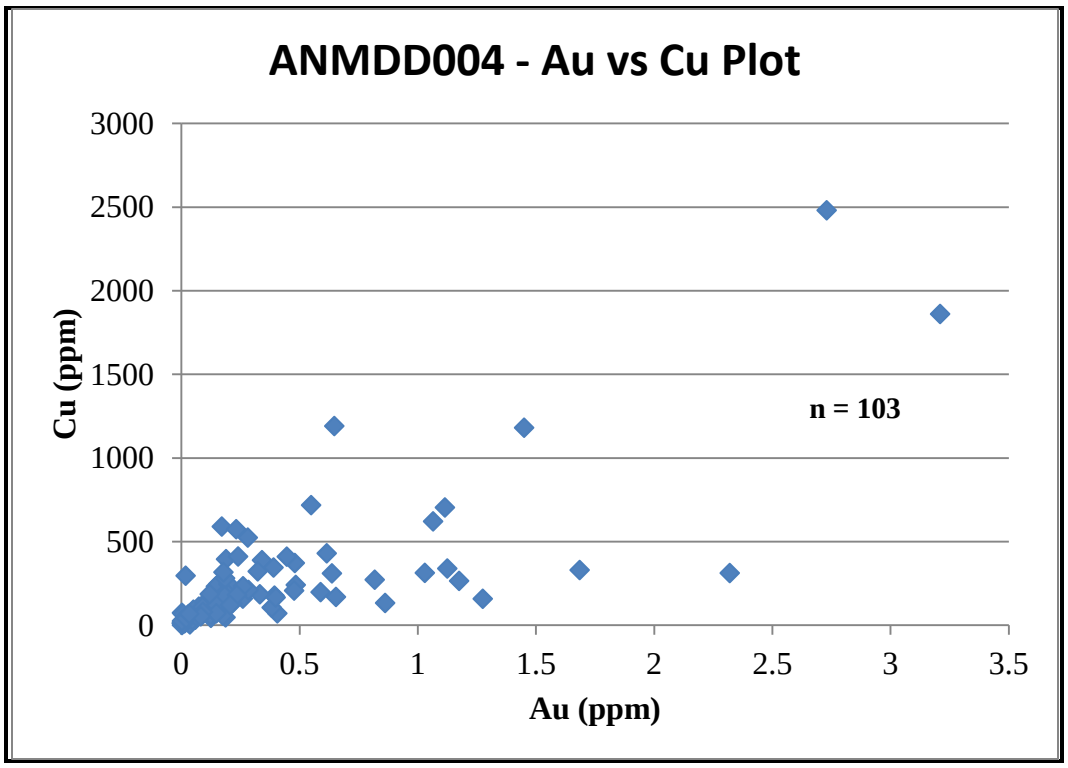

Figure 68. Scatter plot showing correlation between gold and copper mineralisation in ANMDD004.

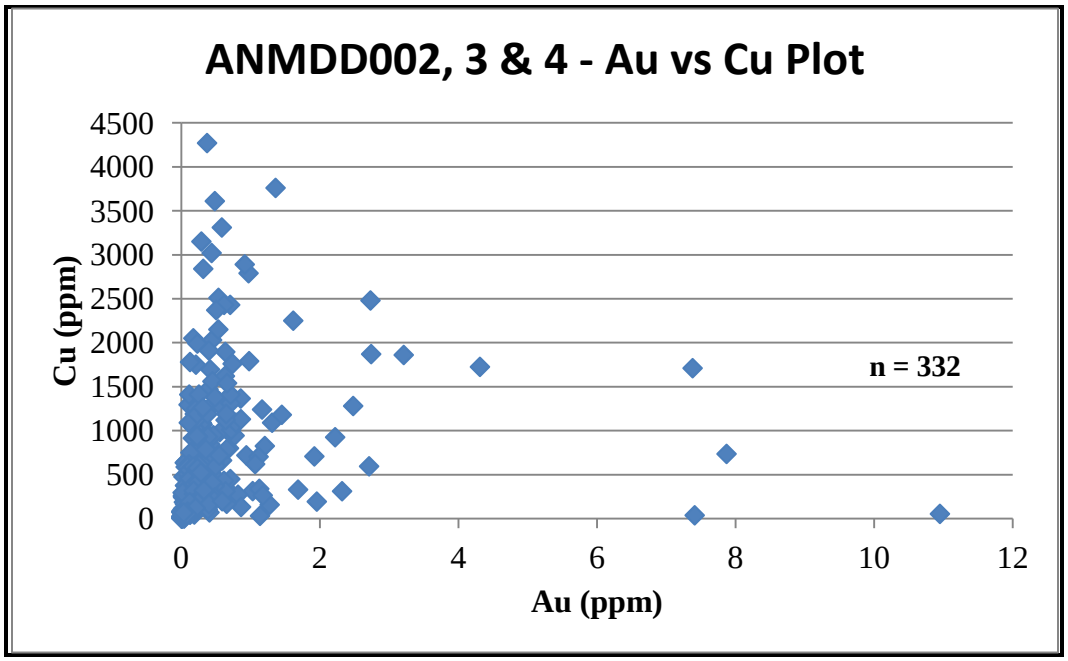

Figure 69. Scatter plot showing correlation between gold and copper mineralisation in all three drill-holes (ANMDD002, 3 & 4).

CHAPTER 9 DISCUSSION & INTERPRETATION

9.1 Gangue mineralogy

Quartz and plagioclase feldspar are the most abundant gangue minerals in both the intrusive rocks and the volcanic rocks from the study area. Plagioclase phenocrysts, often strongly altered to sericite, occur in a groundmass composed of coarsely granular quartz and commonly chloritised biotite. Minor gangue minerals include calcite, hornblende, augite and magnetite. Euhedral to subhedral grains of rutile and sphene were also observed as inclusions in pyrite grains. The mineralogy of the intrusive rocks is typical of quartz-diorite, tonalite and granodiorite and is consistent with mineral modal compositions determined by Crawford (2011).

The mineralogy of the volcanic rocks is similar to the mineralogy of the intrusive rocks; the volcanics rocks are largely classified as dacites (Crawford, 2011). In general, upon applying the total alkali-silica (TAS) classification system of volcanic rocks to plutonic rocks, dacites and granodiorites plot in the same field making dacites extrusive equivalents of granodiorites (Middlemost, 1994).

9.2 Ore mineralogy

9.2.1 Sulphides

The sulphides identified using ore microscopy and EPMA techniques include in decreasing order of abundance, pyrite, chalcopyrite and galena. These sulphides are present in both intrusive rocks and volcanics rocks. Pyrite is generally restricted to narrow veinlets where it may be intergrown with quartz, carbonate, chlorite and epidote. It often occurs as idio- to hypidiomorphic coarse crystals characterised by xenomorphic inclusions of pre-existing chalcopyrite as shown in Figures 33, 35, 53 and 55. In places, the pyrite is not compact but rather porous suggesting rapid growth as illustrated in Figure 43 and Figure 53. Chalcopyrite is mostly associated with pyrite in veinlets but it also occurs scattered as discrete blebs outside the veins and often weakly disseminated through the altered rocks. Microscopic grains of galena were observed included in pyrite grains.

9.2.2 Gold

No macroscopic gold was observed, but gold assays on intervals with pyrite indicate its presence, so gold is inferred to be present in pyrite. Careful search for gold grains using an optical microscope was unsuccessful. However, during EPMA examination, rare gold inclusions ranging from 2 µm to 20 µm in size were observed completely enclosed in pyrite grains as shown in Figure 38, Figure 43 and Figure 47. Individual grains of gold have regular forms, including equant and tabular forms.

The grains of gold are variably enriched in silver and their Au/Ag ratios were calculated using the facility of semi-quantitative analysis attached to the WDS software. The Au content of equant gold grains is greater than 90 wt% indicating that they may be classified as native gold, according to Boyle (1979). Elongate gold grains contain silver with >38 wt% suggesting that they may be classified as electrum.

The different forms of the gold grains and their respective different Au/Ag ratios may suggest that there were two generations of gold precipitation.

9.2.3 Bismuth tellurides and selenides

The investigations of thin section samples using the EPMA technique resulted in the identification of other microscopic inclusions in pyrite. These other microscopic inclusions include monazite, tellurides and a selenide. The tellurides identified include tellurobismuthite (Bi_2Te_3) shown in Figures 41, 45, 49 and 57 as well as kawazulite [$Bi_2(Te, Se, S)_3$] shown in Figure 49. Silver tellurides were identified as kurilite (Ag_8Te_3Se), shown in Figure 36, and volynskite ($AgBiTe_2$), shown in Figure 38. The tellurides are typically formed in hydrothermal gold-quartz veins of low sulphur content (Criddle and Stanley, 1993). The selenide identified is Pb-Bi seleniferous sulphosalt wittite ($Pb_3Bi_4S_6Se_3$) and is shown in Figure 53.

Although common in epithermal deposits, close paragenetic association of bismuth tellurides with gold is also observed in orogenic gold deposits (Cook and Ciobanu, 2005; Hagemann and Cassidy, 2000). Bismuth tellurides are common in the orogenic gold deposits of the Lake Victoria Goldfields. The Golden Pride, an orogenic gold deposit in the Nzega Greenstone Belt, contains tetradymite (Bi_2Te_2S) (Vos et al., 2009). Bulyanhulu, an orogenic gold deposit in the Sukumaland Greenstone Belt, also contains bismuth tellurides (Chamberlain, 2003).

9.3 Alteration mineralogy

The common mineral assemblage in all the rock types comprises chlorite and epidote. This assemblage is typical of regional greenschist metamorphic facies grading into amphibolite metamorphic facies and is consistent with the metamorphism of the Nyanzian volcanic rocks throughout Kenya (Ichang'i and MacLean, 1991).

However, chlorite and epidote could possibly be a result of propylitic alteration caused by iron and magnesium bearing hydrothermal fluids altering biotite within the rock groundmass. Figure 26 shows biotite altering to chlorite and this could possibly be a result of propylitic alteration. These fluids could be late stage hydrothermal fluids associated with the magma of the intrusive lithologies. Chalcopyrite has been observed as an inclusion in chlorite as illustrated in Figure 52 suggesting that chalcopyrite could be an earlier phase than some of the chlorite thereby supporting the idea of a propylitic alteration event. Therefore, it is possible that the epidote-chlorite event occurs both in the regional metamorphic stage and the copper ore-forming event, later referred to as ore stage 1.

Magnetite is associated with an early stage alteration assemblage (Tomkinson, 2012). Figure 52 illustrates the association of magnetite with chlorite. This early stage alteration is possibly associated with the copper ore-forming event because chalcopyrite, and pyrite to a lesser extent, is commonly associated with epidote and chlorite as illustrated in Figure 29 and Figure 34 respectively.

Hydrothermal alteration assemblages in these rocks comprise silica, muscovite, sericite, carbonate with the sulphides pyrite and chalcopyrite. The mineralogy of the alteration assemblages is fairly uniform although the intensity of its development varies significantly. The dominant assemblage consists of silica and pyrite. This alteration assemblage is associated with gold mineralisation as microscopic grains of gold are identified as inclusions in pyrite (Figures 38, 43 and 47). In diamond drill cores, silicification appears to be the most important alteration related to the gold mineralisation at Masumbi. The early formed Fe-rich alteration (magnetite-bearing) may have been critical in precipitating the later gold through sulphidation reactions (Tomkinson, 2012).

9.4 Ore paragenesis

Two ore-forming stages can be identified characterising ore paragenesis at the Masumbi deposit: one that precipitated chalcopyrite and another one that precipitated pyrite. In paragenetic determination, primary inclusions result from trapping during growth of the host mineral (Craig et al., 1981). Therefore, paragenetic relationship between chalcopyrite inclusions and pyrite host suggests that pyrite formed later than chalcopyrite. The pyrite may have formed as a result of direct precipitation from a hydrothermal fluid that circulated later than the hydrothermal fluid that generated chalcopyrite.

The occurrence of chalcopyrite as interstitial minerals between pyrite grains as shown in Figure 33 (c) and Figure 35 may suggest that some of the chalcopyrite formed later than pyrite. However, chalcopyrite is softer and more ductile than pyrite such that the pyrite, during its growth, may have squeezed and deformed the pre-existing chalcopyrite. Chalcopyrite also occurs as interstitial material between epidote grains (Figure 59) suggesting that chalcopyrite may be later than these silicate minerals.

In Reef 1 at Bulyanhulu gold mine in Tanzania, Chamberlain (2003) distinguished three generations of pyrite (pyrite 0, pyrite I and pyrite II) and two generations of chalcopyrite (chalcopyrite I and chalcopyrite II). Chalcopyrite I occurs as inclusions in pyrite II while chalcopyrite II is paragenetically later than pyrite II. Chalcopyrite II is closely associated with high gold grades and visible gold (Chamberlain, 2003). Therefore, chalcopyrite at the Masumbi deposit could be correlated to the chalcopyrite I in Reef 1 at the Bulyanhulu gold mine; there is no obvious association between chalcopyrite and gold at Masumbi.

Gold together with tellurides and selenides likely co-precipitated with the pyrite phase from a hydrothermal fluid. Based on paragenetic relationships observed through ore microscopy and EPMA techniques, a suggested summary paragenesis of mineralisation at the Masumbi Prospect is presented graphically in Figure 70.

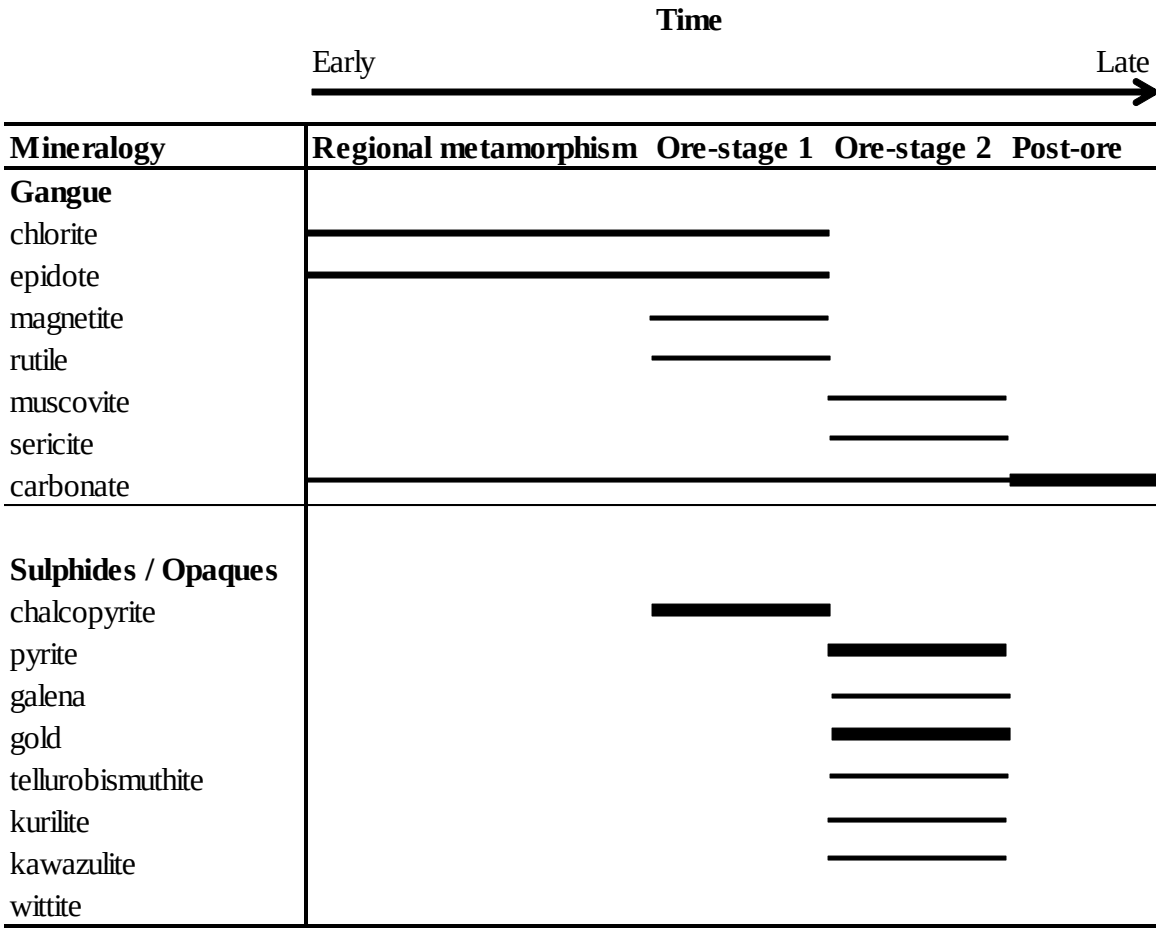

Figure 70. Suggested paragenesis for gangue and ore minerals at the Masumbi Prospect.

9.5 Structure

Structural analysis in section 8.4 shows that all the veins at Masumbi trend northwest-southeast. This trend is consistent with the northwest-southeast trend of mineralisation. Grant (2006) argues that this trend defines shear zones striking north-northwest with shallow to steep east dips. Electron micro-probe analyses show that gold is associated with pyrite grains and this observation resonates with Grant (2006) who documented that gold at Masumbi seems associated with pyrite localised along stringer veins. According to Gray and Jones (2011), the main zone of gold mineralisation appears to be structurally controlled as it cross-cuts a number of different logged lithologies and is associated with the occurrence of pyrite and quartz veins. Therefore, it can be suggested that the gold mineralising event (ore-stage 2) at Masumbi is structurally controlled.

The average strike/dip readings are 304/54 for the quartz-pyrite veins, 322/68 for the pyrite veins and 306/68 for the epidote veins. Based on the petrographic results, the epidote veins are associated with chalcopyrite and formed earlier than the pyrite veins. Similarities in average strike/dip readings of the epidote veins and the pyrite veins suggest that the hydrothermal fluids for the later auriferous ore-forming event utilised the same fluid pathways as early copper-rich hydrothermal fluids.

9.6 Correlation of ore elements

Scatter plots (Figures 66 - 69) illustrate the association of gold and copper. The calculated correlation coefficients presented in Table 9 demonstrate that a simple positive correlation between gold and copper cannot be statistically confirmed. This lack of positive correlation strongly supports the hypothesis that there are two separate ore-forming stages at Masumbi: an earlier stage that is associated with copper and a later stage that is associated with gold. The apparent association of gold and copper over mineralised intervals in drill-holes as shown in Figure 65 could be a result of auriferous hydrothermal fluids from the second ore-forming stage utilising the same fluid pathways that were conduits for the early primary ore-forming stage.

9.7 Timing of gold mineralisation at the Masumbi deposit

As discussed in Chapter 4 and illustrated in Figure 13 and Figure 14, the Aruan metamorphism coincided with granitoid magmatism at 2600 – 2500 Ma in the Tanzania Craton. The granitoids are genetically related to gold mineralisation (Bell and Dodson, 1981; Gabert, 1990; Chamberlain, 2003). Table 1 shows that The Mumias and the Maragoli granites in Kenya are coeval with the Aruan metamorphic event. In Figure 13, Chamberlain (2003) suggests that the main gold-forming event in the Tanzania Craton also coincided with the D_3 deformation event.

Although no age dating has been undertaken, ore-forming hydrothermal fluids at Masumbi may possibly have originated from the intrusion of the granodiorite and diorite that are likely to be coeval with the Mumias and the Maragoli granites that in turn are related to the Aruan metamorphism.

CHAPTER 10 EXPLORATION METHODS FOR MASUMBI-TYPE DEPOSITS

10.1 Introduction

Mineral exploration involves three sequential steps: development of a business strategy, creation and application of a targeting model, and follow-up with direct detection in defined high-priority domains. The conceptual targeting phase is the main geoscientific challenge which can lower geological risk and ensure cost-effective direct-detection exploration (Hronsky and Groves, 2008). A typical exploration programme involves geological mapping, remote sensing, geophysical exploration, geochemical exploration, drilling and evaluation. This chapter proposes exploration methods that may be used to locate orogenic gold deposits that are similar to the Masumbi Au-Cu deposit.

10.2 Geological mapping

Geological mapping forms the basis of mineral exploration and is undertaken in areas of potential mineralisation in order to detail the various rock types, structures, alteration, metamorphic grades and so on. Strong structural control of mineralisation characterises orogenic gold deposits (Groves et al., 1998).

The Masumbi deposit has gold mineralisation trends similar to that of Ramba Lumba deposit, a low-strain, high differential stress planar vein type deposit. The Ramba Lumba deposit is spatially associated with one or more regionally extensive, interpreted late stage fault zones (Mason, 2010). Consequently, late fault zones and the regions that surround them, particularly in the vicinity of homogeneous competent wallrocks, are probably prospective for low-strain, high differential stress planar vein type deposits.

However, at the Masumbi Prospect outcrops are scarce (<5%) so alternative exploration methods may be required to compliment geological mapping.

10.3 Remote sensing

Remote sensing is the science of obtaining and interpreting information from a distance, using sensors that are not in physical contact with the object being observed (Smith, 2001). Remote sensing images are used for mineral exploration in two applications: map geology and the faults and fractures that localise ore deposits; and recognise hydrothermally altered rocks by their spectral signatures.

Landsat Thematic Mapper (TM) satellite images are widely used to interpret both structure and hydrothermal alteration (Sabins, 1999). Since its launch in 1999, Advanced Spaceborne Thermal Emission and Reflection Radiometer (ASTER) has increasingly become the commonly used regional to district scale alteration mapping tool. It enables quick acquisition of useful surface mineralogical information for mapping alteration, lithology and structure, with more mineralogical resolution than is possible using the older Landsat TM imagery (Robert et al., 2007).

Silicification which is an important indicator of hydrothermal alteration is not recognisable on TM and hyperspectral images (Sabins, 1999) but the thermal infrared (TIR) bands of ASTER allow mapping of silica and/or quartz abundance and lithology (Rowan and Mars, 2003). However, ASTER has its limitations in gold exploration in greenstone belt deposits; it may not differentiate lithology related quartz from hydrothermal silicification (Robert et al., 2007).

Very significant technological advances have been made in the field of infrared spectroscopy for alteration mapping. Spatial and spectral resolution, higher signal-to-noise ratio and wider spectral range coverage have been improved by satellite multispectral systems such as ASTER and airborne hyperspectral sensors such as Hymap. Pima, one of the commonly used field portable hyperspectral instruments, was first introduced to the mineral industry in mid-1990s and has become a standard tool for alteration mapping since then (Robert et al., 2007).

Spectral-based alteration mapping has aided in the construction of alteration models for a number of greenstone belt deposits (Robert et al., 2007). A study by Halley (2006) at Kanowna Belle demonstrated zoning in mica composition extending for several kilometres outboard of this 7 Moz greenstone belt deposit in Eastern Goldfield Province of Western Australia (Halley,

2006). This study showed that gold mineralisation is spatially associated with the transition zone between V-bearing phengite and Ba-rich muscovite as illustrated in Figure 71.

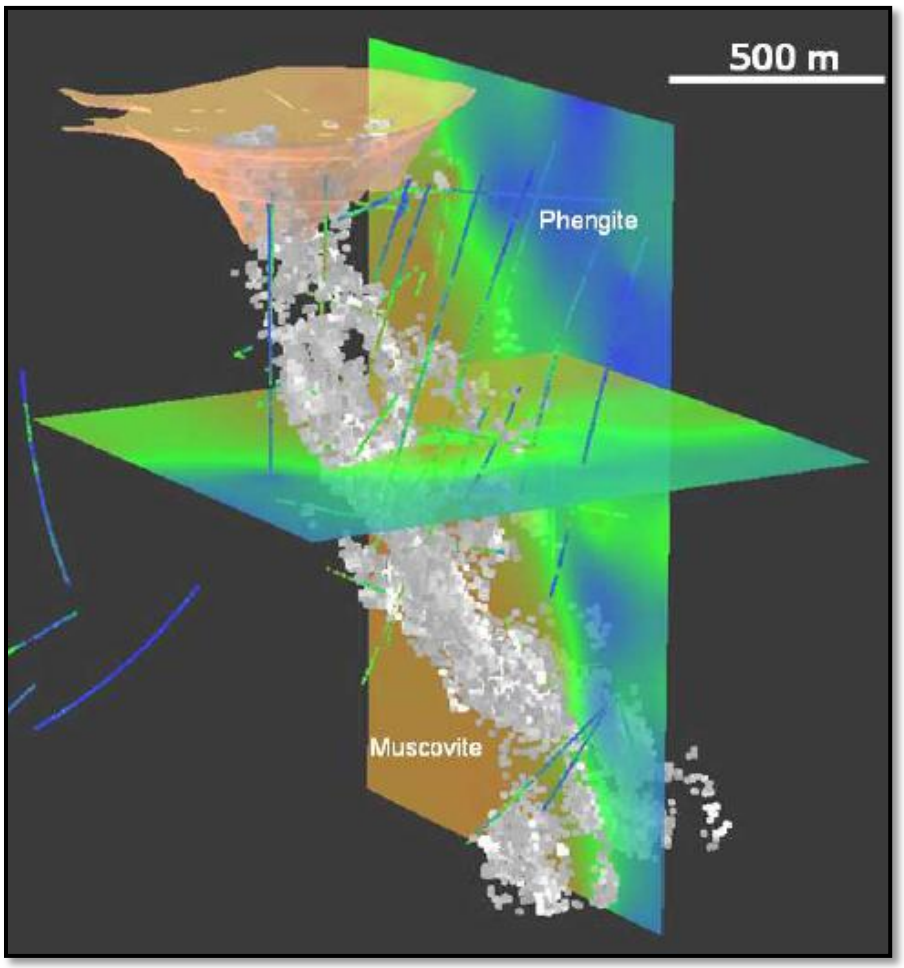

Figure 71. 3D model of gold mineralisation (grey) and white mica chemistry (blue is phengitic, brown is muscovitic) at Kanowna Belle, Eastern Goldfields, Australia. Looking ENE. Adapted from Halley (2006).

Propylitic assemblage minerals (chlorite, epidote and calcite) characterising wallrock alteration of the Masumbi rocks, as observed by Grant (2006) and identified through petrography in this study, make remote sensing an appropriate exploration tool for orogenic deposits that have utilised similar fluid pathways as earlier hydrothermal events similar to the Masumbi Au-Cu deposit.

10.4 Geophysical exploration

Geophysics involves applying the principles of physics to the Earth. The interior of the Earth is investigated by taking surface measurements that are influenced by the internal distribution of physical properties. There is a broad division of geophysical surveying methods into those that make use of natural fields of the Earth and those that require the input into the ground of artificially generated energy (Kearey et al., 2009).

The natural field methods utilise the gravitational, magnetic, electrical and electromagnetic fields of the Earth, searching for local perturbations in these naturally occurring fields that may be caused by concealed geological features of economic interest. Artificial source methods involve the generation of local electrical or electromagnetic fields that may be used analogously to natural fields. Generally, natural field methods can provide information on Earth properties to significantly greater depths and are logistically simpler to carry out than artificial source methods. The latter, however, are capable of producing a more detailed and better resolved picture of the subsurface geology (Kearey et al., 2009).

It is impossible to get a direct geophysical response from gold because of the low grades in deposits, except when electromagnetic detectors are used for individual shallow nuggets (Doyle, 1990). However, indirect geophysical indications may occur through association of gold with particular host rocks or structures.

Magnetic surveys are used in orogenic gold exploration for regional and detailed mapping of structures such as faults, shear zones and veins, with which gold may be associated (Paterson and Hallof, 1993). They can be conducted either as ground surveys or as airborne survey. The magnetic survey is the most commonly used geophysical tool in gold exploration (Doyle, 1990).

Radiometric surveys are usually conducted in conjunction with airborne magnetic surveys. The radiometric data is useful in delineating alteration zones, particularly where high potassium alteration assemblages predominate. High-potassium zones could be a product of sericite alteration which is usually associated with gold mineralisation (Doyle, 1990).

IP and resistivity surveys are often used where gold is closely associated with disseminated sulphides and silicification (Kearey et al., 2009). The two most commonly used IP/resistivity electrode configurations are the dipole-dipole and gradient arrays (Corbett, 1992). The dipole-

dipole array usually produces large anomalies but the anomalies rarely give information on dip of a structure and are strongly influenced by overburden irregularities. The gradient array provides dip information and good horizontal resolution (Coggon, 1973).

A successful IP and resistivity survey conducted over the Masumbi Prospect, as detailed in Chapter 2, revealed that the mineralisation sits within one of several mappable resistive units trending north to northwest, coincident with a wider chargeability zone (Buckingham, 2012). Considering that the second ore-forming stage at Masumbi is associated with silicification (increased resistivity) and the presence of disseminated sulphides (increased chargeability), IP and resistivity surveys would be appropriate geophysical tools in exploration for gold deposits with Masumbi characteristics.

Since the turn of the 21st Century significant advances have been made on proven geophysical methods and on techniques to interpret and to visualise geophysical data. One of the most significant recent advances in geophysics is the routine 3D inversion of potential field data (magnetic and gravity). There are many good examples of 3D inversions being used to map alteration associated with gold systems such as by Coggon (2003) at Wallaby, Western Australia, and by Wallace (2007) at Musselwhite, Canada. However, the lack of petrophysical and geological constraints, and the drive to view data in 3D have also led to inappropriate application of 3D inversion techniques (Robert et al., 2007).

Exploration problems can be solved by acquiring data capable of being processed in 3D. Figure 72 shows an example of the benefits of processing data in 3D, rather than in 2D, from the Dee-Rossi Carlin deposit in Nevada (Petrick, 2007).

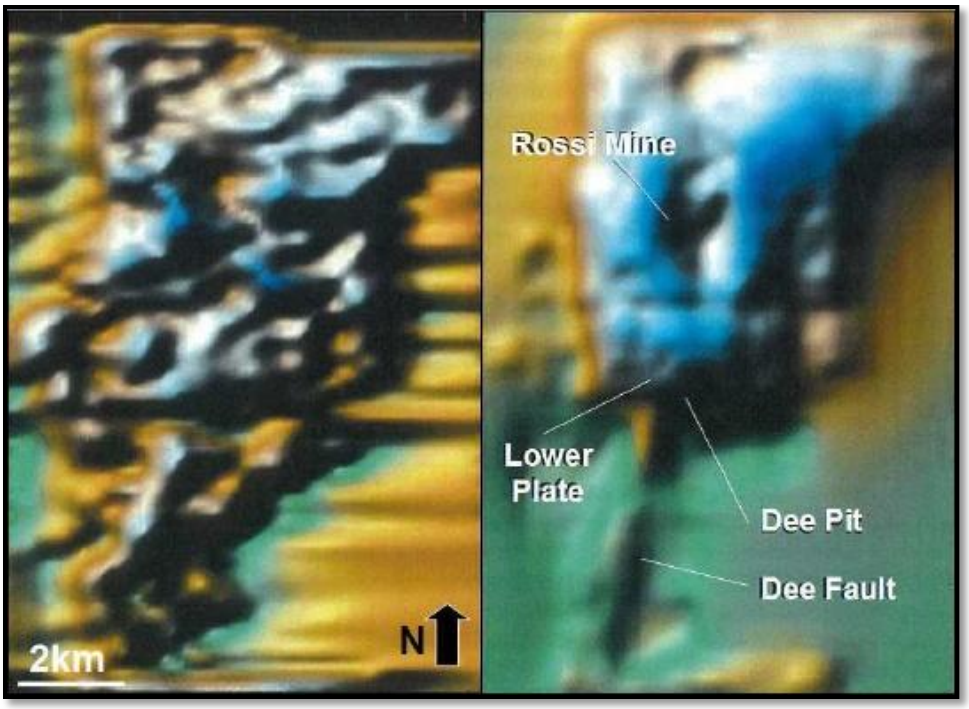

Figure 72. Subsurface conductivity distribution at a depth of 450 m obtained from stitching together 2D-TM (left) inversions and 3D inversions (right) of magnetotelluric data over the the Dee-Rossi region (Petrick, 2007)**.**

A single line of pole-dipole data were collected during the resistivity and IP survey conducted over the Masumbi Prospect as discussed in Chapter 2. The 2D inversion technique was used to invert the data using the UBC 2D IP inversion software. The inversion results provided a model of the subsurface that gave a response that was similar to the actual measure values (Buckingham, 2012). Therefore, 3D inversion techniques could be a suitable geophysical tool in exploration for gold deposits similar to the Masumbi deposit.

10.5 Geochemical exploration

Exploration geochemistry is the practical application of theoretical geochemical principles to mineral exploration (Levinson, 1974). The objective is to find some dispersion of elements or compounds sufficiently above normal to be called an anomaly, which may indicate mineralisation. Geochemical exploration involves mainly lithogeochemical, stream sediment and

soil sampling. However, it is hardly used as a single method but always in conjunction of other methods.

In regional exploration, stream sediment geochemistry, in the form of conventional fine fraction, BLEG (Bulk Leach Extractable Gold), cyanide leach, or pan concentrate sampling, continue to be important tools in gold exploration. At a local scale, geochemical techniques such as soil, lag, and rock-chip sampling are usually effective in defining anomalies associated with outcropping or sub-cropping deposits (Robert et al., 2007).

As discussed in Chapter 2, a gold-in-soil anomaly measuring 5 km by 2km was defined over the Masumbi Prospect through soil geochemical sampling. This anomaly definition makes soil geochemistry a suitable exploration technique when searching for deposits similar to the Masumbi mineralisation. While gold remains to be its own best pathfinder element (Zeegers and Leduc, 1993), Ag, As, Sb, Bi, Te and Se are some of the most useful pathfinder elements for gold (Niskavaara and Kontas, 1990). The broadest anomaly surrounding the Late Archaean Bronzewing orogenic gold deposit in Western Australia is defined by tellurium (Eilu et al., 2001). Based on the EPMA results for this study, Ag, Bi, Se and Te are potential pathfinder elements for geochemical dispersion of gold in orogenic deposits similar to Masumbi.

10.6Drilling

The main purpose of drilling is to test geophysical and geochemical anomalies in order to delineate mineralisation. Three-dimensional geological modelling and resource calculation are only possible if sufficient mineralisation data is generated through drilling. Drilling can be done in three phases: reconnaissance drilling, target drilling and resource evaluation drilling.

The reconnaissance drilling phase is aimed at increasing geological knowledge. Widely spaced (>100 m) drill-holes, usually rotary air blast (RAB) holes are recommended for regolith mapping and bedrock interface geochemistry as well as to test conceptual models of mineralisation (Marjoribanks, 2010). Reverse circulation (RC) drilling or aircore drilling is a cost effective and the preferred drilling method for the reconnaissance drilling phase. However, limited diamond drilling could provide information on the structural controls of the mineralisation.

The target drilling phase is aimed at achieving an intersection of ore, or potential ore. The conventional method used is usually by means of carefully targeted diamond or rotary-percussion drill-holes, but more rarely trenching, pitting, sinking a shaft or driving an adit may be employed. This is arguably the most critical stage of exploration since, depending on its results, decisions involving high costs and potential costs have to be made. If a decision is made that a potential ore body has been located, the costs of exploration will then dramatically escalate. If it is decided to write a prospect off after this stage, there is always the possibility that an ore body has been missed (Marjoribanks, 2010).

The resource evaluation drilling phase provides answers to economic questions relating to the grade, tonnage and mining/metallurgical characteristics of the potential ore body. Sound understanding of the nature of the mineralisation should already have been achieved. A detailed pattern drilling and sampling are required to provide the data to answer the economic questions. Because resource evaluation drilling can be such an expensive and time-consuming process, this drilling is often undertaken in two stages with a minor decision point in between: an initial evaluation drilling stage and a later definition drilling stage. Evaluation and definition drilling provide the detail and confidence levels required to proceed to the feasibility study (Marjoribanks, 2010).

10.7Evaluation

Detailed feasibility studies must now be conducted on potential ore bodies in order to determine their economic viability. This is a desk-top due-diligence study that assesses all factors, including geological, mining, environmental, political and economic factors, relevant to the decision to mine. With very large projects, the costs involved in evaluation are such that a preliminary feasibility study is often carried out during the preceding resource evaluation phase. The preliminary feasibility study identifies whether the costs involved in exploration are appropriate to the returns that can be expected. It also identifies the nature of the data that must be acquired in order to bring the project to the final feasibility phase (Marjoribanks, 2010).

Based on previous work, the best combination of exploration methods for the Masumbi-type deposits appears to be soil geochemical sampling, resistivity and IP geophysical survey and drilling.

CHAPTER 11 CONCLUSIONS AND RECOMMENDATIONS

11.1 Conclusions

The Masumbi deposit is characterised by gold and copper mineralisation that are both associated with quartz-sulphide veinlets. EPMA results from this study indicate that gold is closely associated with pyrite and its pathfinder elements silver, lead, bismuth, tellurium and selenium. The gold occurs in two forms: as native gold with Au content greater than 90% and as electrum with silver content greater than 38%. Copper mineralisation is almost entirely chalcopyrite. The petrogenetic relationship between pyrite and chalcopyrite suggests that there is no temporal relationship between gold and copper mineralisation, which is also indicated by the statistical analysis of the gold and copper.

Although there is a strong Au-Ag association within individual gold grains, mineralisation at Masumbi appears atypical of Archaean orogenic gold deposits because of the abundance of copper; Archaean orogenic gold deposits usually contain copper in trace amounts. Nonetheless, this peculiar copper abundance has been reported at other Archaean orogenic gold deposits in the Lake Victoria Goldfields; Bulyanhulu quartz-sulphide-gold deposit in Tanzania is one very good example.

The common alteration assemblage in the Masumbi rocks comprises chlorite and epidote. Propylitic alteration within the rock groundmass could possibly have been the source of the early chlorite and epidote veining. However, this mineral assemblage is typical of regional greenschist metamorphic facies grading into amphibolite metamorphic facies and is consistent with the metamorphism of the Nyanzian volcanic rocks in Kenya. The sulphide phases are later than the silicate phases with the same fractures being reopened to allow for the sulphide mineralisation. Other alteration assemblages comprise silica, muscovite, sericite and carbonate with the sulphides pyrite and chalcopyrite. These are common alteration assemblages associated with hydrothermal fluids related to orogenic gold deposits. In diamond drill cores silicification appears to be the most important alteration related to the gold mineralisation at Masumbi. Pyrite appears to be the sulphide most commonly associated with gold. Gold is generally not associated with chalcopyrite.

Although two distinct ore-forming events are suggested from the proposed paragenetic sequence for the mineralisation at the Masumbi deposit, these events are probably the early and late stages of a continuum of the same metamorphic or deformation event. The hydrothermal fluids associated with the ore-forming events may possibly have originated from the intrusion of the granodiorite, tonalite and diorite that are likely coeval with Mumias and Maragoli granites. These granites are in turn coincident with the Aruan metamorphic event and consequently genetically-related to the main gold-forming event in the Tanzania Craton.

Exploration methods have been proposed to locate undiscovered Masumbi-type gold deposits in the Ndori Greenstone Belt. These methods could probably be applied, with modifications, to low-strain, high differential stress planar vein-type gold deposits in other granite-greenstone terranes in the Lake Victoria Goldfields.

11.2 Recommendations

The following recommendations are suggested:

- Late fault zones and the regions that surround them, particularly in the vicinity of homogeneous competent wallrocks, be targeted for locating undiscovered low-strain, high differential stress planar vein type deposits.
- Geochemical exploration programmes targeting Masumbi-type gold deposits should analyse for Ag, Pb, Bi, Te and Se as pathfinders for gold.
- Following a successful survey over the Masumbi Prospect, Resistivity and IP geophysical surveys are highly recommended when exploring for Masumbi-type gold deposits that are associated disseminated sulphides and silicification.
- 3D inversion techniques should be considered as a suitable geophysical tool in exploration for gold deposits similar to the Masumbi deposit, especially in conjunction with resistivity and IP surveys.
- Areas surrounding granitoids that are coeval with the Mumias and the Maragoli granites could also be targeted in search for Masumbi-type gold deposits.

REFERENCES

Allibone, A.H., Windh, J., Etheridge, M.A., Burton, D., Anderson, G., Edwards, P.W., Miller, A., Graves, C., Fanning, C.M. and Wysoczanski, R., 1998, Timing relationships and structural controls on the location of Au-Cu mineralization at the Boddington gold mine, Western Australia: Economic Geology, v. 93, p. 245-270.

Bakken, B.M., 1990, Gold mineralization, wall-rock alteration, and the geochemical evolution of the hydrothermal system in the Main orebody, Carlin mine, Nevada, Stanford University.

Begg, G., Griffin, W., Natapov, L., O'Reilly, S.Y., Grand, S., O'Neill, C., Hronsky, J., Djomani, Y.P., Swain, C. and Deen, T., 2009, The lithospheric architecture of Africa: Seismic tomography, mantle petrology, and tectonic evolution: Geosphere, v. 5, p. 23-50.

Bell, K. and Dodson, M., 1981, The geochronology of the Tanzanian Shield: The Journal of geology, v. 89, p. 109-128.

Boniface, N. and Mruma, A.H., 2012, Structural analysis, metamorphism, and geochemistry of the Archean granitoids-greenstones of the Sukumaland Greenstone Belt around Geita Hills, Northern Tanzania: Natural Science, v. 4, 526-535.

Borg, G. and Krogh, T., 1999, Isotopic age data of single zircons from the Archaæan Sukumaland Greenstone Belt, Tanzania: Journal of African Earth Sciences, v. 29, p. 301-312.

Borg, G. and Shackleton, R., 1997, The Tanzania and NE-Zaire cratons: Oxford Monographs on Geology and Geophysics, v. 35, p. 608-619.

Borg, G., Lyatuu, D. and Rammlmair, D., 1990, Genetic aspects of the Geita and Jubilee Reef Archean BIF-hosted gold deposits, Tanzania: Geologische Rundschau, v. 79, p. 355-371.

Borg, G., 1994, The Geita Gold deposit, NW-Tanzania: Geology, Ore petrology, Geochemistry and timing of events.: Geologische Jahrbuch, v. 100, p. 545-595.

Boyle, R.W., 1960, The Geology, Geochemistry, and Origin of the Gold, Deposits of the Yellowknife District, Department of mines and technical surveys.

Boyle, R.W., 1979, The Geochemistry of Gold and Its Deposits, Geological Survey of Canada, v. 280, 584p.

Buckingham, A., 2012, Report on the Resistivity and Induced Polarisation Survey carried out at the Masumbi & Barding project area, West Kenya, Aviva Corporation.

Burrows, D., Wood, P. and Spooner, E., 1986, Carbon isotope evidence for a magmatic origin for Archaean gold-quartz vein ore deposits.

Cahen, L. and Snelling, N., 1966, The geochronology of equatorial Africa, North-Holland Publishing Company Amsterdam, The Netherlands.

Cahen, L., Snelling, N., Delhal, J., Vail, v.J., Bonhomme, M. and Ledent, D., 1984, The geochronology and evolution of Africa, Clarendon press Oxford.

Chamberlain, C.M., 2003: Geology and genesis of the Bulyanhulu gold deposit, Sukumaland Greenstone Belt, Tanzania.

Clifford, T., 1970, The structural framework of Africa: African magmatism and tectonics, Oliver and Boyd, Edinburgh, p. 1-26.

Coggon, J., 1973, A comparison of IP electrode arrays: Geophysics, v. 38, p. 737-761.

Colvine, A., 1984, An Integrated Model for the Origin of Archean Lode QGS Gold Deposits, Ontario Ministry of Natural Resources.

Colvine, A.C., 1988, Archean lode gold deposits in Ontario, Ontario Ministry of Northern Development and Mines.

Cook, N.J. and Ciobanu, C.L., 2005, Tellurides in Au deposits: implications for modelling: Mineral Deposit Research: Meeting the Global Challenge, Proceedings, p. 1387-1390.

Corbett, J., 1992, A comparison of dipole? dipole and gradient arrays: Exploration Geophysics, v. 23, p. 75-82.

Craig, J.R., Vaughan, D.J. and Hagni, R.D., 1981, Ore microscopy and ore petrography, Wiley New York.

Crawford, A., 2011, Petrographic Report, 23 Rocks from the Masumbi Prospect (W Kenya): Unpublished, Aviva Corporation.

Criddle, A.J. and Stanley, C.J., 1993, Quantitative data file for ore minerals, Chapman & Hall.

Doyle, H.A., 1990, Geophysical exploration for gold-A review: Geophysics, v. 55, p. 134-146.

Eilu, P., Mikucki, E.J. and Dugdale, A.L., 2001, Alteration zoning and primary geochemical dispersion at the Bronzewing lode-gold deposit, Western Australia: Mineralium Deposita, v. 36, p. 13-31.

Foster, R. and Piper, D., 1993, Archaean lode gold deposits in Africa: Crustal setting, metallogenesis and cratonization: Ore Geology Reviews, v. 8, p. 303-347.

Gabert, G., 1990, Lithostratigraphic and tectonic setting of gold mineralization in the Archean cratons of Tanzania and Uganda, East Africa: Precambrian Research, v. 46, p. 59-69.

Gebre-Mariam, M., Hagemann, S. and Groves, D., 1995, A classification scheme for epigenetic Archaean lode-gold deposits: Mineralium Deposita, v. 30, p. 408-410.

Goldfarb, R.J., Baker, T., Dube, B., Groves, D.I., Hart, C.J. and Gosselin, P., 2005, Distribution, character, and genesis of gold deposits in metamorphic terranes: Economic Geology 100th Anniversary Volume, p. 407-450.

Goldfarb, R., Groves, D. and Gardoll, S., 2001, Orogenic gold and geologic time: a global synthesis: Ore geology reviews, v. 18, p. 1-75.

Grant, D., 2006, An assessment of some hydrothermal gold prospects in the Ndori Greenstone Belt, Southwestern Kenya, Unpublished.

Gray, D. and Jones, M., 2011, Review of the gold grade and mineralisation extents at the Masumbi Prospect, West Kenya: Unpublished, Aviva Corporation.

Groves, D.I., Condie, K.C., Goldfarb, R.J., Hronsky, J.M. and Vielreicher, R.M., 2005, 100th Anniversary Special Paper: secular changes in global tectonic processes and their influence on the temporal distribution of gold-bearing mineral deposits: Economic Geology, v. 100, p. 203-224.

Groves, D.I., Goldfarb, R.J., Gebre-Mariam, M., Hagemann, S. and Robert, F., 1998, Orogenic gold deposits: a proposed classification in the context of their crustal distribution and relationship to other gold deposit types: Ore geology reviews, v. 13, p. 7-27.

Groves, D., Knox-Robinson, C., Ho, S. and Rock, N., 1990, An overview of Archaean lode-gold deposits: Gold deposits of the Archaean Yilgarn Block, Western Australia: nature, genesis, and exploration guides.Geology Department and University Extension, University of WA Publication, v. 20, p. 2-18.

Hagemann, S. and Cassidy, K.F., 2000, Archean orogenic lode gold deposits: In Hagemann, S.G., Brown, P.E. (Eds), Gold in 2000, Society of Economic Geologists, Reviews in Economic Geology, v. 13, p. 9-68.

Halley, S., 2006, Alteration vectors to blind, high grade, Archaean Gold Deposits: AIG-AMEC 2006.

Harpum, J., 1970, Summary of the Geology of Tanzania, Mineral Resources Division.

Hitchen, C.S., 1936, Geological survey of No. 2 Mining Area, Kavirondo: Interim report and map of north-west quadrant: Kenya, Geological Survey Dept.

Hronsky, J. and Groves, D., 2008, Science of targeting: definition, strategies, targeting and performance measurement: Australian Journal of Earth Sciences, v. 55, p. 3-12.

Huddleston, A., 1954, Geology of the Kakamega District: Degree Sheet 33, SE Quadrant, Government Printer.

Ichang'i, D. and MacLean, W., 1991, The Archaen volcanic facies in the Migori segment, Nyanza greenstone belt, Kenya: stratigraphy, geochemistry and mineralisation: Journal of African Earth Sciences (and the Middle East), v. 13, p. 277-290.

Kearey, P., Brooks, M. and Hill, I., 2009, An introduction to geophysical exploration, Wiley. com.

Kerrich, R. and Wyman, D., 1994, The mesothermal gold-lamprophyre association: significance for an accretionary geodynamic setting, supercontinent cycles, and metallogenic processes: Mineralogy and Petrology, v. 51, p. 147-172.

Kerrich, R. and Fyfe, W., 1981, The gold—carbonate association: Source of CO< sub> 2</sub>, and CO< sub> 2</sub> fixation reactions in Archaean lode deposits: Chemical Geology, v. 33, p. 265-294.

Kerrich, R. and Cassidy, K.F., 1994, Temporal relationships of lode gold mineralization to accretion, magmatism, metamorphism and deformation—Archean to present: A review: Ore Geology Reviews, v. 9, p. 263-310.

Kerrich, R., Goldfarb, R., Groves, D., Garwin, S. and Jia, Y., 2000, The characteristics, origins, and geodynamic settings of supergiant gold metallogenic provinces: Science in China Series D: Earth Sciences, v. 43, p. 1-68.

Klver, K., 1975, O 100 200M: Preliminary Report of African Studies, p. 14.

Knox-Robinson, C.M. and Gardoll, S.J., 1998, GIS-stereoplot: an interactive stereonet plotting module for ArcView 3.0 geographic information system: Computers & Geosciences, v. 24, p. 243-250.

Krogh, T., 1993, High precision U-Pb ages for granulite metamorphism and deformation in the Archean Kapuskasing structural zone, Ontario: implications for structure and development of the lower crust: Earth and Planetary Science Letters, v. 119, p. 1-18.

Kröner, A., 1977, The Precambrian geotectonic evolution of Africa: plate accretion versus plate destruction: Precambrian Research, v. 4, p. 163-213.

Kuehn, S., Ogola, J. and Sango, P., 1990, Regional setting and nature of gold mineralization in Tanzania and southwest Kenya: Precambrian Research, v. 46, p. 71-82.

Lee Rodgers, J. and Nicewander, W.A., 1988, Thirteen ways to look at the correlation coefficient: The American Statistician, v. 42, p. 59-66.

Leggo, P.J., 1974, A geochronological study of the basement complex of Uganda: Journal of the Geological Society, v. 130, p. 263-276.

Levinson, A.A., 1974, Introduction to exploration geochemistry, Applied Publishing Ltd.

MacCall, G.J.H., 1958, Geology of Gwasi area. Degree sheet 41, south-west quarter: Geological Survey Kenya, Government Printers.

Manya, S. and Maboko, M., 2003, Dating basaltic volcanism in the Neoarchaean Sukumaland Greenstone Belt of the Tanzania Craton using the Sm–Nd method: implications for the geological evolution of the Tanzania Craton: Precambrian Research, v. 121, p. 35-45.

Manya, S., Kobayashi, K., Maboko, M.A. and Nakamura, E., 2006, Ion microprobe zircon U–Pb dating of the late Archaean metavolcanics and associated granites of the Musoma-Mara Greenstone Belt, Northeast Tanzania: Implications for the geological evolution of the Tanzania Craton: Journal of African Earth Sciences, v. 45, p. 355-366.

Marjoribanks, R.W., 2010, Geological methods in mineral exploration and mining, Springer.

Mason, R., 2011, Structure and Mineralisation - Kenya: Unpublished, Aviva Corporation.

Mason, R., 2010, Structural Mapping and Interpretation - Ndori Greenstone Belt, West Kenya: Unpublished, Aviva Corporation.

Mathu, E. and Davies, T., 1996, Geology and the environment in Kenya: Journal of African Earth Sciences, v. 23, p. 511-539.

McCuaig, T., Kerrich, R., Groves, D. and Archer, N., 1993, The nature and dimensions of regional and local gold-related hydrothermal alteration in tholeiitic metabasalts in the Norseman goldfields: the missing link in a crustal continuum of gold deposits?: Mineralium Deposita, v. 28, p. 420-435.

Middlemost, E.A., 1994, Naming materials in the magma/igneous rock system: Earth-Science Reviews, v. 37, p. 215-224.

Mueller, A.G. and Groves, D.I., 1991, The classification of Western Australian greenstone-hosted gold deposits according to wallrock-alteration mineral assemblages: Ore Geology Reviews, v. 6, p. 291-331.

Ngecu, W.M. and Gaciri, S.J., 1995, Lithostratigraphy, provenance and facies distribution of Archaean cratonic successions in western Kenya: Journal of African Earth Sciences, v. 21, p. 359-372.

Niskavaara, H. and Kontas, E., 1990, Reductive coprecipitation as a separation method for the determination of gold, palladium, platinum, rhodium, silver, selenium and tellurium in geological samples by graphite furnace atomic absorption spectrometry: Analytica Chimica Acta, v. 231, p. 273-282.

Ödman, O.H., 1929, Preliminary report on the Archaean geology of western Nzoya Province, Kenya Colony: GFF, v. 51, p. 77-90.

Opiyo-Akech, N., Tarney, J. and Hoshino, M., 1999, Petrology and geochemistry of granites from the Archaean terrain north of Lake Victoria, western Kenya: Journal of African Earth Sciences, v. 29, p. 283-300.

Patel, J. and Raja, P., 1979, A palaeomagnetic study of lower Proterozoic granites from Western Kenya: Geophysical Journal International, v. 58, p. 279-286.

Paterson, N. and Hallof, P., 1993, Geophysical exploration for gold, Gold metallogeny and exploration, Springer, p. 360.

Petrick, W.R., 2007, Practical 3D Magnetotelluric Inversion: Finally Dispensing with TE and TM: Barrick Gold Corporation, Unpublished Internal Report.

Pinna, P., Cocherie, A. and Jezequel, P., 2000, The Kisii Group of western Kenya: an end-Archaean (2.53 Ga) late orogenic volcano sedimentary sequence: Journal of African Earth Sciences, v. 30, p. 79-97.

Poulsen, K., 1996, Lode gold: Geology of Canadian Mineral Deposit Types: Geological Survey of Canada, Geology of Canada, v. 8, p. 323-328.

Pulfrey, W., 1946, Geological survey of Maragoli, North Kavirondo, Report No. 9.: Nairobi, Government Printer.

Quennel, A., McKinlay, A. and WG, A., 1956, Summary of the Geology of Tanganyika, Part I: Introduction and Stratigraphy.Geological Survey of Tanganyika Memoir, v. 1.

Rammlmair, D., Höhndorf, A., Borg, G. and Hiza, G., 1990, Nouvelles Datations Isotopiques des granites et des gabbros de la Region "greenstone" Granitique du Sukumaland, NW Tanzanie: 15th Colloquium African Geology (Abstract Volume), Nancy.

Ridley, J.R. and Diamond, L.W., 2000, Fluid chemistry of orogenic lode gold deposits and implications for genetic models: In Hagemann, S.G., Brown, P.E. (Eds), Gold in 2000, Society of Economic Geologists, Reviews in Economic Geology, v. 13, p. 141-162.

Robert, F., Brommecker, R., Bourne, B., Dobak, P., McEwan, C., Rowe, R., Zhou, X. and Milkereit, B., 2007, Models and exploration methods for major gold deposit types: proceedings of Exploration, Proceedings, p. 691-711.

Rock, N., Groves, D., Perring, C. and Golding, S., 1989, Gold, lamprophyres, and porphyries: what does their association mean: Economic Geology Monograph, v. 6, p. 609-625.

Rowan, L.C. and Mars, J.C., 2003, Lithologic mapping in the Mountain Pass, California area using advanced spaceborne thermal emission and reflection radiometer (ASTER) data: Remote Sensing of Environment, v. 84, p. 350-366.

Sabins, F.F., 1999, Remote sensing for mineral exploration: Ore Geology Reviews, v. 14, p. 157-183.

Saggerson, E., 1952, Geology of the Kisumu District, Degree Sheet 41, NE Quadrant, Government Printer.

Sanders, L.D., 1965, Geology of the Contact between the Nyanza Shield and the Mozambique Belt in western Kenya, Government Printer.

Shackleton, R.M., 1950, A contributon to the geology of the Kavirondon Rift Valley: Quarterly Journal of the Geological Society, v. 106, p. 345-392.

Smith, R.B., 2001, Introduction to Remote Sensing of Environment (RSE): United States of America, TNTmips, MicroImages, Inc, 31 p.

Stockley, G., 1943, The pre-Karoo stratigraphy of Tanganyika, Geol. Mag, 161 p.

Tomkinson, M., 2012, Observations on Au and base metal mineralisation,western Kenya - Aviva Corporation: Unpublished, Aviva Corporation.

Vos, I., Bierlein, F., Standing, J. and Davidson, G., 2009, The geology and mineralisation at the Golden Pride gold deposit, Nzega Greenstone Belt, Tanzania: Mineralium Deposita, v. 44, p. 751-764.

Walraven, F., Pape, J. and Borg, G., 1994, Implications of Pb-isotopic compositions at the Geita gold deposit, Sukumaland Greenstone Belt, Tanzania: Journal of African Earth Sciences, v. 18, p. 111-121.

Weinberg, R.F., Hodkiewicz, P.F. and Groves, D.I., 2004, What controls gold distribution in Archean terranes?: Geology, v. 32, p. 545-548.

Whittaker, A., Cope, J., Cowie, J., Gibbons, W., House, M., Jenkins, D., Rawson, P., Rushton, A., Smith, D. and Thomas, A., 1991, A guide to stratigraphical procedure: Journal of the Geological Society, v. 148, p. 813-824.

Zeegers, H. and Leduc, C., 1993, Geochemical exploration for gold in temperate, arid, semi-arid, and rain-forest terrains, Gold metallogeny and exploration, Springer, p. 309.

APPENDIX A – QUARTER CORE SAMPLES FROM MASUMBI DIAMOND DRILL-HOLES

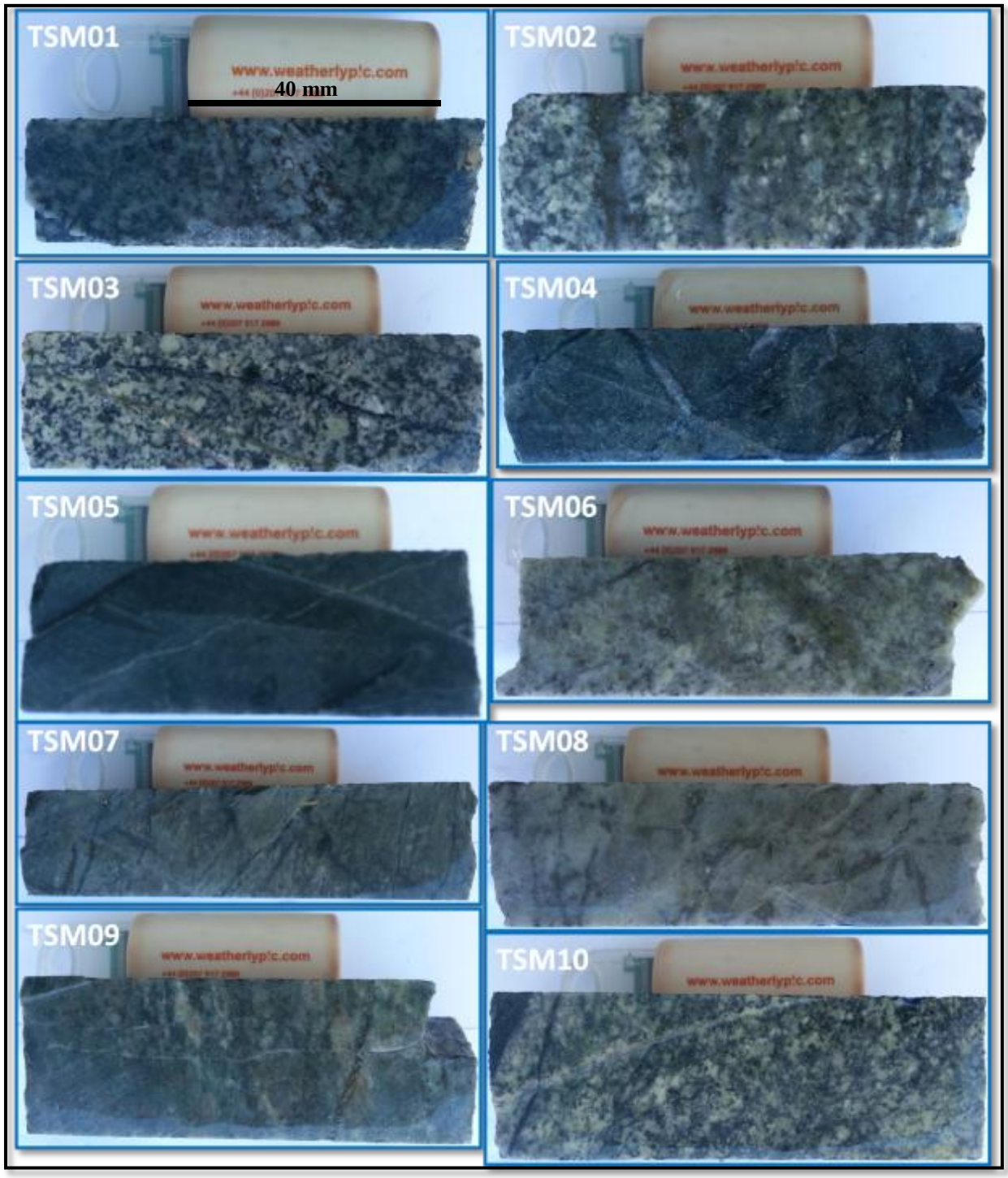

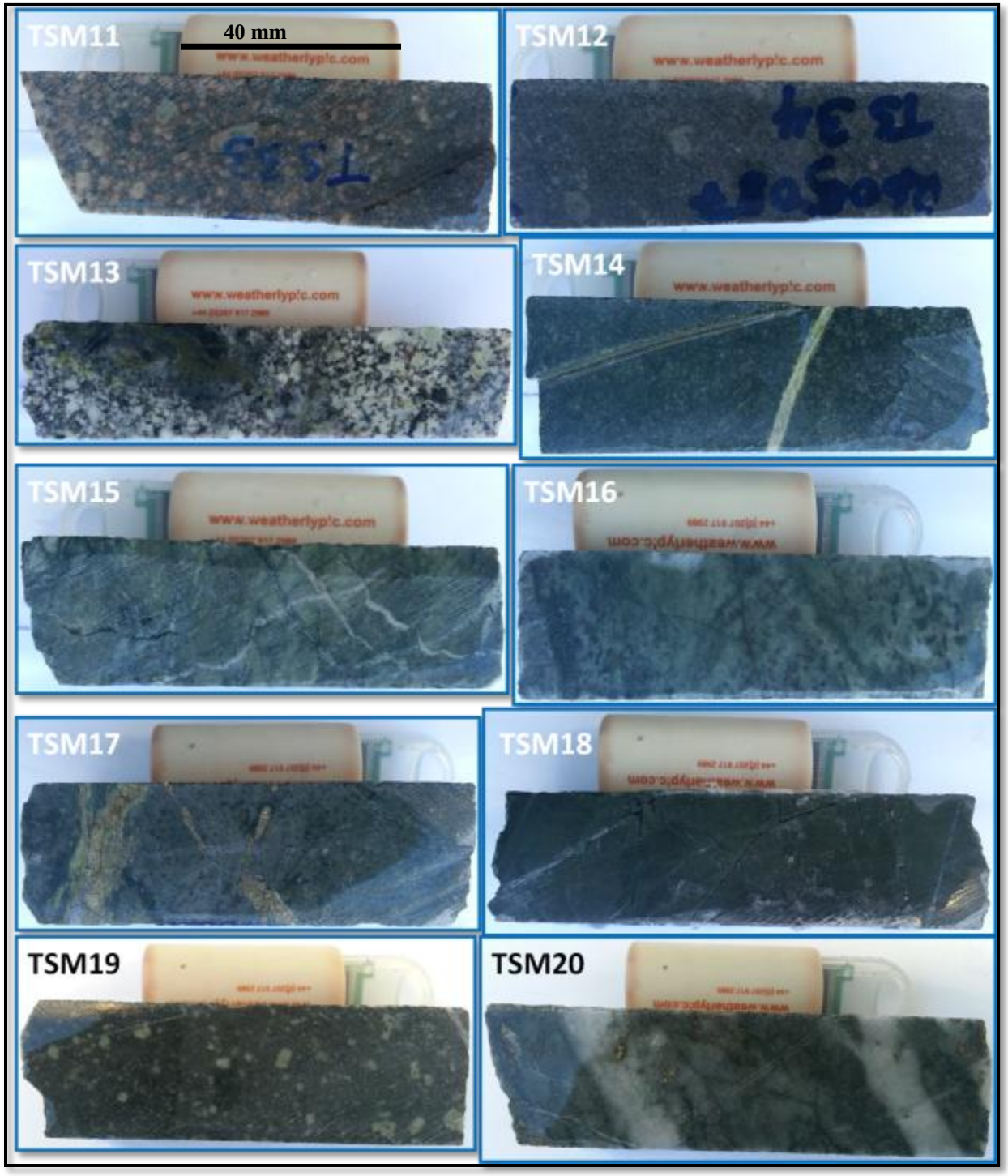
TSM11
40 mm
TSM12
TSM13
TSM14
TSM15
TSM16
TSM17
TSM18
TSM19
TSM20

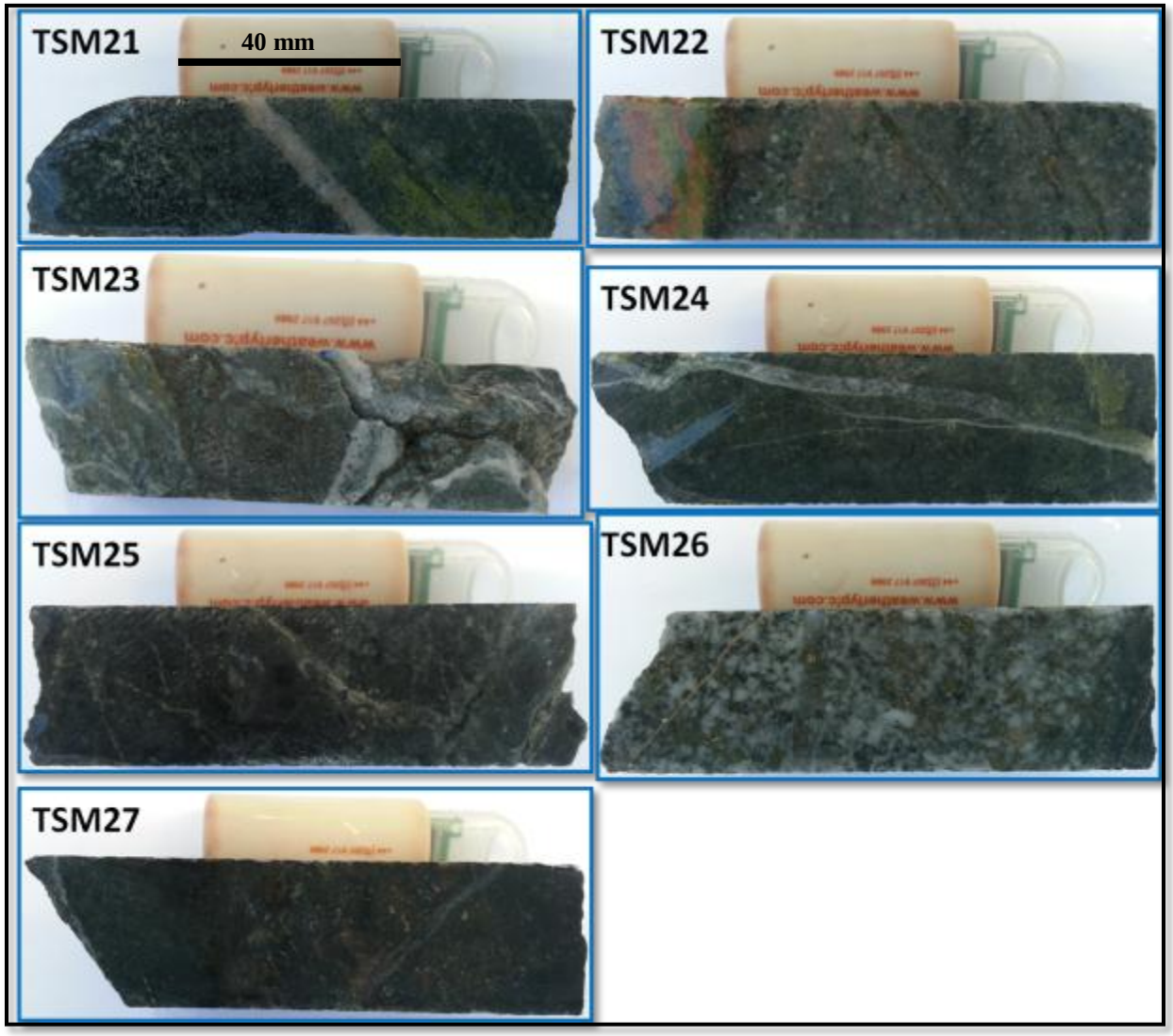
TSM21
40 mm
TSM22
TSM23
TSM24
TSM25
TSM26
TSM27

APPENDIX B – MASUMBI DIAMOND DRILL ASSAY LOGS

ProjectCode: NDORI123
PROSPECT: MASUMBI

HoleID: ANMDD002
Depth: 200.82

Aviva Mining - Kenya

AVIVA MINING KENYA LTD

rock & stock INVESTMENTS

Company: AVIVA_KENY
Geologist: JD
Driller: HALL

Geology Items

From	To	Weathering	Lithology	Comments	Alteration
0	8	ND		Clay - Transported/	
8	16.68	EXTR-V		Saprolite/ Creamy brown, crumbly, extremely weathered. Protolith probably a granite.	OXIDATION Intensely Developed
16.68	18.68	MOD		Alkali Feldspar Granite/ Khaki, massive. Moderately weathered.	OXIDATION Moderately Developed
18.68	18.89			Core Loss/	
18.89	26.61	SL-MOD		Alkali Feldspar Granite/ Light brown, massive.	OXIDATION Weakly to Moderately Developed
26.61	26.82			Core Loss/	OXIDATION
26.82	27.18	SL-MOD		Alkali Feldspar Granite/ Creamy orange, massive. Moderately weathered.	Moderately Developed
27.18	27.68			Core Loss/	
27.68	28.53	FRESH-SL		Alkali Feldspar Granite/ Light pink grey, massive.	
28.53	29.67			Core Loss/	
29.67	38.14	SL-MOD		Alkali Feldspar Granite/ Light orange, massive. Very fractured.	OXIDATION Weakly to Moderately Developed
38.14	40.86			Dacite/ Grey, massive. Interbedded with alkali feldspar granite. Very fractured.	OXIDATION Weakly to Moderately Developed
40.86	44.72	FRESH-SL		Dacite/ with Veined Pyrite. Grey to light grey, massive. Slightly silicified with zones of more intense silicification. Occasional thin quartz carbonate pyrite veinlets. Moderate development of carbonate veinlets.	SILICIFICATION Strongly Developed
44.72	45.58	FRESH		Dacite/ Creamy grey, massive. Intensely silicified due to underlying granite vein.	SILICIFICATION Intensely Developed
45.58	46.48			Granite/ Creamy grey, massive. Unusual irregular top contact.	SILICIFICATION Weakly to Moderately Developed
46.48	49.79			Dacite/ with Veined Pyrite. Grey green, massive. Slight to moderate development of granite forming a ghost texture. Slight to moderate development of quartz pyrite veinlets.	

Assay

From	To	Sample No	Cu (ppm)	Au (ppm)
18	18.68	RS03279		0.096
18.89	20	RS03280		0.394
20	21	RS03281		0.081
21	22	RS03282		0.113
22	23	RS03283		0.152
23	24	RS03284		0.187
24	25	RS03285		0.38
25	25.8	RS03448		0.037
25.8	26.61	RS03449		0.093
26.82	27.18	RS03450		0.121
27.68	28.53	RS03451		0.011
29.67	30.67	RS03452		0.172
30.67	31.67	RS03453		0.039
31.67	32.67	RS03454		0.047
32.67	33.33	RS03455		0.218
33.33	34	RS03456		0.193
34	35	RS03286		0.035
35	36	RS03288		0.027
36	37	RS03289		0.071
37	38.14	RS03290		0.057
38.14	39.14	RS03291		0.551
39.14	40.1	RS03292		0.014
40.1	40.86	RS03293		0.021
40.86	41.86	RS03294	29	0.005
41.86	42.86	RS03295	130	0.058
42.86	43.86	RS03296	67	0.022
43.86	44.72	RS03297	90	0.065
44.72	45.58	RS03298	186	0.074
45.58	46.48	RS03299	394	0.316
46.48	47.67	RS03301	166	0.161

Cu (ppm): 2135. / 4270. | Au (ppm): 7.5 / 15. / 22.5 | Mag Susc: 1. / 97.9 / 969.4 / 9594.

ProjectCode: NDORI123
PROSPECT: MASUMBI

HoleID: ANMDD002
Depth: 200.82

Aviva Mining - Kenya

AVIVA MINING KENYA LTD

rock & stock INVESTMENTS

Company: AVIVA_KENY
Geologist: JD
Driller: HALL

Depth	Geology Items						Assay					Mag Susc
	From	To	Weathering	Lithology	Comments	Alteration	From	To	Sample No	Cu (ppm)	Au (ppm)	
										2135. 4270.	7.5 15. 22.5	1. 97.9 969.4 9594.
	46.48	49.79	FRESH		Dacite/ with Veined Pyrite. Grey green, massive. Slight to moderate development of granite forming a ghost texture. Slight to moderate development of quartz pyrite veinlets.	SILICIFICATION Weakly to Moderately Developed	46.48	47.67	RS03301	166	0.161	
							47.67	48.67	RS03302	800	0.688	
							48.67	49.79	RS03303	1060	0.224	
50	49.79	49.96			Granite/ with Veined Pyrite. Creamy grey granite vein. Pyrite veinlets cross cutting granite.		49.79	49.96	RS03304	279	0.129	
							49.96	51	RS03305	2050	0.173	
							51	52.38	RS03306	4270	0.371	
							52.38	53.13	RS03307	914	0.166	
	49.96	57.97			Dacite/ with Veined Pyrite. Grey to light grey, massive. Granite forming a ghost texture. Slight to moderate development of quartz pyrite veinlets occasionally with chalcopyrite. Mild development of pegmatite from 53.13 to 54.13m.	SILICIFICATION Weakly to Moderately Developed	53.13	54.13	RS03308	1095	0.235	
55							54.13	55.13	RS03309	2790	0.97	
							55.13	56.24	RS03310	304	0.11	
							56.24	57.29	RS03312	1210	0.244	
							57.29	57.97	RS03313	2030	0.444	
	57.97	59.08			Breccia/ with Veined Pyrite. Fault zone. Intensely silicified causing a bleached effect. Brecciated. Silcrete.	SILICIFICATION Intensely Developed	57.97	58.63	RS03314	761	0.16	
							58.63	59.09	RS03315	290	0.15	
	59.08	60.18			Dacite/ with Disseminated Pyrite. Grey green, slightly foliated. Occasional granite veins. Poory mineralized.	SILICIFICATION Weakly to Moderately Developed	59.09	60.18	RS03316	3020	0.437	
60	60.18	61.24			Granite/ with Disseminated Pyrite. Light grey , massive. Silicified. Disseminated pyrite as blebs less than 1 percent.		60.18	61.24	RS03317	1990	0.231	
	61.24	63.46			Dacite/ with Veined Pyrite. Green grey, massive. Pervasive granite throughout unit forming a ghost texture. Mild development of quartz pyrite veins.	SILICIFICATION Strongly Developed	61.24	62.36	RS03319	1695	0.415	
							62.36	63.46	RS03320	2840	0.316	
							63.46	64.46	RS03321	1295	0.104	
65	63.46	67.39			Dacite/ with Veined Pyrite. Green grey, massive. Mildly silicified. Occasional thin quartz pyrite vein, often broken. Occasional thin granite vein.	SILICIFICATION Weakly Developed	64.46	65.46	RS03322	716	0.522	
							65.46	66.46	RS03323	405	0.391	
							66.46	67.39	RS03324	533	0.222	
	67.39	67.76			Dacite/ with Disseminated Pyrite. Creamy brown, massive. Disseminated pyrite less than 1 percent.	SILICIFICATION Intensely Developed	67.39	67.76	RS03325	513	0.25	
							67.76	68.76	RS03326	825	1.205	
	67.76	71.62			Dacite/ with Disseminated Pyrite. Creamy grey green, massive. Strongly silicified. Minor disseminated pyrite less than 0.1 percent.	SILICIFICATION Strongly Developed	68.76	69.76	RS03327	537	0.176	
70							69.76	70.76	RS03328	940	0.359	
							70.76	71.62	RS03330	3610	0.483	
	71.62	72.14			Dacite/ with Disseminated Pyrite. Light grey, massive. Intensely silicified with quartz vein. Mildy mineralized [pyrite less than 1 percent].	SILICIFICATION Intensely Developed	71.62	72.14	RS03331	1015	0.643	
							72.14	73.32	RS03332	2510	0.536	
							73.32	74.19	RS03333	2430	0.705	
	72.14	78.12			Dacite/ with Disseminated Pyrite. Light grey to grey, massive to occasionally foliated. Mild to moderate disseminated pyrite [0.1 to 3 percent]. Strong to intensely silicified. Occasional small quartz pyrite veinlets, typically broken.	SILICIFICATION Intensely Developed	74.19	75.1	RS03334	1895	0.634	
75							75.1	75.73	RS03335	220	0.169	
							75.73	76.65	RS03336	641	0.33	
							76.65	78.12	RS03337	719	0.938	
	78.12	79.6			Dacite/ with Disseminated Pyrite. Brown grey, massive and fractured. Moderately silicified. Mild to moderate disseminated pyrite mineralization [up to apprx 1 percent]. Occasional thin quartz pyrite veinlet.	SILICIFICATION Moderately Developed	78.12	79.6	RS03338	193	1.955	
	79.6	80.2			Diorite/ with Disseminated Pyrite. Micro diorite. Grey to green grey, massive. Mild to moderately silicified decreasing downwards. Epidote alteration near bottom contact. Generally poory mineralized.	SILICIFICATION Moderately Developed	79.6	80.2	RS03340	478	0.444	
80	80.2	81.85			Dacite/ with Disseminated Pyrite. Grey to brown grey, massive. Moderately silicified with a ghost granite texture in places. Slightly mineralized [less than 1 percent pyrite].	SILICIFICATION Strongly Developed	80.2	81.2	RS03341	232	0.27	
							81.2	81.85	RS03342	1725	4.31	
							81.85	82.6	RS03343	735	7.87	
	81.85	85.08			Dacite/ Pink green, massive. Pink color due to influence of pervasive granite throughout unit. Generally poory mineralized. Moderate epidote alteration often as veins.		82.6	83.6	RS03344	205	0.29	
							83.6	84.54	RS03345	274	0.22	
85							84.54	85.08	RS03346	1365	0.857	
	85.08	87.29			Dacite/ with Veined Pyrite. Grey to light grey, massive. Moderately silicified. Moderate development of quartz pyrite veinlets.	SILICIFICATION Moderately Developed	85.08	86.12	RS03348	1870	2.74	
							86.12	86.59	RS03349	982	0.553	
							86.59	87.29	RS03350	272	0.285	
							87.29	88.29	RS03351	390	0.428	
							88.29	88.95	RS03352	302	0.7	
							88.95	89.95	RS03353	302	0.511	
90	87.29	115.1			Diorite/ with Veined Pyrite. Micro diorite. Grey green, massive. Occasional zones with mild to moderate epidote alteration commonly as veins. Occasional pegmatite vein. Occasional zones with quartz pyrite veinlets.		89.95	90.95	RS03354		0.192	
							90.95	91.95	RS03355		0.094	
							91.95	92.95	RS03356		0.327	
							92.95	93.93	RS03357		0.195	
							93.93	94.93	RS03358		0.06	

ProjectCode: NDORI123
PROSPECT: MASUMBI

HoleID: ANMDD002
Depth: 200.82

Aviva Mining - Kenya

Company: AVIVA_KENY
Geologist: JD
Driller: HALL

Depth	Geology Items						Assay					Mag Susc
	From	To	Weathering	Litholog y	Comments	Alteration	From	To	Sample No	Cu (ppm)	Au (ppm)	
										2135. 4270.	7.5 15. 22.5	1. 97.9 969.4 9594.
95			FRESH				93.93	94.93	RS03358		0.06	
							94.93	95.93	RS03359		0.455	
							95.93	96.93	RS03361		0.466	
							96.93	97.93	RS03362		0.072	
							97.93	98.29	RS03363		0.048	
							98.29	98.67	RS03364		0.067	
							98.67	99.5	RS03365		0.014	
100							99.5	100.5	RS03366		0.267	
							100.5	101.5	RS03367		0.151	
							101.5	102.5	RS03368		1.56	
							102.5	103.5	RS03370		0.123	
							103.5	104.5	RS03371		0.099	
	87.29	115.1			Diorite/ with Veined Pyrite. Micro diorite. Grey green, massive. Occasional zones with mild to moderate epidote alteration commonly as veins. Occasional pegmatite vein. Occasional zones with quartz pyrite veinlets.		104.5	104.8	RS03372		0.211	
105							104.8	105.8	RS03373		0.373	
							105.8	106.43	RS03374		5	
							106.43	106.83	RS03375		0.148	
							106.83	107.83	RS03376		0.136	
							107.83	108.83	RS03377		0.013	
							108.83	109.83	RS03378		0.0025	
110							109.83	111	RS03379		0.005	
							111	112.3	RS03381		0.0025	
							112.3	113.3	RS03382		0.009	
							113.3	114	RS03383		0.005	
							114	115.1	RS03384		0.693	
115							115.1	116.1	RS03458		0.007	
	115.1	117.14			Diorite/ Dark grey, massive.		116.1	117.12	RS03459		0.0025	
							117.12	118.12	RS03460		0.0025	
							118.12	119.12	RS03461		0.0025	
	117.14	122			Diorite/ Micro diorite, massive. Mildly to moderately epidotized.		119.12	120.12	RS03462		0.0025	
120							120.12	121.12	RS03463		0.0025	
							121.12	122	RS03464		0.0025	
							122	122.85	RS03385		0.0025	
	122	124.95			Diorite/ Micro diorite. Green yellow to dark grey, foliated. Mildly silicified, moderately epidotized. Minor disseminated pyrite [less than 1 percent].	SILICIFICATIO N Weakly to Moderately Developed	122.85	124.05	RS03386		0.085	
							124.05	124.95	RS03388		0.038	
125							124.95	126	RS03389		0.03	
	124.95	128.55			Diorite/ Mildly epidotized commonly as veins. Pegmatite vein from 128.03 to 128.16m.		126	127	RS03390		0.077	
							127	127.92	RS03391		0.005	
							127.92	128.55	RS03392		0.051	
							128.55	129.55	RS03393		0.085	
130	128.55	132.5			Diorite/ with Veined Pyrite. Micro diorite, green grey, massive to slightly foliated. Moderate development of thin [less than 1 cm] pegmatite veins with associated pyrite and epidote alteration. Mildly silicified.	SILICIFICATIO N Weakly to Moderately Developed	129.55	130.55	RS03394		0.053	
							130.55	131.55	RS03395		0.765	
							131.55	132.5	RS03396		0.927	
	132.5	133.32			Diorite/ Green grey, massive.		132.5	133.32	RS03397		0.044	
							133.32	134.32	RS03398		0.021	
135	133.32	136.48			Diorite/ with Veined Pyrite. Micro diorite. Dark grey green, massive. Moderate development of epidote veins with associated pyrite at bottom contact area. Mild development of quartz pyrite veinlets.		134.32	135.32	RS03399		0.144	
							135.32	136.48	RS03401		0.148	
	136.48	138.94			Diorite/ with Layered Pyrite. Grey, massive. Moderately epidotized with associated pyrite. Occasional pegmatite. Small sliver of dolerite at 137.88m.		136.48	137.62	RS03402		0.413	
							137.62	138.94	RS03403		0.741	
							138.94	139.94	RS03465		0.026	
140	138.94	152.58			Diorite/ Micro diorite, grey, massive. Generally poorly epidotized and mineralized. Occasional pegmatite veins [less than 1cm]. Poor core recovery from 149.18 to 149.82m. BQ size core.		139.94	140.94	RS03466		0.076	
							140.94	141.94	RS03468		0.028	

ProjectCode: NDORI123
PROSPECT: MASUMBI

HoleID: ANMDD002
Depth: 200.82

Aviva Mining - Kenya

Company: AVIVA_KENY
Geologist: JD
Driller: HALL

Depth	From	To	Weathering	Lithology	Comments	Alteration
145	138.94	152.58	FRESH		Diorite/ Micro diorite, grey, massive. Generally poorly epidotized and mineralized. Occasional pegmatite veins [less than 1cm]. Poor core recovery from 149.18 to 149.82m. BQ size core.	
150	152.58	160.19			Diorite/ Grey, massive. Occasionally mildly epidotized. Occasional thin [less than 2cm] pegmatite veins.	
160	160.19	161.24			Mafic Dyke/ Dolerite dyke.	
	161.24	163.36			Diorite/ Grey , massive. Occasionally mildly epidotized.	
165	163.36	167.12			Diorite/ with Veined Pyrite. Micro diorite. Light grey, massive to slightly foliated. Appears bleached. Moderately silicified. Mildly epidotized commonly as veins. Mild to moderate development of disseminated pyrite [1 percent].	SILICIFICATION Weakly to Moderately Developed
	167.12	167.51			Diorite/ Grey, massive, medium grained. Poory mineralized.	
	167.51	169.07			Diorite/ with Disseminated Pyrite. Micro diorite, massive to slightly foliated. Strongly silicified. Mildly epidotized commonly as veins. Moderate development of disseminated pyrite [1 to 2 percent].	SILICIFICATION Strongly Developed
170	169.07	172.36			Diorite/ Grey, massive. Mildly epidotized often as veins. Mild pyrite mineralization as large blebs.	
175	172.36	176.48			Diorite/ with Disseminated Pyrite. Micro diorite, creamy green, massive to slightly foliated. Strongly silicified, Mild to moderate disseminated pyrite. Occasional chalcopyrite. Abundant quartz [pyrite] veinlets.	SILICIFICATION Strongly Developed
	176.48	177.22			Diorite/	SILICIFICATION Weakly Developed
180	177.22	182.4			Diorite/ with Disseminated Pyrite. Micro diorite, creamy green, massive to slightly foliated. Moderately to strongly silicified. Mildly to moderately epidotized often as veins. Mild development of disseminated pyrite.	SILICIFICATION Strongly Developed
185	182.4	195.38			Diorite/ Grey, massive. Mildly epidotized commonly as veins especially at upper contact area.	

From	To	Sample No	Cu (ppm)	Au (ppm)	Mag Susc
140.94	141.94	RS03468		0.028	
141.94	142.94	RS03469		0.008	
142.94	143.94	RS03470		0.292	
143.94	144.94	RS03471		0.007	
144.94	145.94	RS03472		0.006	
145.94	146.94	RS03473		0.35	
146.94	147.94	RS03474		0.243	
147.94	148.94	RS03475		0.026	
148.94	149.94	RS03476		0.041	
149.94	150.94	RS03478		0.025	
150.94	151.58	RS03479		0.007	
151.58	152.58	RS03404		0.133	
152.58	153.58	RS03480		0.175	
153.58	154.58	RS03481		0.17	
154.58	155.58	RS03482		0.195	
155.58	156.58	RS03483		0.848	
156.58	157.58	RS03484		0.031	
157.58	158.58	RS03485		0.034	
158.58	159.58	RS03486		0.492	
159.58	160.21	RS03488		0.061	
160.21	161.21	RS03489		0.0025	
161.21	162.36	RS03490		0.089	
162.36	163.36	RS03405		0.24	
163.36	164.36	RS03406		0.079	
164.36	165.36	RS03407		0.354	
165.36	166.36	RS03408		0.135	
166.36	167.12	RS03409		0.159	
167.12	167.51	RS03410		0.012	
167.51	168.51	RS03412		0.708	
168.51	169.07	RS03413		0.153	
169.07	170.07	RS03414		0.104	
170.07	171.07	RS03415		0.199	
171.07	172.36	RS03416		0.213	
172.36	173.36	RS03417		0.099	
173.36	174.36	RS03418		0.092	
174.36	175.36	RS03419		0.29	
175.36	176.48	RS03421		0.146	
176.48	177.22	RS03422		0.199	
177.22	178.22	RS03423		0.06	
178.22	179.22	RS03424		0.017	
179.22	180.22	RS03425		0.077	
180.22	181.22	RS03426		0.085	
181.22	182.4	RS03427		0.205	
182.4	183.4	RS03429		0.009	
183.4	184.7	RS03430		0.168	
184.7	185.7	RS03491		0.007	
185.7	186.7	RS03492		0.007	
186.7	187.7	RS03493		0.005	
187.7	188.7	RS03494		0.0025	

ProjectCode: NDORI123
PROSPECT: MASUMBI

HoleID: ANMDD002
Depth: 200.82

Aviva Mining - Kenya

Company: AVIVA_KENY
Geologist: JD
Driller: HALL

Depth	Geology Items						Assay					Mag Susc
	From	To	Weathering	Lithology	Comments	Alteration	From	To	Sample No	Cu (ppm)	Au (ppm)	
										2135.	7.5 15. 22.5	1. 97.9 969.4 9594.
190	182.4	195.38	FRESH		Diorite/ Grey, massive. Mildly epidotized commonly as veins especially at upper contact area.		187.7	188.7	RS03494		0.0025	
							188.7	189.7	RS03495		0.007	
							189.7	190.7	RS03496		0.344	
							190.7	191.7	RS03498		0.006	
							191.7	192.7	RS03499		0.0025	
							192.7	193.7	RS03500		0.0025	
195							193.7	194.7	RS03501		0.0025	
							194.7	195.4	RS03502		0.053	
	195.38	198.26			Diorite/ Micro diorite, dark grey to black, with a porphyritic texture. Possibly a dyke.		195.4	196.4	RS03503		0.017	
							196.4	197.4	RS03504		0.022	
							197.4	198.24	RS03505		0.0025	
							198.24	199.24	RS03506		0.006	
200	198.26	200.82			Diorite/ Green grey, occasional epidote vein.		199.24	200.03	RS03508		0.0025	
							200.03	200.82	RS03509		0.0025	
205												
210												
215												
220												
225												
230												
235												

ProjectCode: NDORI123
PROSPECT: MASUMBI

HoleID: ANMDD003
Depth: 200.91

Aviva Mining - Kenya

Company: AVIVA_KENY
Geologist: LS
Driller: HALL

Depth	Geology Items						Assay					Mag Susc
	From	To	Weathering	Lithology	Comments	Alteration	From	To	Sample No	Cu (ppm)	Au (ppm)	
										2135. 4270.	7.5 15. 22.5	1. 97.9 969.4 9594.
0	0	4.82	EXTR		Overburden/ Reddish brown soil							
5	4.82	7.2			Overburden/							
	7.2	8.63			Saprolite/ Creamish yellow in colour and micaceous in places		7.2	8.63	RS05029	1090	1.31	
10	8.63	10.76			Core Loss/							
	10.76	26.63	EXTR-V		Saprolite/		10.76	11.76	RS05030	809	0.233	
							11.76	12.76	RS05031	749	0.39	
							12.76	13.76	RS05032	937	0.415	
							13.76	14.76	RS05034	943	0.285	
15							14.76	15.76	RS05035	842	0.419	
							15.76	16.76	RS05036	943	0.769	
							16.76	17.76	RS05037	1240	1.165	
							17.76	18.76	RS05038	1270	0.415	
20							18.76	19.76	RS05039	1010	0.719	
							19.76	20.76	RS05040	1090	0.789	
							20.76	21.76	RS05041	1190	0.194	
							21.76	22.76	RS05043	921	0.42	
							22.76	23.76	RS05044	786	0.249	
							23.76	24.76	RS05045	648	0.068	
25							24.76	25.76	RS05046	587	0.062	
							25.76	26.63	RS05047	635	0.049	
	26.63	28.58	V		Saprock/ Creamish yellow in colour, with iron-stained fractures.		26.63	27.63	RS05048	166	0.081	
							27.63	28.58	RS05049	313	0.427	
							28.58	29.58	RS05050	252	0.176	
30	28.58	32.35	SL-MOD		Diorite/ Medium grained, massive, greenish coloured dioritic unit. Magnetic		29.58	30.58	RS05051	304	0.2	
							30.58	31.58	RS05052	291	0.139	
	32.35	32.52			Quartz Vein/		31.58	32.35	RS05053	449	0.707	
	32.52	32.78			Diorite/		32.35	32.52	RS05054	707	1.92	
	32.78	33.08	MOD		Core Loss/		32.52	32.78	RS05055	83	0.089	
	33.08	33.16	V		Diorite/ Extremely weathered material		33.08	33.16	RS05057	242	0.025	
	33.16	33.73	EXTR		Core Loss/		33.73	33.82	RS05058	16	0.024	
	33.73	33.82	FRESH-SL		Diorite/ Magnetic		34.28	34.38	RS05059	155	0.113	
	33.82	34.28			Core Loss/							
	34.28	34.38	V		Diorite/							
35	34.38	35.63			Core Loss/							
	35.63	36.19	V		Diorite/		35.63	36.19	RS05060	476	0.03	
	36.19	37.58	MOD		Silcrete/ Fine-grained, pale greenish white, siliceous unit - '??silcrete'		36.19	37.58	RS05061	177	0.371	
	37.58	38.63	MOD-V		Diorite/ Weathered, porphyritic dioritic unit		37.58	38.63	RS05062	257	0.021	
	38.63	39.23	MOD		Silcrete/ Pale greenish white, fine-grained siliceous unit - '??silcrete'. Broken up		38.63	39.23	RS05063	279	0.602	
40							39.23	40.23	RS05065	149	0.08	
	39.23	42.63			Silcrete/ Pale greenish white. fine grained siliceous unit - '??silcrete' unit. Badly broken up		40.23	41.23	RS05066	66	0.131	
							41.23	42.63	RS05067	271	0.034	
					Core Loss/							
	42.63	43.1			Diorite/ with Disseminated Pyrite. Fine-medium grained, epidotised, magnetic, (?micro) dioritic unit. Mineralised with fine sulphide (py) disseminations and very thin sulphide veins. Oxidised along fractute planes.	EPIDOTIZATIO N Weakly to Moderately Developed						
	43.1	44.2	FRESH-SL		Core Loss/		43.1	44.2	RS05068	566	0.167	
	44.2	44.38			Diorite/ with Stringer Pyrite. Selectivel weathered, fine grained and magnetic (?micro) dioritic unit with occasional very thin sulphide stringers. Weakly epidotised. Silicified from 45.17m to 45.32m.	EPIDOTIZATIO N Weakly Developed SILICIFICATIO N Moderately Developed						
45	44.38	45.84	FRESH-SL		Diorite/ with Stringer Pyrite. Silicified, with very thin pyrite stringers		44.38	45.38	RS05069	750	0.13	
	45.84	46			Core Loss/		45.38	45.84	RS05070	1330	0.548	
	46	46.46			Diorite/ with Stringer Pyrite. Silicified, with occasional pyrite stringers	SILICIFICATIO N Moderately Developed	45.84	46	RS05071	453	0.22	
	46.46	46.88	FRESH-SL		Diorite/ Magnetic, oxidised along fractures, with occasional pyrite stringers and blebs. Weakly silicified in places.		46.46	46.88	RS05072	594	2.71	
	46.88	47.33					46.88	47.33	RS05073	486	0.127	

ProjectCode: NDORI123
PROSPECT: MASUMBI

HoleID: ANMDD003
Depth: 200.91

Aviva Mining - Kenya

Company: AVIVA_KENY
Geologist: LS
Driller: HALL

Geology Items						Assay					Mag Susc
From	To	Weathering	Lithology	Comments	Alteration	From	To	Sample No	Cu (ppm)	Au (ppm)	
46.88	47.33	FRESH-SL		Diorite/ Magnetic, oxidised along fractures, with occasional pyrite stringers and blebs. Weakly silicified in places.		46.88	47.33	RS05073	486	0.127	
47.33	47.91			Core Loss/							
						47.91	49	RS05075	236	0.183	
47.91	51	FRESH-SL		Diorite/ with Stringer Pyrite. Epidotised and silicified in places, with occasional pyrite stringers and blebs. Magnetic	EPIDOTIZATION Weakly Developed	49	50	RS05076	500	0.266	
						50	51	RS05077	210	0.168	
51	51.21			Core Loss/							
51.21	53.24	FRESH-SL		Diorite/ Silicified in places, magnetic, with very thin sulphide stringers. Cubic pyrite and chalcopyrite blebs present in places and along fracture planes.	SILICIFICATION Weakly to Moderately Developed	51.21	52.21	RS05078	205	0.425	
						52.21	53.24	RS05079	948	0.461	
						53.24	54.24	RS05080	89	0.047	
53.24	56.04	FRESH		Granite/ Medium-coarse grained, leucocratic, inequigranular granitic unit. With sporadic sulphide disseminations and blebs, especially along fracture planes. Plagioclase feldspar is the dominant feldspar.		54.24	55.24	RS05081	131	0.084	
						55.24	56.04	RS05083	268	0.128	
56.04	57.7	FRESH-SL		Alkali Feldspar Granite/		56.04	57.04	RS05084		0.007	
						57.04	57.7	RS05085		0.01	
57.7	59.17			Diorite/ Melanocratic and porphyritic, especially towards bottom contact.		57.7	58.5	RS05086		0.049	
				Granite/ With thin sulphide stringers of pyrite and chalcopyrite		58.5	59.17	RS05087	31	1.135	
59.17	59.36			Dacite/ with Stringer Weakly silicified and epidotised in places, with occasional fine disseminations and blebs of chalcopyrite. Very magnetic (?magnetite) in places.	SILICIFICATION Weakly Developed	59.17	59.36	RS05088	136	0.298	
59.36	59.91					59.36	59.91	RS05089	316	0.536	
						59.91	60.91	RS05090	24	0.047	
						60.91	61.91	RS05091	40	0.025	
59.91	64.93			Granite/ Medium-coarse grained granitic unit with abundant plagioclase feldspar. Weak alteration of epidote as thin veinlets. With occasional K-feldspar veins (5-10mm wide) and sporadic sulphide stringers and blebs.		61.91	62.91	RS05092	106	0.186	
						62.91	63.91	RS05094	115	0.133	
						63.91	64.93	RS05095	55	0.119	
						64.93	65.93	RS05096	705	0.415	
						65.93	66.93	RS05097	373	0.062	
						66.93	67.93	RS05098	247	0.173	
						67.93	68.93	RS05099	1070	0.307	
64.93	74.41			Dacite/ with Stringer Pyrite. Fine-medium grained, fresh, green, magnetic unit. Weakly to moderately silicified and epidotised. With occasional pyrite and minor chalcopyrite stringers and blebs. Intercalated with minor dioritic and granitic units.	SILICIFICATION Weakly to Moderately Developed	68.93	69.93	RS05101	566	0.205	
						69.93	70.93	RS05102	1760	0.74	
						70.93	71.93	RS05103	461	0.121	
						71.93	72.93	RS05104	112	0.025	
						72.93	74.41	RS05105	661	0.588	
						74.41	75.41	RS05106	158	0.105	
74.41	76.85	FRESH		Diorite/ Porphyritic dioritic unit. Weakly silicified in places, with hairline sulphide stringers.		75.41	76.85	RS05108	168	0.182	
						76.85	77.85	RS05109	150	0.075	
76.85	80.26			Dacite/ Fine grained, magnetic in places, with occasional epidote veins. Very thin sulphide stringers are present, oxidised in places.		77.85	78.85	RS05110	365	0.128	
						78.85	79.85	RS05111	157	0.176	
						79.85	80.26	RS05112	205	0.248	
						80.26	81.26	RS05113	611	0.442	
80.26	83.79			Diorite/ Weakly silicified and epidotised, medium grained dioritic unit with occasional hairline sulphide stringers. The sulphide stringers are commonly concordant with epidote veins.	SILICIFICATION Weakly to Moderately Developed	81.26	82.26	RS05114	790	0.656	
						82.26	83.79	RS05115	520	0.315	
						83.79	84.79	RS05117	1150	0.224	
						84.79	85.79	RS05118	1270	0.584	
						85.79	86.79	RS05119	640	0.475	
						86.79	87.79	RS05120	1090	0.294	
						87.79	88.79	RS05121	1470	0.392	
83.79	95.23			Dacite/ with Disseminated Pyrite. Moderately epidotised, magnetic, intercalated in places with granite. Well mineralised with pyrite and chalcopyrite disseminations and stringers, usually in association with epidote veins.	EPIDOTIZATION Weakly to Moderately Developed	88.79	89.79	RS05122	1310	0.709	
						89.79	90.79	RS05123	1620	0.629	
						90.79	91.79	RS05124	2250	1.615	
						91.79	92.79	RS05125	2430	0.617	
						92.79	93.79	RS05126	1560	0.448	
						93.79	94.79	RS05127	2370	0.503	

ProjectCode: NDORI123
PROSPECT: MASUMBI

HoleID: ANMDD003
Depth: 200.91

Aviva Mining - Kenya

Company: AVIVA_KENY
Geologist: LS
Driller: HALL

Geology Items						Assay					Mag Susc
From	To	Weathering	Lithology	Comments	Alteration	From	To	Sample No	Cu (ppm)	Au (ppm)	
									2135. 4270.	7.5 15. 22.5	1. 97.9 969.4 9534.
83.79	95.23	FRESH		Dacite/ with Disseminated Pyrite. Moderately epidotised, magnetic, intercalated in places with granite. Well mineralised with pyrite and chalcopyrite disseminations and stringers, usually in association with epidote veins.	EPIDOTIZATION Weakly to Moderately Developed	93.79	94.79	RS05127	2370	0.503	
						94.79	95.23	RS05129	1250	0.215	
95.23	97.4			Dacite/ with Stringer Pyrite. Silicified, fine grained, light green coloured unit, with pyrite mineralisation as stringers and very thin veinlets.	SILICIFICATION Moderately Developed	95.23	96.23	RS05130	1210	0.259	
						96.23	97.4	RS05131	2150	0.534	
97.4	109.23			Dacite/ with Stringer Pyrite. Fresh, fine grained, green coloured horizon. Moderately epidotised and weakly silicified in places, with occasional cross cutting quartz carbonate veining. Mineralised with minor to moderate amounts of pyrite and chalcopyrite as stringers and blebs, especially along veins and veinlets usually associated with epidote.	EPIDOTIZATION Weakly to Moderately Developed	97.4	98.4	RS05132	1750	0.21	
						98.4	99.4	RS05133	1130	0.86	
						99.4	100.4	RS05134	560	0.219	
						100.4	101.4	RS05135	553	0.384	
						101.4	102.4	RS05137	930	0.382	
						102.4	103.4	RS05138	236	0.163	
						103.4	104.4	RS05139	583	0.155	
						104.4	105.4	RS05140	522	0.273	
						105.4	106.4	RS05141	1120	0.638	
						106.4	107.4	RS05142	1380	0.485	
						107.4	108.4	RS05143	1410	0.71	
						108.4	109.23	RS05144	1540	0.66	
109.23	114.91			Dacite/ Silicified, fine grained, light green coloured horizon. With sporadic minor chalcopyrite and pyrite stringers and blebs. Mild quartz carbonate veining present. Brecciated in places and very subtle faulting observed.	SILICIFICATION Moderately Developed	109.23	110.23	RS05145	1030	0.189	
						110.23	111.23	RS05146	222	0.429	
						111.23	112.23	RS05148	214	0.105	
						112.23	113.23	RS05149	1710	7.38	
						113.23	114.23	RS05150	1280	2.48	
						114.23	114.91	RS05151	545	0.245	
114.91	116.31			Intermediate Dyke/ Massive, fine-medium grained mesocratic ?dyke.		114.91	115.6	RS05152	86	0.0025	
						115.6	116.31	RS05153	78	0.0025	
116.31	116.73			Dacite/ with Blebs Pyrite. Silicified ?dacitic horizon, with minor pyrite mineralisation as blebs and stringers.	SILICIFICATION Moderately Developed	116.31	116.73	RS05154	87	0.054	
						116.73	117.73	RS05155	92	0.067	
						117.73	118.73	RS05156	75	0.0025	
						118.73	119.73	RS05157	252	0.037	
						119.73	120.73	RS05159	616	0.112	
116.73	127.76			Dacite/ Weakly to moderately silicified and epidotised, fine grained ?dacitic horizon. Mineralised with minor sulphide as stringers and blebs.	EPIDOTIZATION Weakly to Moderately Developed	120.73	122.25	RS05160	344	0.12	
						122.25	123.73	RS05161	1910	0.398	
						123.73	124.73	RS05162	939	0.211	
						124.73	125.73	RS05163	1120	0.21	
						125.73	126.73	RS05164	376	0.052	
						126.73	127.76	RS05165	1090	0.107	
127.76	130.99			Diorite/ Medium grained ?dioritic unit characterized by epidote alteration. Oxidised along fracture planes.	EPIDOTIZATION Moderately Developed	127.76	128.76	RS05166	101	0.02	
						128.76	129.76	RS05167	519	0.431	
						129.76	130.76	RS05168	634	0.347	
130.99	131.06			Quartz Vein/ with Blebs Chalcopyrite. With distinct chalcopyrite and pyrite blebs		130.76	131.06	RS05170	1790	0.978	
						131.06	132.06	RS05171	188	0.092	
						132.06	133.06	RS05172	321	0.131	
						133.06	134.06	RS05173	336	0.508	
						134.06	135.06	RS05174	479	0.476	
131.06	140.05			Diorite/ Fine-medium grained, green coloured, dioritic-dacitic unit. Epidotised in places, with cross cutting quartz carbonate veining. Sulphide mineralisation present as hairline stringers.	EPIDOTIZATION Weakly to Moderately Developed	135.06	136.06	RS05176	334	0.579	
						136.06	137.06	RS05177	925	2.22	
						137.06	138.06	RS05178	341	0.356	
						138.06	139.06	RS05179	743	0.42	
						139.06	140.05	RS05180	349	0.259	
140.05	140.5			Dacite/ Vuggy in places and moderately carbonated.	SILICIFICATION Strongly Developed	140.05	140.5	RS05181	1190	0.228	
140.5	149.27			Diorite/		140.5	141.5	RS05182	598	0.497	

ProjectCode: NDORI123
PROSPECT: MASUMBI

HoleID: ANMDD003
Depth: 200.91

Aviva Mining - Kenya

Company: AVIVA_KENY
Geologist: LS
Driller: HALL

Depth	From	To	Weathering	Lithology	Comments	Alteration	From	To	Sample No	Cu (ppm)	Au (ppm)	Mag Susc
										2135. 4270.	7.5 15. 22.5	1. 97.9 969.4 9594.
145	140.5	149.27	FRESH		Diorite/		140.5	141.5	RS05182	598	0.497	
							141.5	142.5	RS05183	353	0.221	
							142.5	143.5	RS05184	47	0.039	
							143.5	144.5	RS05185	1190	0.379	
							144.5	145.5	RS05186	227	0.082	
							145.5	146.5	RS05187	255	0.086	
							146.5	147.5	RS05189	290	0.181	
							147.5	148.5	RS05190	239	0.095	
							148.5	149.27	RS05191	178	0.233	
150	149.27	155.89			Dacite/ with Stringer Chalcopyrite. Silicified dacitic-dioritic horizon, well mineralised with chalcopyrite stringers and blebs as well as stringers and cubic blebs of pyrite.	SILICIFICATION Moderately Developed	149.27	150.27	RS05192	1410	0.114	
							150.27	151.77	RS05193	2890	0.915	
							151.77	153.27	RS05194	1780	0.125	
							153.27	154.27	RS05195	3310	0.584	
155							154.27	155.27	RS05196	1410	0.254	
							155.27	155.89	RS05197	3760	1.36	
	155.89	159.36			Dacite/ Strongly epidotised and moderately silicified in places. With minor pyrite stringers.	EPIDOTIZATION Strongly Developed	155.89	156.89	RS05198	610	0.254	
							156.89	157.89	RS05199	786	0.352	
							157.89	158.89	RS05201	3150	0.289	
							158.89	159.36	RS05202	187	0.036	
160							159.36	160.36	RS05203	932	0.239	
							160.36	161.36	RS05204	938	0.226	
							161.36	162.36	RS05205	303	0.351	
							162.36	163.36	RS05206	365	0.143	
							163.36	164.36	RS05207	586	0.09	
165							164.36	165.36	RS05208	508	0.091	
							165.36	166.36	RS05209	550	0.118	
							166.36	167.36	RS05211	490	0.22	
	159.36	177.65			Dacite/ with Stringer Pyrite. Weakly to strongly silicified dacitic horizon, mineralised with stringers and blebs of pyrite and chalcopyrite.Quartz carbonate veining present in places.	SILICIFICATION Weakly to Moderately Developed	167.36	168.36	RS05212	1260	0.311	
							168.36	169.36	RS05213	455	0.121	
170							169.36	170.36	RS05214	421	0.237	
							170.36	171.36	RS05215	166	0.052	
							171.36	172.36	RS05216	37	7.41	
							172.36	173.36	RS05217	53	10.95	
							173.36	174.36	RS05219	45	0.068	
175							174.36	175.36	RS05220	60	0.133	
							175.36	176.36	RS05221	64	0.057	
							176.36	177.65	RS05222	8	0.0025	
	177.65	178.52			Diorite/	EPIDOTIZATION Weakly to Moderately Developed	177.65	178.52	RS05223	6	0.005	
							178.52	179.52	RS05224		0.009	
180	178.52	181.47	FRESH-SL		Dacite/ Moderately silicified and epidotised, fine grained ?dacitic horizon. Very broken up in places.	SILICIFICATION Weakly to Moderately Developed	179.52	180.52	RS05225		0.084	
							180.52	181.47	RS05226		0.0025	
							181.47	182.47	RS05227		0.035	
							182.47	183.47	RS05228		0.037	
							183.47	184.47	RS05229		0.016	
185	181.47	200.91	FRESH		Diorite/ Porphyritic and epidotised, medium grained ?dioritic unit, oxidised along fracture planes.	EPIDOTIZATION Weakly to Moderately Developed	184.47	185.47	RS05231		0.038	
							185.47	186.47	RS05232		0.034	
							186.47	187.47	RS05233		0.016	
							187.47	188.47	RS05234		0.014	

ProjectCode: NDORI123
PROSPECT: MASUMBI

HoleID: ANMDD003
Depth: 200.91

Aviva Mining - Kenya

Company: AVIVA_KENY
Geologist: LS
Driller: HALL

Geology Items						Assay					Mag Susc
From	To	Weathering	Lithology	Comments	Alteration	From	To	Sample No	Cu (ppm)	Au (ppm)	
									2135.	7.5 15. 22.5	1. 97.9 969.4 9594.
						187.47	188.47	RS05234		0.014	
						188.47	189.47	RS05235		0.023	
						189.47	190.47	RS05236		0.089	
						190.47	191.47	RS05237		0.071	
						191.47	192.47	RS05238		0.078	
						192.47	193.47	RS05240		0.0025	
						193.47	194.47	RS05241		0.0025	
181.47	200.91	FRESH		Diorite/ Porphyritic and epidotised, medium grained ?dioritic unit, oxidised along fracture planes.	EPIDOTIZATION Weakly to Moderately Developed	194.47	195.47	RS05242		0.014	
						195.47	196.47	RS05243		0.088	
						196.47	197.47	RS05244		0.059	
						197.47	198.47	RS05245		0.081	
						198.47	199.47	RS05246		0.211	
						199.47	200.91	RS05248		0.042	

ProjectCode: NDORI123
PROSPECT: MASUMBI

HoleID: ANMDD004
Depth: 158.64

Aviva Mining - Kenya

AVIVA MINING KENYA LTD

rock & stock INVESTMENTS

Company: AVIVA_KENY
Geologist: JD
Driller: HALL

Depth	Geology Items						Assay					Mag Susc
	From	To	Weathering	Litholog y	Comments	Alteration	From	To	Sample No	Cu (ppm)	Au (ppm)	
										2135. 4270.	7.5 15. 22.5	1. 97.9 969.4 9594.
	0	4.2	ND		Clay - Residual/							
5							4.2	5.63	RS05313		0.032	
							5.63	8.46	RS05314		0.017	
	4.2	13.26	EXTR		Saprolite/	OXIDATION Intensely Developed	8.46	9.46	RS05315		0.058	
10							9.46	10.49	RS05316		0.014	
							10.49	11.49	RS05317		0.083	
							11.49	12.49	RS05319	70	0.038	
							12.49	13.26	RS05320	43	0.125	
							13.26	14.46	RS05321	32	0.059	
15							14.46	16	RS05322	46	0.187	
	13.26	20.32	EXTR-V		Saprock/ Poor core recovery (70 percent). Crumbly.	OXIDATION Strongly Developed	16	17.46	RS05323	55	0.037	
							17.46	19	RS05324	58	0.029	
20							19	20.32	RS05325	93	0.072	
	20.32	23.37	V		Saprock/	OXIDATION Strongly Developed	20.32	23.37	RS05326	60	0.123	
	23.37	24.57	SL-MOD		Micro diorite/ Fractured with zones of saprolite.	OXIDATION Weakly Developed	23.37	24.57	RS05327	111	0.011	
25	24.57	26.46			Core Loss/							
	26.46	26.98	EXTR		Saprock/ Creamy orange, crumbly.	OXIDATION Intensely Developed	26.46	26.88	RS05328	63	0.041	
	26.98	27.21			Core Loss/		27.21	27.91	RS05330	62	0.05	
	27.21	29.93	EXTR-V		Saprolite/ Creamy orange, crumbly.	OXIDATION Intensely Developed	28.44	29.03	RS05331	114	0.123	
30							29.03	29.93	RS05332	176	0.394	
							29.93	32.01	RS05333	157	1.275	
	29.93	34.37	SL		Micro diorite/ with Disseminated Pyrite. Green grey. Mildly epidotized in places with disseminated pyrite. Very broken with poor core recovery (40 percent).	OXIDATION Very Weakly Developed	32.01	33.16	RS05334	184	0.332	
							33.16	34.37	RS05335	311	2.32	
35	34.37	36.53	FRESH-SL		Dacite/ with Veined Pyrite. Grey, massive. Mild development of quartz pyrite veinlets. Mildly epidotized.	EPIDOTIZATIO N Weakly Developed	34.37	35.33	RS05336	312	1.03	
							35.33	36.53	RS05337	1360	3.21	
	36.53	36.77			Core Loss/							
	36.77	38.53	SL		Dacite/ with Veined Pyrite. Grey, fractured. Mild development of quartz pyrite veinlets, mildly silicified.	SILICIFICATIO N Weakly Developed	36.77	37.81	RS05339	1180	1.45	
							37.81	38.53	RS05340	429	0.615	
							38.53	39.41	RS05341	388	0.341	
40	38.53	41.05	FRESH		Dacite/ Grey, massive. Mildly silicified.	SILICIFICATIO N Very Weakly Developed	39.41	40.29	RS05342	246	0.157	
							40.29	41.05	RS05343	231	0.146	
	41.05	42.05	MOD		Dacite/ Brown grey. Fracture zone.	OXIDATION Moderately Developed	41.05	42.05	RS05344	245	0.199	
							42.05	43	RS05345	158	0.26	
							43	44	RS05346	157	0.135	
							44	45	RS05347	129	0.215	
45	42.05	57	FRESH		Dacite/ Grey green, massive. Occasional quartz pyrite veinlet.		45	46	RS05348	65	0.062	
							46	47	RS05349	46	0.053	
							47	48	RS05351	86	0.136	

ProjectCode: NDORI123
PROSPECT: MASUMBI

HoleID: ANMDD004
Depth: 158.64

Aviva Mining - Kenya

Company: AVIVA_KENY
Geologist: JD
Driller: HALL

Geology Items

From	To	Weathering	Lithology	Comments	Alteration
42.05	57			Dacite/ Grey green, massive. Occasional quartz pyrite veinlet.	
57	72.46	FRESH		Dacite/ Grey green, massive. Mildly to moderately epidotized.	EPIDOTIZATION Weakly Developed
72.46	113.58			Dacite/ with Veined Pyrite. Grey green, massive. Rock appears to be near diorite intrusive as there are patches of coarser dioritic zones that appear as large blobs. Occasional quartz pyrite veinlets throughout.	SILICIFICATION Weakly Developed

Assay

From	To	Sample No	Cu (ppm)	Au (ppm)
47	48	RS05351	86	0.136
48	49	RS05352	126	0.094
49	50	RS05353	18	0.007
50	51	RS05354	110	0.074
51	52	RS05355	271	0.818
52	53	RS05356	92	0.051
53	54	RS05357	11	0.0025
54	55	RS05358	57	0.176
55	56	RS05359	73	0.0025
56	57	RS05360	66	0.007
57	58	RS05362	28	0.007
58	59	RS05363	45	0.057
59	60	RS05364	20	0.008
60	61	RS05365	13	0.0025
61	62	RS05366	12	0.0025
62	63	RS05367	13	0.013
63	64	RS05368	295	0.018
64	65	RS05370	18	0.026
65	66	RS05371	4	0.036
66	67	RS05372	12	0.015
67	67.8	RS05373	62	0.028
67.8	69.2	RS05374	59	0.031
69.2	70.13	RS05375		0.0025
70.13	71.2	RS05376	7	0.007
71.2	72.46	RS05377	31	0.047
72.46	73.46	RS05379	77	0.1
73.46	74	RS05380	132	0.862
74	75	RS05381	114	0.166
75	76	RS05382	38	0.027
76	77	RS05383	168	0.654
77	78	RS05384	70	0.406
78	79	RS05385	589	0.171
79	80	RS05386	177	0.174
80	81	RS05387	280	0.185
81	82	RS05388	54	0.062
82	83	RS05390	24	0.0025
83	84	RS05391	573	0.232
84	85	RS05392	105	0.382
85	86	RS05393	121	0.165
86	86.8	RS05394	108	0.09
86.8	87.82	RS05395	210	0.284
87.82	89	RS05396	309	0.637
89	89.69	RS05397	394	0.189
89.69	90.62	RS05398	410	0.24
90.62	91.32	RS05399	717	0.549
91.32	92.24	RS05401	2480	2.73
92.24	93	RS05402	371	0.48
93	94	RS05403	1190	0.647
94	94.96	RS05404	316	0.178

Cu (ppm) scale: 2135. / 4270.
Au (ppm) scale: . / 7.5 / 15. / 22.5
Mag Susc scale: 1. / 97.9 / 969.4 / 9594.

ProjectCode: NDORI123
PROSPECT: MASUMBI

HoleID: ANMDD004
Depth: 158.64

Aviva Mining - Kenya

Company: AVIVA_KENY
Geologist: JD
Driller: HALL

Geology Items						Assay					Mag Susc
From	To	Weathering	Lithology	Comments	Alteration	From	To	Sample No	Cu (ppm)	Au (ppm)	
									2135. 4270.	7.5 15. 22.5	1. 97.9 969.4 9594.
72.46	113.58	FRESH		Dacite/ with Veined Pyrite. Grey green, massive. Rock appears to be near diorite intrusive as there are patches of coarser dioritic zones that appear as large blobs. Occasional quartz pyrite veinlets throughout.	SILICIFICATION Weakly Developed	94	94.96	RS05404	316	0.178	
						94.96	96	RS05405	523	0.281	
						96	97.05	RS05406	703	1.115	
						97.05	98.05	RS05407	344	0.39	
						98.05	99.05	RS05409	409	0.446	
						99.05	100	RS05410	182	0.199	
						100	100.93	RS05411	232	0.261	
						100.93	102	RS05412	240	0.484	
						102	103	RS05413	173	0.184	
						103	104	RS05414	321	0.323	
						104	105	RS05416	180	0.235	
						105	105.91	RS05417	206	0.477	
						105.91	107.04	RS05418	120	0.147	
						107.04	108	RS05419	70	0.148	
						108	109.4	RS05420	338	1.125	
						109.4	110.04	RS05421	620	1.065	
						110.04	111	RS05422	165	0.399	
						111	111.6	RS05423	264	1.175	
						111.6	112.68	RS05424	185	0.12	
						112.68	113.58	RS05425	197	0.589	
113.58	114.54			Feldspar Porphyry/ with Disseminated Pyrite. Grey massive intermediate feldspar porphyry.		113.58	114.54	RS05426	41	0.02	
114.54	119.46			Dacite/ with Veined Pyrite. Grey green, massive, moderately silicified. Moderate development of quartz pyrite veinlets throughout.	SILICIFICATION Weakly Developed	114.54	115.54	RS05427	329	1.685	
						115.54	116.49	RS05429	78	0.091	
						116.49	117.49	RS05430	120	0.206	
						117.49	118.49	RS05431	52	0.082	
						118.49	119.46	RS05432	67	0.033	
119.46	136.14			Feldspar Porphyry/ with Disseminated Pyrite. Grey, massive and porphyritic. Poorly mineralized with trace to minor disseminated pyrite.		119.46	120.46	RS05433		0.04	
						120.46	121.46	RS05434		0.016	
						121.46	122.46	RS05435		0.015	
						122.46	123.46	RS05436		0.009	
						123.46	124.46	RS05438		0.011	
						124.46	125.46	RS05439		0.014	
						125.46	126.46	RS05440		0.023	
						126.46	127.46	RS05441		0.008	
						127.46	128.46	RS05442		0.011	
						128.46	129.46	RS05443		0.023	
						129.46	130.46	RS05444		0.187	
						130.46	131.46	RS05446		0.02	
						131.46	132.46	RS05447		0.02	
						132.46	133.46	RS05448		0.012	
						133.46	134.46	RS05449		0.007	
						134.46	135.46	RS05450		0.011	
						135.46	136.14	RS05451		0.015	
136.14	146.8			Dacite/ with Disseminated Pyrite. Light green grey, massive, highly silicified, mildly mineralized [pyrite].	SILICIFICATION Strongly Developed	136.14	137.11	RS05452		0.009	
						137.11	138.38	RS05453		0.028	
						138.38	139.66	RS05454		0.035	
						139.66	140.77	RS05455		0.349	
						140.77	141.82	RS05456		0.164	

ProjectCode: NDORI123
PROSPECT: MASUMBI

HoleID: ANMDD004
Depth: 158.64

Aviva Mining - Kenya

AVIVA MINING KENYA LTD

rock & stock INVESTMENTS

Company: AVIVA_KENY
Geologist: JD
Driller: HALL

Geology Items

From	To	Weathering	Lithology	Comments	Alteration
136.14	146.8	FRESH		Dacite/ with Disseminated Pyrite. Light green grey, massive, highly silicified, mildly mineralized [pyrite].	SILICIFICATION Strongly Developed
146.8	158.64	FRESH		Dacite/ with Veined Pyrite. Green grey, massive. Generally poorly mineralized with occasional quartz pyrite vein. Moderate development of thin carbonate veinlets, mildly silicified.	SILICIFICATION Weakly Developed

Assay

From	To	Sample No	Cu (ppm)	Au (ppm)
140.77	141.82	RS05456		0.164
141.82	142.82	RS05458		0.035
142.82	143.82	RS05459		0.021
143.82	144.65	RS05460		0.036
144.65	145.65	RS05461		0.01
145.65	146.8	RS05462		0.073
146.8	147.78	RS05463		0.017
147.78	148.78	RS05464		0.031
148.78	149.88	RS05465		0.016
149.88	151	RS05467		0.063
151	152	RS05468		0.057
152	153	RS05469		0.119
153	154	RS05470		0.048
154	155	RS05471		0.032
155	156	RS05473		0.042
156	156.88	RS05474		0.055
156.88	157.64	RS05475		0.02
157.64	158.64	RS05476		0.012

Cu (ppm): 2135. 4270.
Au (ppm): . 7.5 15. 22.5
Mag Susc: 1. 97.9 969.4 9594.